VAN ROOYEN, GERT CORNELIS

VIBRATIONAL ANALYSIS OF THE LOW-TEMPERATURE MODIFICATION OF THE CHLORIDE SPINELS: Li_2MCl_4 (M = Fe, Co and Cr)

MSc (Chemistry) UP 1992

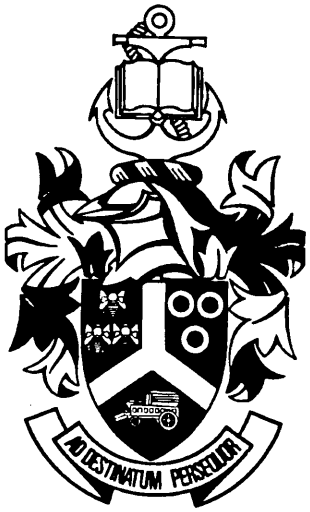

Vibrational analysis of the low-temperature modification of the chloride spinels: Li_2MCl_4 (M = Fe, Co and Cr)

by

Gert Cornelis van Rooyen

Presented for the fulfilment of a part of the requirements for the degree:

M.Sc (Chemistry)

In the Faculty of Science

University of Pretoria

Pretoria

South Africa

December 1992

Acknowledgements

First, I would like to thank my promoter Prof Anton Heyns, head of the Department of Chemistry, at the University of Pretoria. Without a good promoter, successful study is impossible. He introduced me to the subject of vibrational spectroscopy during my Honours year, and thus started an interest that shapes to become a career. Studying under him is never easy, but always interesting, because of comments, suggestions, assignments and challenges.

Secondly, my thanks is due to the people sharing the laboratory (Dr De Waal and Mrs Prinsloo). An M.Sc-student is very green at the commencement of his studies and their invaluable help and instruction in sample preparation and the recording of spectra, is greatly appreciated.

Thirdly, my gratitude extends to my parents, who encouraged scientific interest from an early age on, stressing the value of a good education. They always supported but never prescribed.

Lastly, but not the least, I must thank the Foundation for Research Development in South Africa, for easing the huge financial implication of post-graduate study, by kindly providing a bursary.

English abstract

Title: **Vibrational analysis of the low-temperature modification of the chloride spinels: Li_2MCl_4 (M = Fe, Co and Cr)**

Author: Gert Cornelis van Rooyen
Promotor: Prof AM Heyns

Degree: M.Sc(Chemistry)
Institution: Faculty of Science
Department of Chemistry
University of Pretoria
Pretoria
South Africa
Date: December 1992

A vibrational analysis is carried out for the low-temperature modification of the chloride spinels: Li_2MCl_4 (M = Fe, Co and Cr), with special emphasis on the theoretical interpretation and representation of the vibrational modes found. Infrared spectra were recorded at room temperature and 80 K in the mid-infrared (1000 cm^{-1} to 500 cm^{-1}) and far-infrared (500 cm^{-1} to 100 cm^{-1}) regions. Raman spectra could not be obtained, due to sample burning.

Several theoretical methods are explored for extending structure information (X-ray crystallographic data) to the interpretation of vibrational spectra. Starting with a factor group correlation, the theory is extended with the aid of a line group analysis, stretching-mode analysis, and finally a vibrational analysis, implemented by allowing every atom three degrees of vibrational freedom.

The vibrational behaviour of the lithium atoms in the tetrahedral positions is resolved, but the assignment of the rest of the spectra was not feasible, due to insufficient data.

Special emphasis was placed on graphical representations using the three-dimensional stereographic method. The possibility that these representations may greatly assist the understanding of crystal structures and the interpretation of vibrational spectra, is explored. Crystal structures and vibrations are represented, and a method for viewing and obtaining these representations are discussed.

Afrikaanse abstrak

Titel: **Vibrasie-analise van die lae-temperatuur modifikasie van die chloried-spinelle: Li_2MCl_4 (M = Fe, Co en Cr)**

Outeur: Gert Cornelis van Rooyen
Promotor: Prof AM Heyns

Graad: M.Sc(Chemie)
Instansie: Fakulteit vir Natuurwetenskap
Departement Chemie
Universiteit van Pretoria
Pretoria
Suid-Afrika
Datum: Desember 1992

'n Vibrasie-analise is uitgevoer vir die lae-temperatuur modifikasie van die chloried-spinelle: Li_2MCl_4 (M = Fe, Co en Cr), met spesiale verwysing na die teoretiese interpretasie en grafiese voorstelling van die vibrasies teenwoordig. Infrarooispektra is by kamertemperatuur en 80 K opgeneem in die mid-infrarooi (1000 cm^{-1} tot 500 cm^{-1}) en ver-infrarooi (500 cm^{-1} tot 100 cm^{-1}) gebiede. Raman-spektra kon nie opgeneem word nie, aangesien die monsters gebrand het.

Verskeie teoretiese metodes word ondersoek om die vibrasiespektra te verklaar, uitgaande van struktuurdata (X-straal kristallografie). Vanaf 'n faktorgroep korrelasie, is die teorie uitgebrei na 'n lyngroep-analise, 'n rekvibrasie-analise en uiteindelik 'n vibrasie-analise gebaseer op die beginsel dat elke atoom drie vibrasie-vryheidsgrade toegelaat word.

Die vibrasie van die litium in the tedraedriese posisies word beskryf, maar die toekenning van die res van die spektra was nie moontlik nie, as gevolg van te min data.

Spesiale vermelding word gemaak van grafiese voorstelling, deur van die drie-dimensionele, stereografiese tegniek gebruik te maak. Die moontlikheid dat hierdie voorstellings grootliks kan bydra tot die interpretasie van kristalstrukture en vibrasie van verbindings, word ondersoek. Kristalstrukture en vibrasies is stereografies voorgestel, en 'n verduideliking vir die gebruik van die voorstellings word gegee. 'n Metode vir die konstruksie van hierdie voorstellings word verskaf.

Table of Contents

Introduction

In the introduction, the main aims of the study are discussed. In the background section, the vibrational problem of the solid state is placed in context with solid-state chemistry in general. The twofold aims of this study is given and each of the aims, viz. the choice of the chloride spinel compounds and the assignment of their spectra; and the theoretical methods tried and the use of stereographic representations, is discussed.

Background

A thorough background in group theory, with special emphasis on representation theory, is crucial to the understanding of the vibrational problem. Two texts, explaining the mathematical and chemical background of the necessary theory are Cotton [4] (an excellent introductory text) and Flurry [6] (a more advanced text covering a range of topics). The application of these methods to the vibrational problem has been much discussed during the past five decades, starting with the text by Hertzberg [9] and the important text by Wilson, Decius and Cross [10].

Because of a substantial increase in importance of materials during the past few decades (with the emphasis on materials designed to meet precise and specific needs), a huge growth in research and development in this aria resulted. An understanding of the forces at work within these materials should aid the understanding of their properties and behaviour under various conditions. Because many of these materials are of inorganic nature (e.g. ceramics and superconductors), it is not surprising that this branch of chemistry, together with physical chemistry, is taking its place amongst the more popular branches of chemistry such as organic or analytical chemistry.

One important aspect of the behaviour of the solid state, is its vibration at various temperatures. An understanding of the vibrational behaviour of solids, should aid the investigation of these materials and will probably contribute largely to the eventual

understanding of the forces at work within these materials. Probably the most important development in the vibrational interpretation of the solid state, is the text by Fateley, Dollish and co-workers [5], in which they describe the application of vibrational selection rules to various types of solid substances.

A huge gap exists however, between the results obtained by the application of the method developed by Fateley, Dollish and co-workers, and the interpretation of the results of the two most important techniques for measuring the vibrational behaviour of substances, viz. infrared and Raman spectroscopy. In many cases the theoretical interpretation is stopped at a correlation (with the method of Fateley, Dollish and co-workers), and further investigations proceed empirically.

Main aims of the investigation

The aims of this study are twofold in nature. The first is to clarify and explore the theoretical means of extending structure information to the interpretation of vibrational spectra. It is the author's belief that clear three-dimensional representations of crystal structure and the vibrations involved, aid the understanding of these properties, and should contribute heavily to the solving of the vibrational problem. The second aim is to apply these methods to the spectra of compounds, not yet interpreted. With this aim in mind the three chloride spinels (Li_2MCl_4, M = Co, Fe and Cr) were chosen.

Overview of the compounds chosen for this study

A review of recent literature on solid state compounds, revealed three interesting compounds described by Kanno, Takeda and co-workers [30,31,32]. These are the low-temperature modification of the chloride spinels: Li_2MCl_4 (M = Co, Fe and Cr). These three compounds were chosen for a vibrational study, because of the following reasons:

First, the compounds were synthesized for the first time only very recently (1987) and to the author's knowledge, only one publication described vibrational spectra of some of the compounds (Wussow, Haeuseler and co-workers [61]).

Secondly, the normal and inverse spinel structures display reasonably simple vibrational spectra and the perturbation, from the inverse spinel structure, present in the compounds of the study, should not be too difficult to describe.

Thirdly, the synthesis is not very difficult and all the reactants are easily obtainable.

These motivations proved to be naive, mainly because the vibrational spectra are substantially more complex than believed at first and because a few serious obstacles were met with, during sample preparation for infrared spectroscopy.

Probably because of the large amount of disorder in the compounds (as discussed in Chapter 5), the infrared spectra are not very good, consisting of broad bands, difficult to resolute and impossible to assign accurately. The spectra are represented in Chapter 4 and a discussion of the assignment is given in Chapter 9.

The author was also unable to obtain Raman spectra, for reasons which are discussed in Chapter 3.

Although the synthesis and sample preparation presented some problems, mainly because of the extremely hygroscopic nature of the compounds, all were overcome, as discussed in Chapter 3.

Overview of the theoretical methods explored

One of the main aims of this study is to develop and explore various methods to construct and describe the vibrational modes obtained by the method of Fateley Dollish and co-workers. After examining the results of this method (Chapter 6) several other methods were tried.

The feasibility of a line group analysis (Chapter 6) is explored, to determine whether it may be applicable in cases where the chains under consideration, are interconnected and not completely independent. The findings confirm the condition that all chains must be completely independent, and consist of strong internal bonds, for the line group analysis to be of any help.

Because of its ease of implementation and the fact that in a crystal lattice, all bending of bond angles must imply some bond stretching, a stretching-mode analysis was attempted, as discussed in Chapter 7. Sets of imaginary bonds are defined in the crystal, to represent the structure, and the behaviour of stretching in these bonds, under the symmetry present in the crystal, is examined. The main conclusion is that the stretching-mode analysis does not produce all the vibrational modes predicted by the correlation, although some modes (the *gerade* modes) are rather well described.

If each atom in the crystal is allowed three degrees of vibrational freedom, the behaviour of these movements under the space group symmetry, should produce all the normal modes present in the crystal. The vibrational analysis carried out in Chapter 8, shows that this is indeed the case.

Although these methods proceed somewhat further than a mere correlation, it does not bridge the gap between theory and practice completely. As discussed in Chapter 8 mixing of modes of similar symmetry must occur, but it seems impossible to predict the nature and size of this mixing from theoretical and structural considerations only.

A discussion and development of these techniques in general, presents some problems, and the treatment of a favourable example with these methods greatly enhances understanding. The chloride spinels were chosen to be examined by these methods. If good graphical representations of the crystal structure and vibrational behaviour of this example can be obtained, the application of the method should be eased.

The first step in most types of studies of crystalline compounds, is to obtain a clear understanding of the structure and structural properties. The spinel structures are discussed in detail in Chapter 4. It is in structure representation, that the enormous aid of three

dimensional visioning of structure, comes to the fore. Stereographic representation mimics the three-dimensions perceived by normal vision, and are used throughout this text (for a discussion of how this representations are constructed and how they should be viewed, see Appendix A). The three-dimensional images of vibrational modes aids the interpretation of these modes enormously, and some interesting observations of the vibration of the tetrahedral lithium are made with the aid of these representations.

Conclusions

Can theoretical methods, based on the crystal structures of compounds, be extended all the way to the vibrational spectra of these compounds? This question summarises the one aim of this study. Can the vibrational spectra of the chloride spinel compounds, be interpreted with the theoretical methods developed? This question summarises the other aim of this study.

PART 1

Background

Chapter 1

Background on the spinel structure

Some background information on the normal and inverse spinel structures is given. The structure and the composition of the spinel family of compounds are discussed and mention is made of some important spinels.

Structure information

The name spinel was originally given to the mineral spinel, with formula composition $MgAl_2O_4$. This mineral is fairly common, especially in the earth's mantle, and is a source of both iron and magnesium. Later, the name spinel was extended to include all compounds with the formula AB_2X_4, that crystallize with the same structure as the mineral spinel. In this way the spinel became one of the basic inorganic crystal structures, like sodium chloride, olivine, wurtzite, etc.

Spinel, therefore, has a formula unit of AB_2X_4 and usually crystallizes in the cubic space group Fd3m. Both the composition and the structure may vary and a good discussion of the various structures possible within the spinel group of compounds, may be found in Haas [24]. The Fd3m space group is cubic (O_h^7) and there are eight formula units in the unit-cell, to yield a unit-cell composition of $A_8B_{16}X_{32}$.

The spinel may be seen as a cubic lattice, in which the 32 anions (X) pack close in a cubic array (cubic close-packed: ccp). As may be seen in Figure 1.1, the ccp lattice consists of three interchanging planes of anions (planes A, B and C) to build the structure ABCABCABC.... The unit-cell is constructed to yield a face-centred cubic lattice (fcc) (indicated in the figure). Each anion is surrounded by twelve other anions, which, together with hexagonal close-packing, is the optimum way of space-filling for anions of similar size and charge, in the solid state.

In such a cubic lattice, consisting of N anions, there are N interstitial holes within the lattice that have a tetrahedral environment of anions. In the same way there are 2N interstitial holes with an octahedral environment. Crystallographically, 1/2N of the octahedral holes and 1/8N of the tetrahedral holes are equivalent respectively. In a unit-cell consisting of 32 anions (as is the case with the spinel structure) there are therefore 8 tetrahedral and 16 octahedral holes. In the normal spinel, the A cations fill the tetrahedral holes and the B cations the octahedral holes, to yield the unit-cell composition of $A_8B_{16}X_{32}$. This way of representing the spinel structure is not the only one however, and a formula unit of A_2BX_4 is sometimes written, with the octahedral and tetrahedral cation labels exchanged.

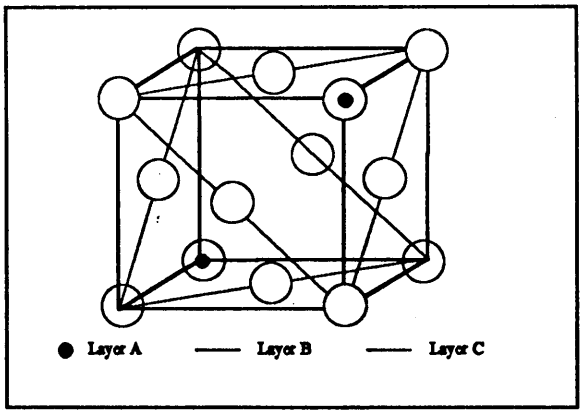

Figure 1.1: Unit-cell (face centred cubic (fcc) unit-cell) in a cubic array of anions. Note the three interchanging layers A, B and C.

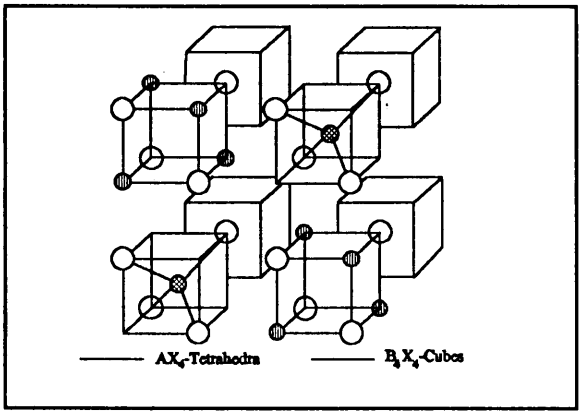

Figure 1.2: Part of the spinel structure, consisting of eight interchanging AX_4-tetrahedra and B_4X_4-cubes.

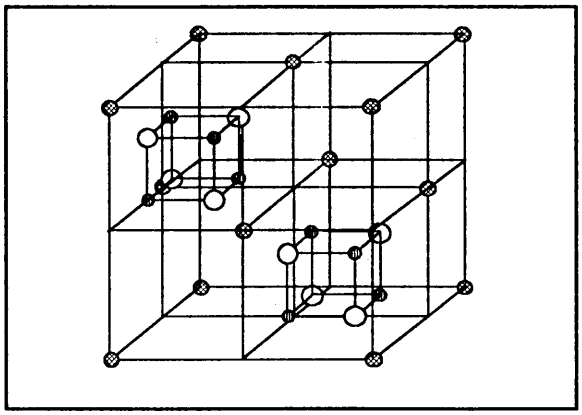

Figure 1.3: The fcc lattice of A ions, superimposed over the structure depicted in the previous figure, to yield the unit-cell.

The spinel structure may be seen as eight octants of alternating AX_4-tetrahedra and B_4X_4-cubes. This may be seen in Figure 1.2 (This and the next figure were taken from Greenwood and Earnshaw [7]). It may also be seen as alternating pieces of a zinc sulphide (AX_4) and rock salt (sodium chloride) (B_4X_4) lattice. It is clear, from the figure, that the B cations are in the octahedral positions and the A cations in the tetrahedral positions. In the structure represented in Figure 1.2 however, there are only four of the of the eight A cations

present and the question arises, how the other four may be explained. This problem can be solved by superimposing a face-centred cubic (fcc) lattice of A cations over the eight octants described above. This situation may be seen in Figure 1.3. The position of the B_4X_4-cubes are indicated in the figure. This lattice is shared by the six neighbouring unit-cells and contributes four A cations to each unit-cell, to complete the $A_8B_{16}X_{32}$ spinel unit-cell composition.

Composition of the spinel structure

In the AB_2X_4 structure discussed in the previous section, it was mentioned that the X-ions represent the anions the spinel structure. This anion is in more than 95 % of all spinel structures known, the oxide anion. Other anions include chloride, sulphide, telluride, selenite and even ionic species like the cyanide ion may in exceptional cases form the anionic lattice needed for the spinel structure.

The cations must be chosen to complete the charge balance. If the formula unit is inspected with the oxide ion as anion, viz. AB_2O_4, it is clear that to balance the eight negative charges of the four oxygen atoms, the following combinations of cations are possible: $A^{II}B_2^{III}O_4$, $A^{IV}B_2^{II}O_4$ and $A^{VI}B_2^{I}O_4$. The first structure is by far the most common (more than 80 % of the compounds known) and examples of the cations are:

A^{II}: Mg; Cr, Mn, Fe, Co, Ni, Cu; Zn, Cd, Sn

B^{III}: Al, Ga, In; Ti, V, Cr, Mn, Fe, Co, Ni, Rh

Examples of spinels with other oxidation states of the cations and anions are:

$A^{IV}B_2^{II}X^{-II}$: $TiMg_2O_4$, $PbFe_2O_4$, $SnCu_2S_4$

$A^{VI}B_2^{I}X^{-II}$: $MoAg_2O_4$, $MoNa_2O_4$, WNa_2O_4

$A^{II}B_2^{I}X^{-I}$: $NiLi_2F_4$, $ZnK_2(CN)_4$, $CdK_2(CN)_4$ and the examples of this study.

In some cases the A cations prefer the octahedral positions over the tetrahedral positions forced onto them by the spinel lattice. In such cases the A cations, together with half of the B cations, fill the octahedral positions, and the other half of the B cations fill the tetrahedral positions, to complete a formula unit of $B_{Td}(AB)_{Oh}X_4$. This form of the spinel structure is

known as the inverse spinel. A very important example of this type of compound is the ferrite magnetite (Fe_3O_4), a natural occurring mineral with formula unit $Fe^{III}_{Td}(Fe^{III}Fe^{II})_{Oh}O_4$.

Between these two extremes (the normal and inverse spinels) a whole range compounds, with mixing of cations between the positions, is possible. The cation distribution of the spinel is often described with the structural parameter λ, which represents the fraction of B cations in the tetrahedral holes, and for the inverse spinel $\lambda = ½$. Intermediate values are possible (e.g. $\lambda = ⅓$, in a random spinel), and λ may even vary for a given spinel if it is heated. These spinels are known as disordered spinels, because different ions occupy crystallographic similar sites.

Several reasons have been suggested to explain why some compounds prefer the normal and others the inverse spinel structure. No all-encompassing theory has been suggested yet, mainly because several factors contribute to the problem more or less. Some reasons for the adoption of one structure over the other, are: First, bigger cations usually prefer the octahedral positions while smaller cations prefer the tetrahedral positions. Secondly, the crystal field stabilization energy of the tetrahedral and octahedral fields for each cation, may play a role. Thirdly, the Madelung constants for the normal and inverse spinel structures have to be considered and fourthly, polarization or covalency effects have to be taken into account. A reasonably successful attempt to classify the structures may be found in a paper by Burdett, Price and Price [15], in which they used structural sorting maps.

In the case of the spinels studied in this text, the anion is chloride, with formula unit AB_2Cl_4 ($A^{II}B^{I}_2Cl_4$). Most of these spinels are inverse; $B_{Td}(AB)_{Oh}Cl_4$. These structures will be discussed fully in subsequent chapters.

Some important spinels

The best known member of the spinel family is the ferrite (a ferrite is a spinel with unit formula $M^{II}Fe_2O_4$, where Fe is in the III+ oxidation state; there are both normal and inverse ferrites) magnetite, Fe_3O_4. This mineral has been known for thousands of years, and was known to the alchemists as 'lodestone'. This mineral was used for compass needles, because

it is ferromagnetic and retains magnetism well. It is an inverse spinel with both Fe^{III} and Fe^{II} cations in the octahedral environment. The Fe^{III}–octahedra and the Fe^{II}–octahedra alternate to from chains with the octahedra sharing an edge. The very high electrical conductivity of magnetite can be easily explained by valence electron transfer between the iron ions in the II+ and III+ oxidation states, because the differently charged ions are in very close contact. In contrast to magnetite, the spinel Mn_3O_4 is a very poor electrical conductor because Mn_3O_4 is a normal spinel ($Mn^{II}_{Td}(Mn^{III}_2)_{Oh}O_4$) and the manganese in the II+ and III+ oxidation states are in different environments and electron transfer, between the valence states, is therefore much more difficult.

Another ferrite, with barium as the divalent metal, ($BaFe_2O_4$) is used as the coating on magnetic disks, audio and video tapes. These are just two examples of the varied field of compounds with the spinel structure.

Chapter 2

Review of the vibrational studies on spinels, found in the literature, with emphasis on the last twelve years

In this chapter the vibrational analyses, on the spinel type of structure, found in the literature, is discussed. The last twelve years (1980 to August 1992) are covered comprehensively, although reference is made to earlier studies of importance. In order to facilitate the understanding of the literature, the results of a factor group correlation on the normal spinel structure (space group Fd3m) are given. It should be noted that except for one reference, no other vibrational work has been carried out on the chloride spinels.

Results of a factor group correlation on the normal spinel structure

The first attempt to obtain a theoretical interpretation of the vibrations present in crystals with the spinel type of structure, was made by Waldron [58]. This paper also contains the first infrared spectra of ferrites, a type of spinel, except for a very early reflectance spectrum of magnetite by Coblenz [3] (reference from Waldron). This paper is still one of the most authoritative works on the theoretical interpretation of the spectra of spinels, being quoted in virtually every paper on the subject. It must be stressed that Waldron determined the vibrational behaviour correctly, without the aid of the method devised by Bhagavantum and Venkatarayudu [2], and the later and much simpler method, devised by Fateley, Dollish and co-workers [5]. He obtained the vibrations by taking the asymmetric unit-cell of the cubic ferrites to consist of two MO_4-tetrahedra and a Fe_4-tetrahedron (with the Fe^{3+} ions on the corners). By relating the vibrations of these units to the O_h factor group of the unit-cell, he obtained the 42 (formula of the asymmetric unit: $M_2Fe_4O_8$; there are two asymmetric units in the space unit-cell) vibrations present in the crystal: $\Gamma_{tot.} = 3\ A_1 + 3\ E + 3\ T_1 + 8\ T_2$. It must be noted that Waldron distinguished between the T_2 *gerade* and *ungerade* (T_{2g} and T_{2u})

vibrations by examining each one individually, to obtain the four T_2 vibrations that are *ungerade*, and therefore infrared active (T_{2u}).

The space group information for the spinel with formula unit A_2BO_4 may be found in Table 2.1. The results of a factor group correlation, using the method of Fateley, Dollish and co-workers, may be seen in Table 2.2. As indicated, there are four (4 T_{1u}) infrared active modes and five (A_{1g} + E_g + 3 T_{2g}) Raman active modes. If a factor group correlation for the inverse spinel is carried out, the results are the same as for the normal spinel. It is therefore difficult to distinguish between the two forms on spectral data alone, the spectra differing only in the position of the vibrational bands.

Spinel: A_2BO_4		
Space group: Fd3m, O_h^7, no. 227 Z = 8 Z^B = 2		
Atom	**Wyckoff site**	**Site group**
A (O_h)	16d	D_{3d}
B (T_d)	8a	T_d
O	8e	C_{3v}

Table 2.1: Space group information for the normal spinel with formula unit AB_2O_4.

Atom									
O	A_{1g}		E_g	T_{1g}	2 T_{2g}	A_{2u}	E_u	2 T_{1u}	T_{2u}
B					T_{2g}			T_{1u}	
A						A_{2u}	E_u	2 T_{1u}	T_{2u}
Γ_{total}	A_{1g}		E_g	T_{1g}	3 T_{2g}	2 A_{2u}	2 E_u	5 T_{1u}	2 T_{2u}
$\Gamma_{acoustic}$								T_{1u}	
$\Gamma_{rotational}$				T_{1g}					
$\Gamma_{vibrational}$	A_{1g}		E_g	T_{1g}	3 T_{2g}	2 A_{2u}	2 E_u	4 T_{1u}	2 T_{2u}
Activity	R	N/A	R	N/A	R	N/A	N/A	N/A	IR	N/A

Table 2.2: Results of a factor group analysis on the normal spinel AB_2O_4.

Of the four infrared active bands, only three are usually observed in the infrared spectra, the fourth is usually below 100 cm^{-1} in energy and not seen in most of the experiments. Raman studies are less common but all five active modes have been observed.

Since the first paper by Waldron, because of the vast number of spinel compounds synthesized, a lot of vibrational work on the normal and inverse spinels has appeared. A good review of the early work on oxide spinels may be found in the paper by White and De Angelis [59]. The theoretical interpretation of results and the assignment of modes have been reviewed by Preudhomme and Tartre [43,44].

Although the space group Fd3m is the generally accepted structure for normal and inverse spinels, some doubt does exist and Heuer and Mitchell [25], amongst others, have suggested the lower symmetry space group $F\bar{4}3m$, T_d^2. From a factor group correlation of this space group (Striefler and Barsch in [1, p.75]), it follows that there are seven infrared active modes. In general, three, or sometimes four (the fourth is often below 50 cm^{-1} in energy) strong bands are observed. These are normally attributed to the four T_{1u} modes associated with the Fd3m space group. However, some weak features are sometimes observed in the spectra of spinels, which, together with the three or four strong bands, may account for the seven T_2 modes expected for the $F\bar{4}3m$ space group. In addition, the two space groups are structurally very closely related and no great difference in the position and pattern of the strong bands can be expected, if different space groups are assigned to the crystal. However, these additional features are seldomly observed (they may be obscured by the strong bands), and due to this absence and the fact that small features in the far infrared are often unreliable, as well as a large amount of structural evidence for the Fd3m space group, there seems to be no reliable reason why the structure of the spinel should not be taken as belonging to the Fd3m space group, as is generally done. There may be some examples though, that crystallise in the $F\bar{4}3m$ space group.

After extensive experimental investigations based on solid solutions and isotope effects, Preudhomme and Tartre [45,46] proposed the assignment of the infrared spectra which is generally accepted as correct. They concluded that the highest frequency band (ν_1) may be assigned to vibrations of the octahedral and tetrahedral groups of the III—II and II—IV spinels respectively. They suggested that the second highest frequency band (ν_2) may be assigned to a bending vibration of the tetrahedral-group in the case of the II—IV spinel, and finally proposed that the two lowest frequency bands (ν_3 and ν_4) may be assigned to vibrations of the octahedral lattice. In the case of III—II spinels ν_2 and ν_3 are sometimes exchanged. This assignment has been investigated by many subsequent authors.

Literature review

One of the only papers in the literature that may be of help in the present study, is the work of Tartre [51]. Tartre used ^{7}Li and ^{6}Li substitutions in the spinel $LiCrGeO_4$ to conclude that the LiO_4–tetrahedron is much more strongly defined than the LiO_6–octahedron (in the present study the $LiCl_4$–tetrahedron and $LiCl_6$–octahedron are under consideration). They placed the vibrations of the LiO_4–tetrahedron in the region of 450 cm^{-1} and concluded that the vibration of the LiO_6–octahedron must lie below 300 cm^{-1}, beyond the scope of their instrument. This paper is also an excellent example of structure clarification with the aid of vibrational analysis.

Starting with the eighties, Shaplygin and Lazarev [47] examined the infrared spectra of MRh_2O_4 (M = Mg, Zn and Cd) spinels, as well as various other parameters. They recorded spectra from 1200 cm^{-1} to 200 cm^{-1}, and, using the information presented by White and De Angelis, proposed that ν_1 and ν_3 may be assigned to M—O stretching and bending modes respectively in the MO_4 –tetrahedron, and that ν_2 and ν_4 may be assigned to Rh—O stretching and bending modes respectively in the RhO_6–octahedron. All these spinels are normal.

Baran and Botto [14] recorded and interpreted the infrared spectra of the spinels Co_5TeO_8, $Co_3Zn_2TeO_8$, $NiZn_4TeO_8$ and $Ni_2Zn_3TeO_8$. A full assignment of the TeO_6–group is proposed and force constants and mean amplitudes of vibration were calculated. The normal spinels Fe_2SiO_4 and Co_2SiO_4 were synthesised by Striefler, Barsch and Syun-Iti [50]. They recorded the infrared spectra from 4000 cm^{-1} to 200 cm^{-1}. They examined the proposed assignment of Preudhomme and Tartre [46,47] for II—IV spinels, and found three strong infrared bands for each of the spinels and confirmed the assignment with the aid of the different cations. The effect of cation size on the vibration spectra is discussed.

Ishii, Hiraishi and Yamanaka [27] measured and analyzed the reflectance infrared (1200 cm^{-1} to 20 cm^{-1}) and Raman (850 cm^{-1} to 100 cm^{-1}) spectra of a single crystal of the non-stoichiometric spinel $MgO.(Al_2O_3)_3$ by comparing it to the spectra of the stoichiometric compound. Shirai, Yoshiyuki and Nakagawa [48] measured the infrared transmission and reflectance spectra of the spinels $Co^{II}Co_2^{III}O_4$, $CoAl_2O_4$, $ZnFe_2O_4$ and $MnFe_2O_4$ and the single crystal Raman spectra of $Co^{II}Co_2^{III}O_4$ and $CoAl_2O_4$. They performed lattice dynamical calculations,

with a normal coordinate analysis based on a rigid ion model and discussed the short-range potential constants obtained, in relation to the bond character. They obtained the frequencies of the transverse (TO) and longitudinal (LO) modes of the infrared active species.

Porotnikov, Savenko and Sidorova [42] synthesized Zn_2SnO_4 and Mg_2SnO_4 and recorded the infrared (1000 cm^{-1} to 50 cm^{-1}) and Raman (1000 cm^{-1} to 100 cm^{-1}) spectra. Using $^{24,26}Mg$ and $^{64,70}Zn$ isotope substitution, they identified the vibrations associated with the various metal-oxygen polyhedra. In both the infrared and Raman spectra they found more than the predicted number of bands, which implies that the compounds have lower symmetry than the Fd3m space group suggests.

Lutz, Waeschenbach and co-workers [39] recorded the far-infrared reflectance spectra (700 cm^{-1} to 40 cm^{-1}) of the spinels MCr_2S_4 (M = Mn, Fe, Co, Zn, Cd and Hg), MCr_2Se_4 (M = Zn, Cd and Hg) and MIn_2S_4 (M = Mn, Fe, Co, Ni, Cd and Hg). These spinels show the four infrared active bands expected in the case of the normal spinels, and up to five bands in the case of the inverse spinels. The transverse (TO) and longitudinal (LO) frequencies were calculated and the covalent nature of the bonds examined.

In a study of the Mg_2SiO_4 polymorphs, Akagogi, Ross and co-workers [12], recorded and discussed the infrared and Raman spectra of β-Mg_2SiO_4 and γ-Mg_2SiO_4. What is of interest is that β-Mg_2SiO_4 has a crystal structure apparently similar to the compounds in this study, viz. Imma.

Badarinath [13] synthesized the solid solution series $MgAl_{2-x}Fe_xO_4$ and recorded the far-infrared spectra. The results follow the characteristic pattern for spinels.

Wakaki [55] synthesized the normal spinel $HgIn_2S_4$ and recorded a far-infrared reflectance spectrum (1000 cm^{-1} to 20 cm^{-1}), observing all four of the predicted bands. Dispersion parameters were calculated by dispersion analysis using classical oscillators. The strength of the four kinds of short range force constants were calculated.

Guyot, Boyer and co-workers [23], interested in various mineral compositions, recorded Raman microprobe spectra (1000 cm^{-1} to 600 cm^{-1}) for Mg_2GeO_4 and $(MgFe)_2SiO_4$. They

attributed the three bands they observed in each case, to symmetrical and anti-symmetrical stretching-modes in the SiO_4- and GeO_4-tetrahedra, which may be considered as internal modes. Yamanaka and Ishii [62] recorded the Raman spectra (1200 cm^{-1} to 100 cm^{-1}) of Ni_2SiO_4 in the temperature range 20 to 600 °C. With convincing arguments they assigned all five of the predicted and observed Raman bands (A_{1g} + E_g + 3 T_{2g}). Calculations of the optically active lattice vibrations have been carried out, assuming a potential function which combines general valence and short range force constants. The values of the force constants were calculated.

Wakamura, Iwatani and Takarabe [56] measured the infrared reflectance spectra (900 cm^{-1} to 40 cm^{-1}) for the spinel series $Zn_{1-x}Cd_xCr_2S_4$. Four or possibly five bands were observed throughout the whole series. The three bands of highest frequency show one-mode behaviour and the other, two-mode behaviour. The concentration dependence of these mode frequencies were interpreted by a model based on two basic units and six force constants.

McMillan and Akaogi [41] recorded the Raman spectra of β-Mg_2SiO_4 (modified spinel) and γ-Mg_2SiO_4 (spinel). The spectrum for the γ-spinel showed the expected five bands, while their spectra of the β-spinel differed appreciably from spectra reported in the literature.

Malézieux and Piriou [40] studied the vibrational behaviour of spinels of the series $MgAl_{2-x}Cr_xO_4$, $FeAl_{2-x}Cr_xO_4$, $Mg_{1-x}Fe_xAl_2O_4$, $Mg_{1-x}Fe_xCr_2O_4$ and $Mg_{1-½}Fe_{½}Al_{2-x}Cr_xO_4$ by recording the diffusion Raman spectra (900 cm^{-1} to 200 cm^{-1}). They examined one-mode and two-mode behaviour in the crystals. The fact that this extensive article is in French, makes it difficult to assess.

In a very interesting single crystal Raman study, Graves, Johnston and Campaniello [19], examined the spectra of three ferrites: Fe_2O_4, $NiFe_2O_4$ and $MnFe_2O_4$. Although they observed the five predicted Raman bands, polarization data denies that two bands may be assigned to the two T_{2g} modes predicted for the O_h^7 factor group. After examination of all the possible arrangements of cations described by Haas [24]. they concluded that there may be a small perturbation of the O_h structure to the lower D_{3d} structure. Strong enough to change the symmetry of the bands, but not strong enough to show any great splitting into the A_{1g} and E_g modes predicted by a correlation between the two factor groups. The authors made a

complete assignment and reopens the question that at least some spinels may crystallise in the $F\bar{4}3m$ space group.

Wakamura [57] measured infrared spectra (900 cm^{-1} to 50 cm^{-1}) at 300K and 16K for the spinel series $Cd_xZn_{1-x}Cr_2Se_{4(1-y)}S_{4y}$. One-mode and two-mode behaviour of the four observed T_{1u} bands, were examined. In some of the more mixed spinels, five bands were observed. Lutz, Becker and co-workers [36] did single crystal studies on several spinel systems: MCr_2S_4 (M = Mn, Fe, Co, Zn and Cd), MIn_2S_4 (M = Mn, Fe, Co and Ni), $MnCr_{2-2x}In_{2x}S_4$ and $Co_{1-x}Cd_xCr_2S_4$. They recorded Raman spectra (700 cm^{-1} and 100 cm^{-1}) as well as polarized Raman spectra. Their main results are firstly that large resonance enhancement effects were observed; secondly, a breakdown of the translation symmetry in the inverse spinels (MIn_2S_4), which results in band broadening was noticed and more bands than predicted by group theory seen; thirdly, a large amount of two-mode behaviour was observed and fourthly, frequency shifts of the bands caused by the tetrahedrally coordinated metal ions occurred, due to mass effects, and both bonding and repulsive interactions.

In the only other vibrational work done on the compounds of this study, Wussow, Haeuseler and co-workers [61] recorded reflectance infrared spectra (900 cm^{-1} to 50cm^{-1}) and some Raman spectra of chloride spinels: Li_2MCl_4 (M = Mg, V, Cr, Mn, Fe, Co, Zn and Cd) and Li_2MnBr_4. They found more than the five Raman active and four infrared active modes in some cases, but attributed this to two-mode behaviour and disorder in the structure. It is unlikely that they recorded the spectra of the low-temperature phase in the case of the iron spinel, as no mention is made of annealing, and they grouped it with other examples of inverse spinels. Some discussion about the nature of the spectra is given.

Gupta, Geeta and co-workers [20] studied the composition dependence of the long wavelength optical lattice vibrations of the mixed spinels $Zn_{1-x}Cd_xCr_2S_4$ and $CdCr_2(S_{1-x}Se_x)_4$, using the Launay-type angular force constant model. One-mode type behaviour is predicted for all the vibrational modes in the spinel systems. Gupta, Parashar and co-workers [21] calculated force constants for the $CdCr_2S_4$ and $CdCr_2Se_4$ spinels, with the aid of a analytical solution to the 42x42 dynamical matrix at the zone centre.

In a paper, Himmrich and Lutz [26] the discussed the results of normal coordinate analyses and lattice dynamical calculations on the spinel Zn_2CrO_4. They used various potential models (short-range, rigid ion and polarizable ion) and concluded that the potential energy is mainly controlled by Cr—O (octahedron) and Zn—O (tetrahedron) interactions as well as Cr—Cr repulsive forces, whereas O—O interactions are less important. The ZnO_4-groups are stronger defined than the CrO_6-groups.

Lutz, Müller and Steiner [37] recorded the reflectance infrared (1000 cm^{-1} to 50 cm^{-1}) and Raman (800 cm^{-1} to 100 cm^{-1}) spectra of the spinels MCr_2O_4 (M = Mg, Mn, Fe, Co, Ni, Cu and Zn) and MFe_2O_4 (M = Ni and Cu). Their results agree with the normal assignment of the optical modes. They presented the results of a Kramers-Kronig analyses and oscillator-fit calculations.

Gupta, Sinha and co-workers [22] did zone-centre frequency calculations on the spinels $MnCr_2S_4$ and $FeCr_2S_4$ using the infrared frequencies obtained from the literature. They concluded that second neighbour interactions dominate over other interactions present. Gasanly, El-Hamid and co-workers [18] measured the infrared reflectance spectra (500 cm^{-1} to 50 cm^{-1}) and Raman spectra (500 cm^{-1} to 20 cm^{-1}) of the spinel $CuIn_5S_8$. Their results are in complete agreement with the normal assignment of spinel spectra.

Cynn, Sharma and co-workers [17] studied disorder between the tetrahedral and octahedral sites in the $MgAl_2O_4$ spinel in order to assign the ambiguous Raman spectra of this compound. They produced Raman spectra to demonstrate the rapid disordering of Mg and Al at high temperatures and the subsequent quenching disorder. The spectra are interpreted to resolve divergent interpretations of the vibrational spectra of natural and synthetic $MgAl_2O_4$.

PART 2

Experimental

Chapter 3

Experimental

In this chapters he synthesis of the compounds of this study, is discussed. Attention is given to sample preparation for infrared and the experimental conditions for the recording of the infrared spectra are discussed. The inability to obtain Raman spectra is mentioned.

Synthesis

In three recent papers Kanno, Takeda and co-workers [30,31,32] described the synthesis and structure determination of three new chloride spinels. All three exhibit interesting low-temperature modifications of the inverse spinel structure. Their method of synthesis was used in this study.

Due to the hygroscopic nature of the reactants and the slight sensitivity to oxygen and the extremely hygroscopic nature of the products, the synthesis had to be carried out under an inert atmosphere (nitrogen in this case). All reactants were dried at 300 °C, for three days, under a nitrogen atmosphere. All reactants were analytical grade.

The following solid state reaction were carried out for each of the three divalent metals:

$2\ LiCl + MCl_2 \rightarrow Li_2MCl_4$ (M = Co^{2+}, Fe^{2+} and Cr^{2+})

The reactants were thoroughly ground (in a mortar and pestle) separately. The reactants were then mixed in stoichiometric quantities and ground and mixed together for about ten minutes, to ensure thorough mixing and thus to accelerate the solid state reaction.

All products were fired for a week, under a nitrogen atmosphere, at 400 °C, to ensure that the reactions proceed to completion. Upon cooling, the chromium and cobalt spinels yielded the desired low-temperature phase immediately, but the iron spinel remained in the cubic

high-temperature phase (a meta-stable phase). In order to obtain the desired low-temperature phase, the compound was annealed at 100 °C (a temperature just below the phase transition temperature of about 125 °C), for two weeks. The iron spinel has an intense sky-blue colour, while the cobalt spinel has an intense dark blue colour. The chromium spinel has a deep dark green colour, appearing almost black.

All three compounds are extremely hygroscopic, absorbing more than twice their own mass in moisture in a matter of hours. The hygroscopic activity may easily be observed, with the compounds forming small droplets in a matter of minutes if exposed to the atmosphere. Extreme care has therefore to be taken in the handling and sample preparation.

All samples were inspected for homogeneity with the aid of electron microscopy, and it was observed that all the compounds are crystalline in nature, consisting of clusters of micro-crystals, forming, what appear to be small single crystals at first sight.

A series of solid solutions with composition $Li_2Co_{1-x}Cr_xCl_4$ was tried, but electron microscopy revealed that the samples consist of a mixture of Li_2CoCl_4 and Li_2CrCl_4 phases.

Sample preparation for infrared spectroscopy

In the generally accepted manner, KBr discs were used for the mid-infrared (3000 cm^{-1} to 500 cm^{-1}) and polyethylene discs for the far-infrared transmission spectra (500 cm^{-1} to 50 cm^{-1}).

Unexpected trouble was encountered when preparing the discs necessary for infrared spectroscopy. Due to the extremely hygroscopic nature of the compounds, the prepared discs absorbed enough moisture, when transferred from the die to the instrument, to influence measurements.

After considering several methods, one was found that is both simple and effective in preventing moisture from reaching the samples.

In the case of the discs prepared for far-infrared measurements, AR polyethylene was used. Two discs consisting of 10 mg of polyethylene were pressed separately (all discs were pressed in a 10 mm die, under a pressure of nine tons, for three minutes). Three milligrams of sample were thoroughly mixed with another ten milligrams of polyethylene, under a nitrogen atmosphere, and the die was assembled, under the same atmosphere, by placing first one of the pressed discs, then the mixture and lastly the other pressed disc in the die (as demonstrated in Figure 3.1). The die was sealed and placed in the press. The result is a neat sandwich with the sample sealed off from the atmosphere, in polyethylene. This allowed sufficient time for the discs to be transferred to the instrument and measurements taken, without interference from moisture.

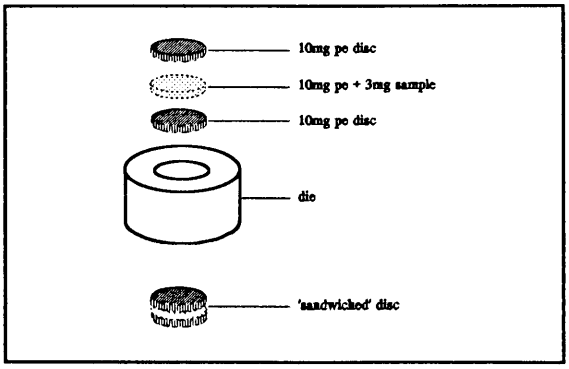

Figure 3.1: Diagrammatical illustration of the preparation of the polyethylene discs (pe = polyethylene).

The same method was applied to the KBr discs required for mid-infrared spectroscopy; two 50 mg KBr discs were pressed and 2 mg of sample was mixed with a further 50 mg of KBr. In the case of KBr however, the above mentioned precautions, to prevent the absorbtion of moisture, were inadequate and the discs had to be dried and then to be handled very rapidly before measurement. The discs were dried under a nitrogen atmosphere for three days, at a temperature just below the first phase transition of the sample (reported by Kanno, Takeda and co-workers). The temperatures may be found in Table 3.1.

Compound	Drying temp. /°C	Phase trans. temp. /°C
Li_2FeCl_4	100	125
Li_2CoCl_4	250	308
Li_2CrCl_4	200	222

Table 3.1: Drying temperature for the KBr discs containing the sample.

Parameters for infrared spectroscopy

All spectra were recorded on a Bruker 113v infrared spectrometer. Details of the experimental parameters may be found in Table 3.2. For measurements in the mid-infrared only one beamsplitter was necessary, but in the far-infrared, it was necessary to use three of the beamsplitters available on the Bruker, to cover the whole region; these spectra were combined, with a feature available on the instrument, afterwards. Spectra were recorded at room temperature, about 398 K, and at 80 K (the lowest temperature available with liquid nitrogen). The whole instrument was evacuated to ensure the absence of any moisture in the beam path.

Parameter	Mid-infrared 3000 to 500 cm^{-1}	Far-infrared 600 to 50 cm^{-1}
Resolution	2 cm^{-1}	2 cm^{-1}
No. Scans	36	128
Reference	150 mg disc KBr	50 mg disc Polyethylene
Mirror vel.	10 $cm.min^{-1}$	1 $cm.min^{-1}$
Baseline correction*	none	no. 1

*Baseline correction method no. 1 of two methods available on the Bruker.

Table 3.2: Parameters for the measurement of infrared spectra, used during this study.

Raman spectroscopy

All attempts to obtain Raman spectra of the compounds failed completely and not even very weak spectra were obtained. This is probably due to the fact that only a single channel instrument was available and the laser power necessary to obtain spectra, caused burning of the samples. The difficulty of obtaining spectra, may also be due to the disorder present in all the samples (lithium in the tetrahedral positions).

Chapter 4

Infrared spectra

All the infrared spectra recorded during this study are presented in this chapter. Spectra were recorded with the conditions mentioned in the previous chapter. Basic problems with the interpretation of the recorded spectra are discussed.

Spectra for Li_2FeCl_4

The mid-infrared spectra (at room temperature and at 80 K) may be seen in Figure 4.1. The far-infrared spectra are given in Figure 4.2. Conditions are as mentioned in the previous chapter. All samples were dried for three days, as mentioned.

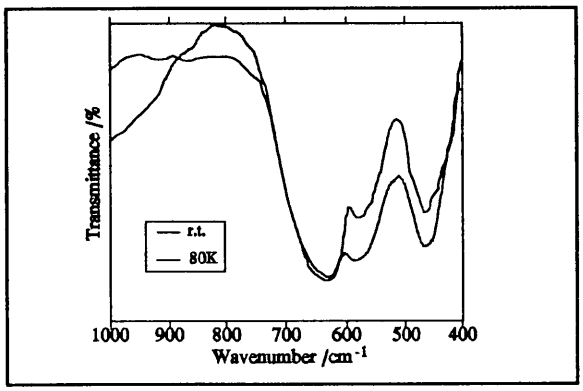

Figure 4.1: Mid-infrared spectra of Li_2FeCl_4. Recorded at room temperature and 80 K.

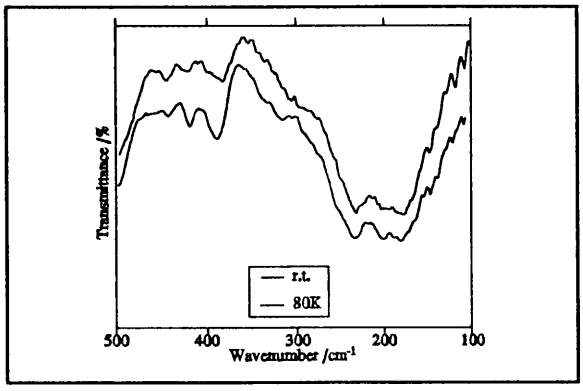

Figure 4.2: Far-infrared spectra for Li_2FeCl_4. Recorded at room temperature and 80 K.

Spectra for Li_2CoCl_4

The mid-infrared spectra (at room temperature and at 80 K) may be seen in Figure 4.3. The far-infrared spectra are given in Figure 4.4. Conditions are as mentioned in the previous chapter. All samples were dried for three days, as mentioned.

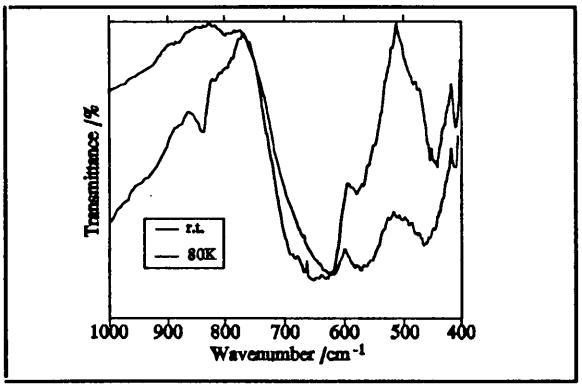

Figure 4.3: Mid-infrared spectra of Li_2CoCl_4. Recorded at room temperature and 80 K.

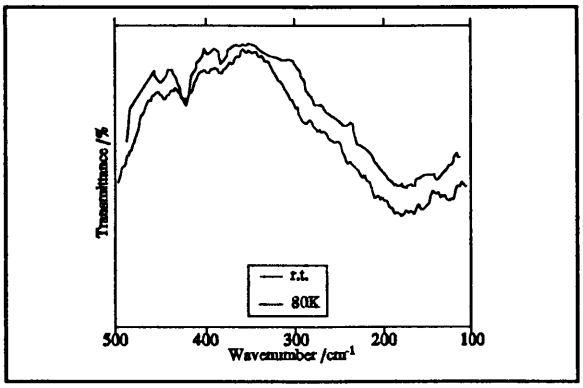

Figure 4.4: Far-infrared spectra for Li_2CoCl_4. Recorded at room temperature and 80 K.

Spectra for Li_2CrCl_4

The mid-infrared spectra (at room temperature and at 80 K) may be seen in Figure 4.5. The far-infrared spectra are given in Figure 4.6. Conditions are as mentioned in the previous chapter. All samples were dried for three days, as mentioned.

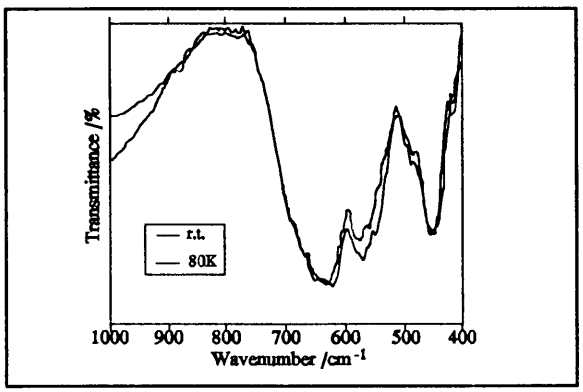

Figure 4.5: Mid-infrared spectra of Li_2CrCl_4. Recorded at room temperature and 80 K.

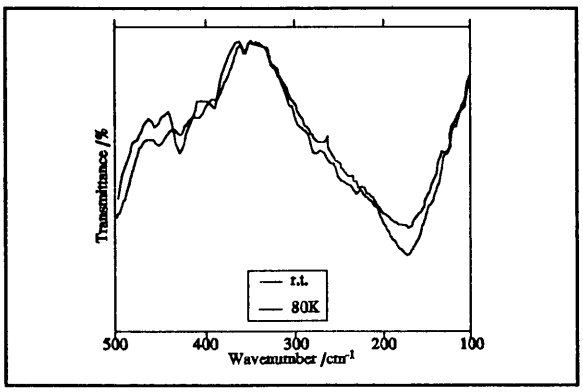

Figure 4.6: Far-infrared spectra for Li_2CrCl_4. Recorded at room temperature and 80 K.

General discussion of spectra

A general discussion of features of the spectra and problems with recording is given here, a more detailed discussion of the spectra, as well as the attempted assignment, will be given

in Chapter 9. A summery of all the spectra may found in Table 4.1. The symbolism used in the table is discussed at the end of the table. The positions of bands indicated are taken mainly from the spectra recorded at 80 K. If some doubt existed however, the spectra recorded at room temperature were consulted. The spectra of the cobalt spinel were not good, and use was made of various spectra of both undried and dried samples.

Li_2FeCl_4		Li_2CoCl_4		Li_2CrCl_4	
FIR	MIR	FIR	MIR	FIR	MIR
~154 sh↓		~155 sh↓		~140 sh↓	
182		172		175	
207		?~202 sh↑		~~185 sh↑	
231		238		~230 sh↑	
				~277 sh↑	
~330 sh↑		~330 sh↑		?~326 sh↑	
				?359	
397		~394		~390 sh↑	
429		430		430	
455	457	452	~456	453	456
	580		574		574
	625		624		630
					~~640 sh↑

sh :	shoulder	**↑,↓ :**	indicates to what band shoulder is attached to.
~ :	some uncertainty in position of band.	**~~ :**	large uncertainty in position of band
? :	existence of band in doubt		**All energies in cm^{-1}**

Table 4.1: Summary of the infrared spectra obtained for the three spinels: Li_2FeCl_4, Li_2CoCl_4 and Li_2CrCl_4.

Another problem with measuring the exact position of spectral bands, is a slight amount of noise on all bands, especially in the low-energy regions of the far-infrared spectra. The program on the infrared instrument, marks the highest of these small disturbances as the position of the main band, a position which is not always correct. To compensate for this, the bands over which some doubt exist were smoothed manually with the aid of a flexi-curve

and the position measured. Some doubt about the position of a shoulder will always exist (it may perhaps be resolved if band shape calculations are carried out) and this doubt is indicated in the table.

In the region below 100 cm^{-1}, and sometimes as high as 150 cm^{-1} (especially in the case of the cobalt spinel measurements) noise is a big problem, and some spikes, which may be attributed to the polyethylene in the discs, are present. This noise is accentuated by the baseline correction programs tried. Because no noticeable bands were observed for the spinels in this region (100 cm^{-1} to 20 cm^{-1}), it was omitted from the spectra. No bands were observed at energies higher than 1000 cm^{-1} either.

Finally, as said in Chapter 3, these spinels are extremely hygroscopic. All absorb water readily, causing great changes in the spectra in the region 1000 cm^{-1} to $\sim$400 cm^{-1} (no significant changes were observed below this energy). In addition to the normal water (or ice) bands, a whole range of bands that must be due to librational modes of the water or ice, appear. The result often is broad bands difficult to resolute. This is the main reason why a clarification of this modes were not attempted during this study, but may prove fruitful matter for further investigation. One exception however, is a very strong band at $\sim$510 cm^{-1} in all the spectra of all three compounds, which may clearly be assigned to a water librational mode.

PART 3

Theoretical Interpretations

Chapter 5

Structure

In this chapter the structure of the compounds synthesized, are discussed. The structure for the three chloride spinels Li_2MCl_4, (M = Fe, Co and Cr), are given from the three papers by Kanno, Takeda and co-workers [30,31,32], and discussed according to the ordering of the various ions in the structures and their relation to the usual inverse spinels. A brief description of the phase transitions, as discussed by Kanno, Takeda and co-workers, is given. Problems with the structure data for the chromium spinel, reported by Kanno, Takeda and co-workers, are discussed.

Basic structure

In recent years a wide variety of compounds, with the spinel structure in which the anion is chloride, have been synthesized [16,28,29,32,33,34,35,38,49,54]. Most of these compounds have the structure Li_2MCl_4. From the I- oxidation state of the chloride anions, it is clear that the oxidation state of the metal must be II+ and therefore the compounds include a large number of transition metals, as well as some of the alkaline earth metals (e.g. M = Mg, Mn, Cd, V). Crystal studies indicate that all these compounds crystallize in the inverse spinel structure, discussed in Chapter 1, in which the transition metal and half of the lithium ions occupy the octahedral positions and the other half of the lithium, the tetrahedral positions.

When Kanno, Takeda and co-workers attempted to synthesize equivalent compounds for Co, Fe and Cr however, distortions from the usual inverse spinel structure, viz. the cubic space group Fd3m, were observed. These distortions, to a space group of lower symmetry, result in a deviation from the simple vibrational spectra obtained from regular spinels. This is the main reason for the selection of these particular compounds for this study. In this chapter the basic structure of each of these compounds is discussed. All the relevant structure data came

from the publications of Kanno, Takeda and co-workers and are repeated for ease of use in this and subsequent chapters.

Li_2CoCl_4 and Li_2FeCl_4: Crystal lattice and the octahedral cations

These were the first two chloride spinels with symmetry other than the normal Fd3m, found by Kanno, Takeda and co-workers. These compounds are treated simultaneously because of their almost complete similarity. Space group information for the iron and cobalt spinels may be seen in Table 5.1 and Table 5.2 respectively. This data was taken directly from the publications mentioned. Kanno, Takeda and co-workers used a Rietveld refinement of powder patterns, because of the difficulty of obtaining large enough single crystals for a single crystal X-ray study.

Space group			Imma	D_{2h}^{28}	
Lattice constants /Å			**a**	**b**	**c**
			7.3067(3)	7.3158(4)	10.3323(5)
Atom	**Site**	**Occup.**	**x**	**y**	**z**
Li (1)	8i	0.5	0.146(15)	0.25	0.196(13)
Li (2)	4b	0.880(13)	0	0	0.5
Fe (1)	4b	0.120	0	0	0.5
Fe (2)	4d	0.880	0.25	0.25	0.75
Li (3)	4d	0.120	0.25	0.25	0.75
Cl (1)	8h	1	0	-0.015(3)	0.245(3)
Cl (2)	8i	1	0.251(6)	0.25	-0.0005(3)

Table 5.1: Space group information for Li_2FeCl_4 (The esd's in parentheses refer to the last significant digits).

Space group			Imma	D_{2h}^{28}	
Lattice constants /Å			**a**	**b**	**c**
			7.1772(2)	7.2478(2)	10.2785(3)
Atom	**Site**	**Occup.**	**x**	**y**	**z**
Li (1)	8i	0.5	0.159(8)	0.25	0.213(13)
Li (2)	4b	0.826(17)	0	0	0.5
Co (1)	4b	0.174	0	0	0.5
Co (2)	4d	0.826	0.25	0.25	0.75
Li (3)	4d	0.174	0.25	0.25	0.75
Cl (1)	8h	1	0	-0.011(1)	0.2442(1)
Cl (2)	8i	1	0.246(2)	0.25	-0.0086(7)

Table 5.2: Space group information for Li_2CoCl_4 (The esd's in parentheses refer to the last significant digits).

Note the great similarity between the data of the two compounds. The lattice constants of the two compounds vary by less than 2 % between them, being slightly bigger in the case of the iron spinel, which is in agreement with the fact that the Fe^{2+} ion is slightly bigger

than the Co^{2+} ion. There is also great similarity between the occupancy of those atoms in mixed sites.

Because of the great similarity between the cobalt and iron spinels, it is impossible to recognize the differences in unit-cell parameters on any but the most accurate of graphical representations. For this reason only the cobalt spinel is represented throughout this chapter and the rest of this text. The iron spinel is almost exactly the same and only involves the substitution of the cobalt cations with iron cations.

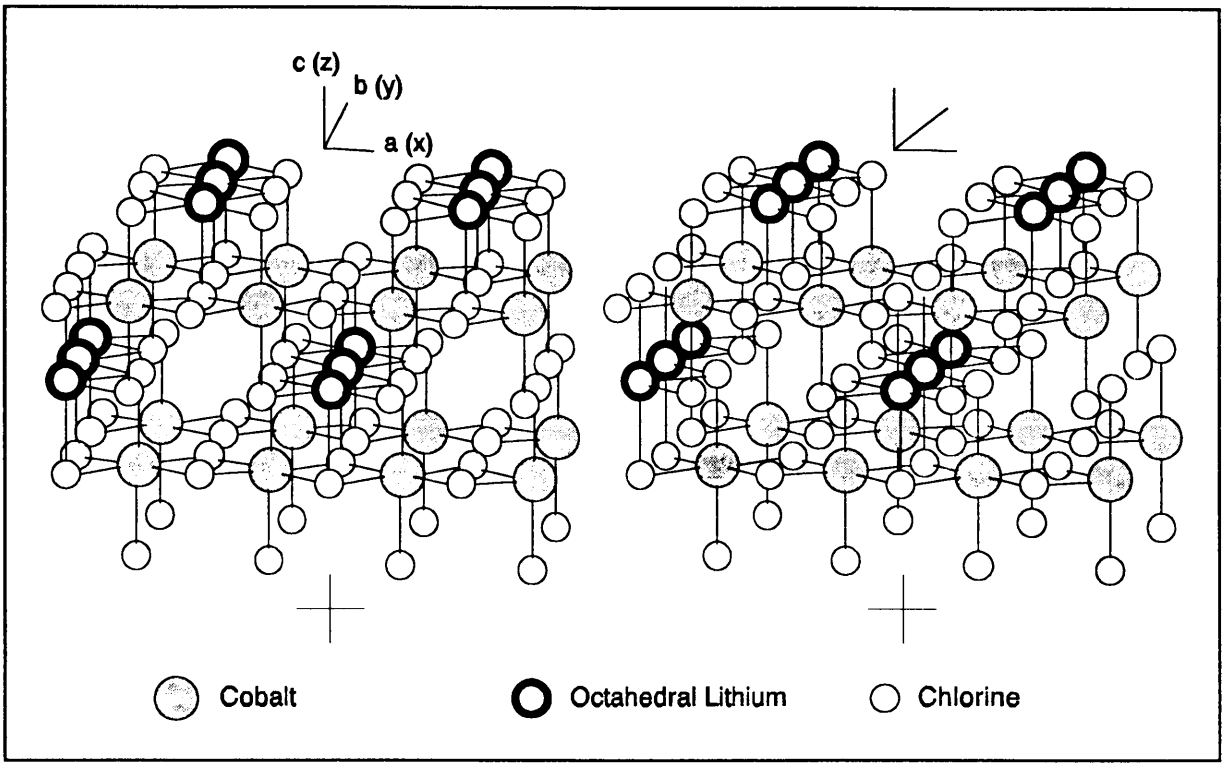

Figure 5.1: Stereographic representation of three adjacent unit-cells for the cobalt spinel, without the tetrahedral lithium.

One simplification is needed in order to facilitate the graphical representations of the crystals in this study. This simplification is to ignore the mixing between the 4b and the 4d crystallographic sites. The 4b site is taken to contain only the lithium in the octahedral positions and the 4d site the transition metal in the octahedral positions. The main reason for this simplification is that a graphical representation of the simplified crystal illustrates the structural properties present in the crystal, much clearer. As the degree of mixing is reasonably small (about 17 % maximum) the actual crystal may be taken as a slight

perturbation of the ideal case. This perturbation may, and probably does have a small effect on the vibrational spectra considered later in this text.

For reasons that are given later in this chapter, the lithium in the tetrahedral positions is considered separately and are omitted in the first graphical representations. Therefore only the metal atoms in the octahedral positions, as well as the chlorine lattice, are considered.

In order to visualize the structural trends present in the crystal, a graphical representation of three connected unit-cells is given (for a discussion of how these representations work and how they were obtained, see Appendix A). This may be seen in Figure 5.1. After the discussion of the structure, a representation of the unit cell will be considered.

Inspection of Figure 5.1 reveals several interesting features. The first thing to notice is that the chlorine atoms remain in a fairly regular cubic closed packed (ccp) array, as is the case with the inverse cubic spinel. The distortion of this array is very small and may in all probability be taken as negligible (the disturbance is less than 1 % relative change in position, to unity and within three standard deviations, in most cases). The lattice of chlorine atoms can therefore not contribute to the change in vibrational spectra observed for these two spinels, and an explanation for this changes should lie with the metal cations.

The metal cations are arranged along the axes of the unit-cell (note the direction of the axes in Figure 5.1; the direction of the axes in all the other stereographic figures in this and subsequent chapters, remains the same, and will not be given again). The cobalt ions are arranged along the a-axis, and the octahedral lithium ions along the b-axis. Each metal atom may be seen as the centre of a MCl_6-octahedron. The metal atoms are therefore arranged in chains along the axes, consisting of MCl_6-octahedra sharing an edge in the direction of the axis. The a- or b-direction chains alternate with chains of 'empty' octahedra, which form the unoccupied interstitial octahedra predicted by a ccp array of large anions (it is the chain of 'empty' octahedra, the interstitial octahedra, between the a-axis chains, that play an important role in the position of the tetrahedral lithium, discussed later in this chapter). The chains of the lithium-octahedra cross the chains of the cobalt-octahedra by sharing opposite faces of an octahedron with the $CoCl_6$-octahedra of a chain above and below the particular lithium chain. Whether these chains are structurally present, or just a convenient way of representing

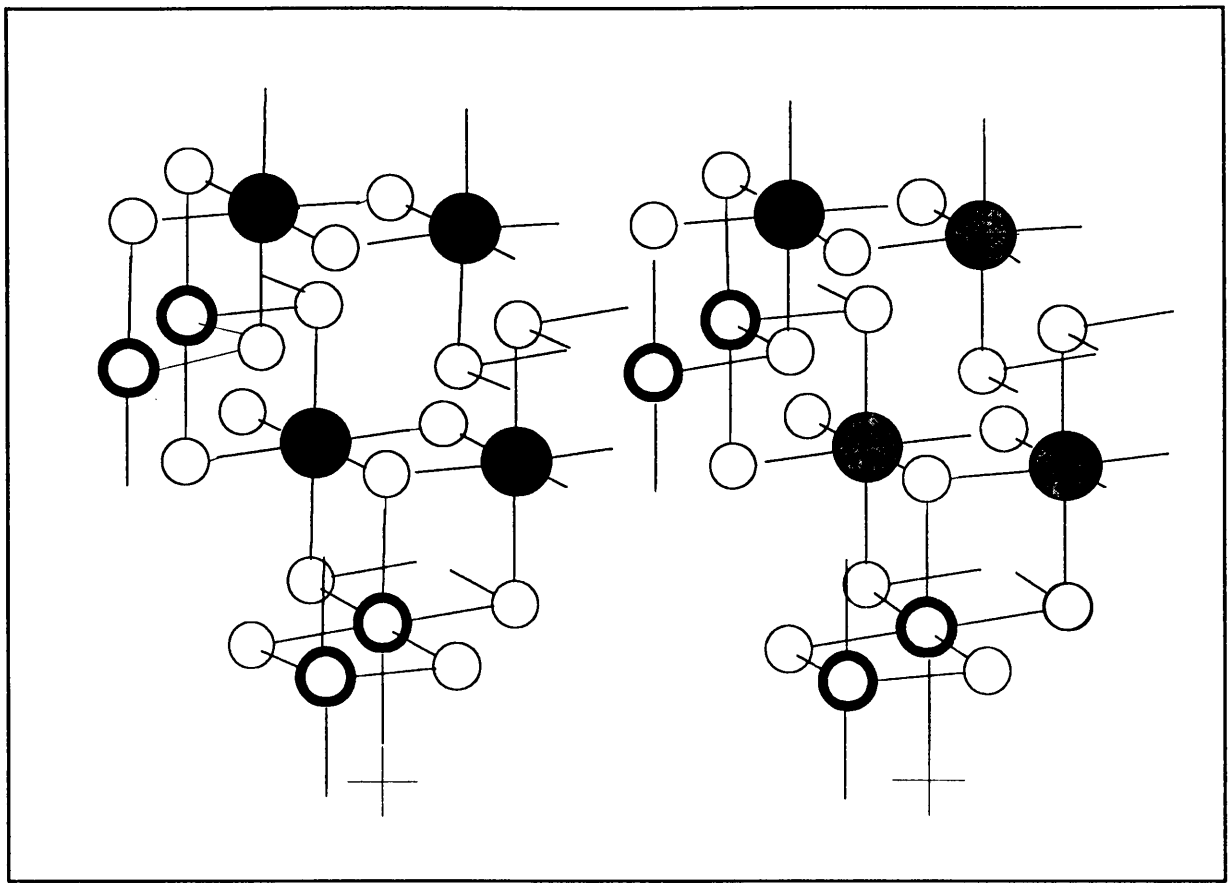

Figure 5.2: Stereographic projection of the unit-cell of the iron and cobalt spinels.

the structure remains to be seen and will be discussed in Chapter 6. The chains do, however, present an accessible way of visualising the structure.

In an article on the phase transitions for compounds with the spinel structure, Haas [24], classified spinels according to structural traits. Although, at the time this article was written, the known spinels consisted mainly of oxide spinels, and Haas applied his theories to these type of compounds, there are no reason why these classification cannot be applied to spinels with other types of anions as well, such as spinels with the chloride anion in this case. According to Haas, the above spinels, belong to a class of spinels with 1:1 ordering on the octahedral sites of type (β). This type differs from the type (α) spinels in that it crystallizes in the Imma space group, whereas the type (α) spinel crystallize in the $P4_1 22$ space group, with factor group D_4^3. Although there is a 1:1 ordering in the octahedral positions between two crystallographically different sites for the (α) type, there is no arrangement along the axes as is the case with the Imma space group.

It is beyond the scope of this text to either present or use the theory on phase transitions developed by Haas, or his use of reciprocal lattices to classify the possible phase transitions of the spinel compounds. The discussion on phase transitions will be concluded with the observation that Haas predicted a first-order phase transition from the orthorhombic Imma space group to the Cubic Fd3m spinel space group. It should be obvious that this phase transition represents an order to disorder type of transition as far as the octahedral sites are concerned. From a definite ordering of the two different cations in the octahedral sites between two crystallographically different sites, the phase transition modifies the crystal to a structure where there is a statistical ordering of the two different cations on a single crystallographical site. This prediction was found to be accurate by Kanno, Takeda and co-workers, who, with the aid of DTA and X-ray crystallography, found phase transitions to the inverse spinel structure, at 308 °C and 126 °C for the cobalt and iron spinels respectively.

This section is concluded with a representation of the unit-cell of the cobalt an iron spinels. A stereographic representation of the unit-cell may be seen in Figure 5.2 (the same legend as in Figure 5.1 applies). The unit-cell is given, because it will be used extensively in subsequent chapters to represent the vibrational movements within the crystal. Note that the lithium in the octahedral positions is again omitted, and is dealt with separately in the next section. As said, the Imma space group is orthorhombic with two primitive units per unit-cell. The unit-cell formula is therefore $Li_8M_4Cl_{16}$. The unit-cell of the parent cubic spinel has therefore divided into two separate unit-cells with the lowering of the symmetry from Fd3m to Imma.

Li_2CoCl_4 and Li_2FeCl_4: Lithium in the tetrahedral positions

In the inverse spinel, half of the one type of cation occupies tetrahedral positions. This is not strictly true for the low-temperature modifications of the iron and cobalt spinels with space group Imma or D_{28}^{2h}. In order to understand the modifications in the D_{28}^{2h} space group, it is necessary to inspect Figure 5.3. In this figure the tetrahedron, at the middle of which lies the tetrahedral position, as well as an adjacent interstitial octahedron, is indicated. Note that the interstitial octahedra form a chain that separates the alternating MCl_6-chains. Similar chains

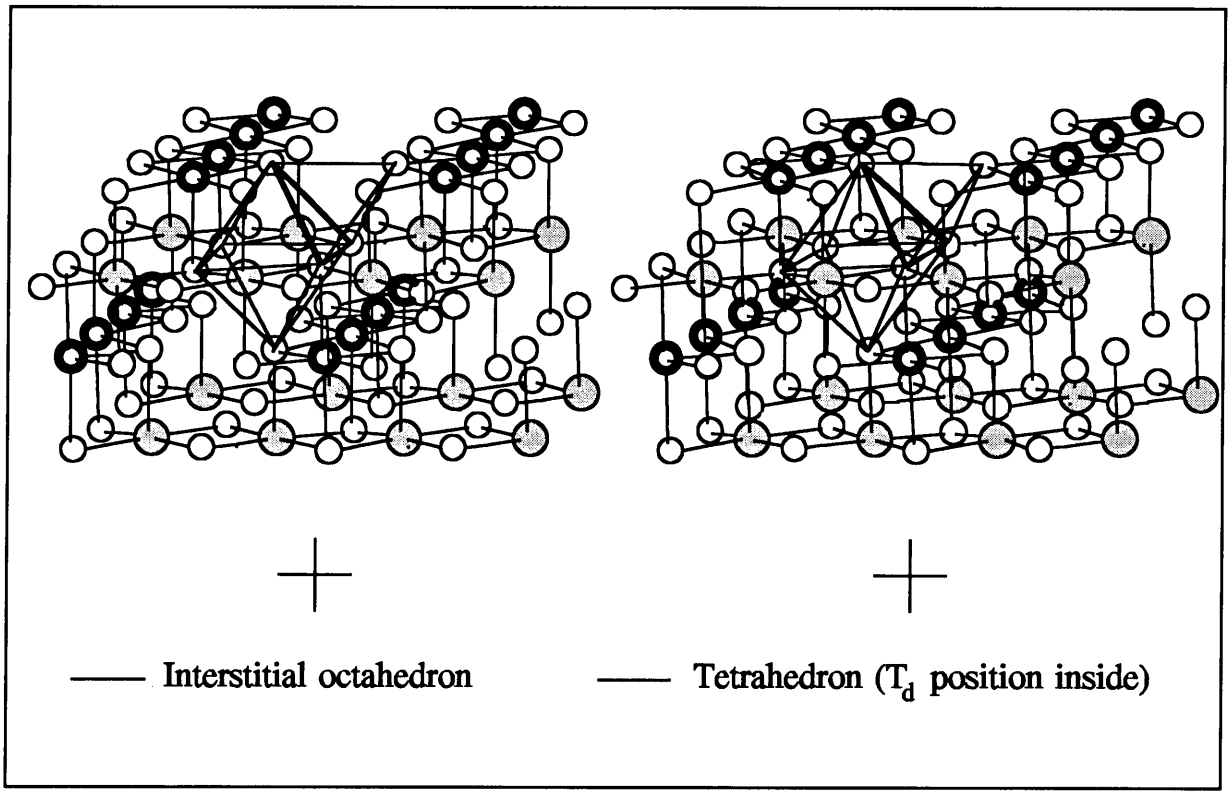

Figure 5.3: Representation of the cobalt spinel, with the interstitial octahedron and tetrahedron containing the tetrahedral position, indicated.

of interstitial octahedra separate the alternating chains of $LiCl_6$–octahedra, but need not be considered here, as they do not take any structural part in the position of the tetrahedral lithium.

In the cobalt and iron spinels the tetrahedral lithium does not occupy the true tetrahedral position, at the centre of the tetrahedron indicated in Figure 5.3, the 4e crystallographical site. In stead, the lithium occupies half of the 8i positions which lie between the 4e site and the 4d site, which, in turn, is at the centre of the adjacent interstitial octahedron indicated in Figure 5.3. All three positions (4e, 4c and 8i) are indicated in Figure 5.4. Note the zig–zag arrangement of the different lithium positions.

If the unit–cell is isolated, the positions become even clearer. The unit–cell, with the interstitial octahedron and the adjacent tetrahedron, as well as al three the lithium sites are indicated in Figure 5.5. The relative positions of the three crystallographic sites concerned (4c, 4e and 8i) are made clear. It is also clear that the 8i site lies on a line drawn from the 4c site to the 4e site, but much nearer to the interstitial octahedral site, 4c. Of these 8i sites,

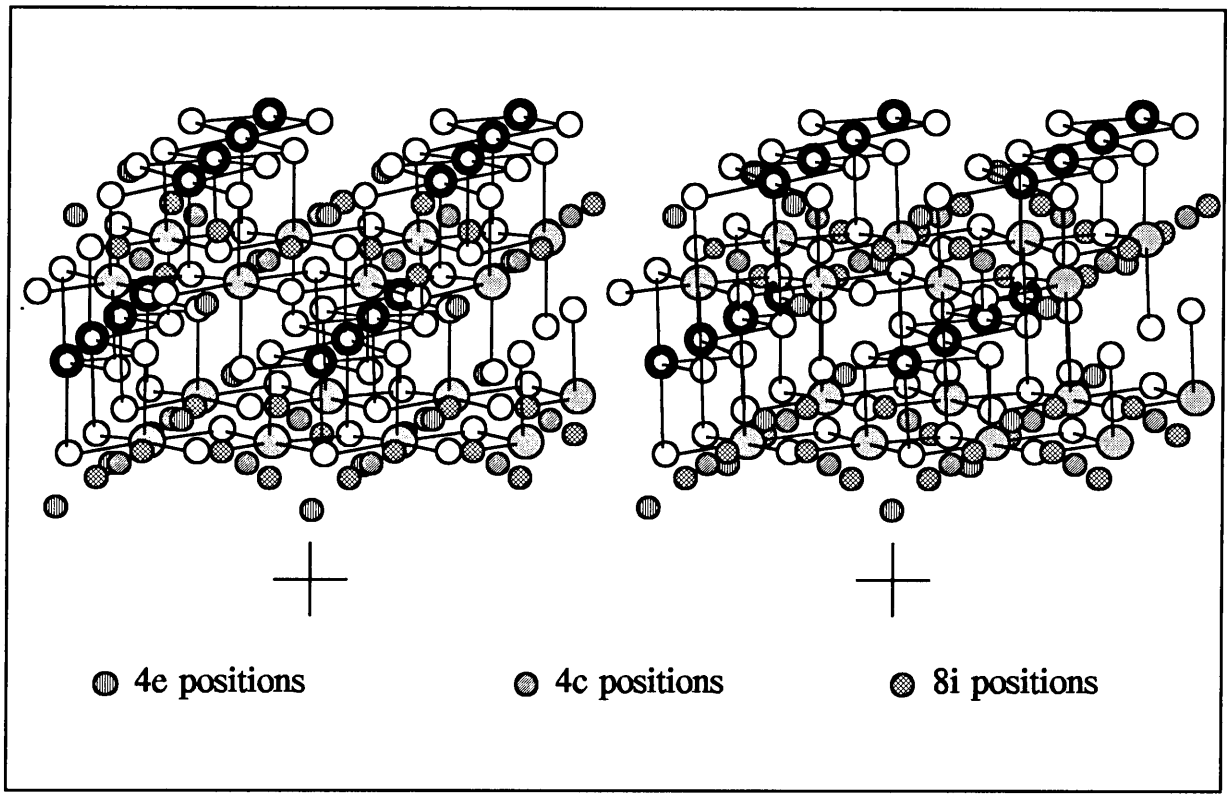

Figure 5.4: Representation of the cobalt spinel, with the 4c, 4e and 8i positions indicated.

only half are occupied by the lithium in the supposed tetrahedral positions (although this lithium is in fact much nearer to octahedral positions than tetrahedral ones, the lithium is still referred to as tetrahedral lithium to distinguish it from the true octahedral lithium). As will be discussed further in Chapters 6, 7, 8 and 9, only one of these positions in each interstitial octahedron is occupied. The result is that the tetrahedron, containing the true tetrahedral position, is completely empty.

The structure of Li_2CrCl_4

The $LiCr_2Cl_4$ spinel crystallises in a space group of even lower symmetry than the other two spinels. It crystallises in the monoclinic space group C2/c (C_{2h}^6). The unit-cell data, as reported by Kanno, Takeda and co-workers [32] may be seen in Table 5.3. As may be seen in the table, the perturbation from the Imma space group is not much, and should not have too great an effect on the spectra.

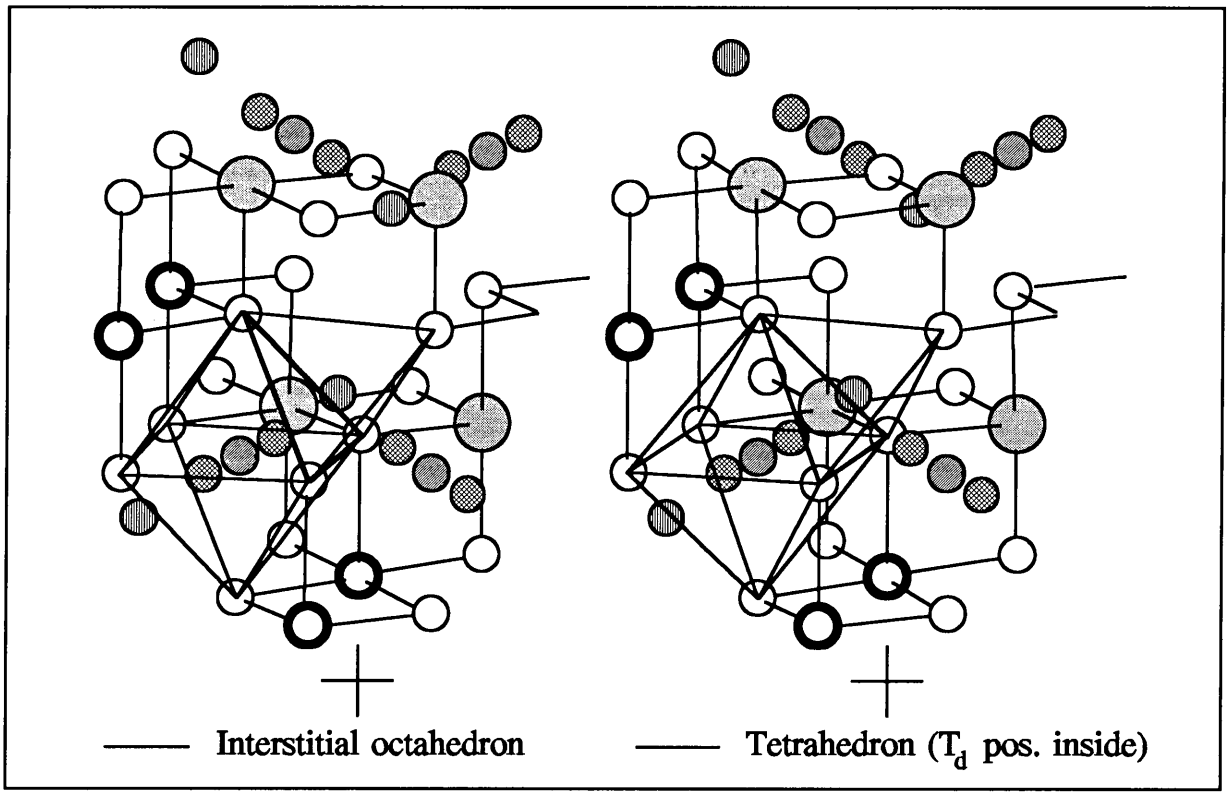

Figure 5.5: Unit-cell of the cobalt spinel, with the interstitial octahedron, tetrahedron, 4c, 4e and 8i positions indicated.

Comparison of the data reported by Kanno, Takeda and co-workers, with information for the C2/c space group, taken from the Tables for Crystallography [8], reveals a startling fact. They seemed to have made an error in reporting the sites occupied by the different types of atoms in the chromium spinel, because the reported positions for atoms in the special positions (Li(1), Li(2) and Cr) do not fit the positions of the sites reported by the Tables for Crystallography. All the special positions, from the Tables for Crystallography, are repeated in Table 5.4, for

Space group			C2/c	C_{2h}^6	
Lattice constants /Å			**a**	**b**	**c**
			7.565(4)	7.443(4)	10.179(8)
angles /°					**γ**
					94.76(6)
Atom	**Site**	**Occup.**	**a**	**b**	**c**
Li (1)	4e	1	0.25	0	-0.188(23)
Li (2)	4b	1	0	0	0.5
Cr	4d	1	0.5	0.25	0.25
Cl (1)	8f	1	-0.002(2)	-0.008(1)	0.258(4)
Cl (2)	8f	1	0.002(6)	0.746(6)	-0.007(1)

Table 5.3: Space group information for Li_2CrCl_4 (The esd's in parentheses refer to the last significant digits).

comparison. If this table is inspected it will be clear that none of the special positions, reported by the Tables for Crystallography, fit the positions reported by Kanno, Takeda and co-workers (except perhaps for their reported 4b site which may be substituted by the 4a site ?). The alternate setting for the same unit-cell (with a unique c axis) B2/b, does not fit any of the positions either.

It is very difficult to overcome this error, as it may be due to a number of reasons. A simple exchange of columns (e.g. the x and y positions), in the publication may be the cause (only some, and not all, all of the positions may have been switched however). The amount of combinations to be tried is large and was not attempted any further after a few trails. The rest of the publication's structure description is still very useful, and is discussed in the rest of this section.

Site	Equivalent positions for the site			
4e	0, y, ¼	0, $\bar{y}$, ¾	½, ½ + y, ¼	½, ½ - y, ¾
4d	¼, ¼, ½	¾, ¼, 0	¾, ¾, ½	¼, ¾, 0
4c	¼, ¼, 0	¾, ¼, ½	¾, ¾, 0	¼, ¾, ½
4b	0, ½, 0	0, ½, ½	½, 0, 0	½, 0, ½
4a	0, 0, 0	0, 0, ½	½, ½, 0	½, ½, ½

Table 5.4: The special positions for the space group C2/c, taken from the Tables for Crystallography.

According to Kanno, Takeda and co-workers, the reason for the perturbation from the Imma space group to the C2/c space group, may be explained by a strong cooperative Jahn-Teller effect of the d^4 state of the Cr^{II} cation. The distortion occurs along one of the axes of the $CrCl_6$-octahedron. The particular axis is the one in the ab-plane in the ab-direction. All the corresponding axes in the $CrCl_6$-chain, elongate slightly to twist the octahedra and distort the shape. This may be seen in Figure 5.6. This representation was taken from the publication of Kanno, Takeda and co-workers [32]. Note the schematic nature of the figure, and the fact that the c-axis extends out of the page. The perturbation is also exaggerated to indicate the trend. Note the alignment of the long axes of the distorted $CrCl_6$-octahedra. This disturbance also causes the $LiCl_6$-octahedra to be distorted.

As is said before, the perturbation is not very big and the general structure follows that of the cobalt and iron spinels. The chromium and the lithium in the octahedral positions form

a 1:1 ordering along the a- and b-axes respectively. The cubic lattice of chloride anions is somewhat distorted.

An interesting feature arises in the position of the lithium atoms in the tetrahedral positions. Kanno, Takeda and co-workers did not refine the position of these lithium atoms exactly, because of too many parameters for the refinement calculations (they used a Rietveld analysis of powder patterns), and the lithium may actually be in the same position (between the tetrahedral positions (used in the refinement) and the interstitial octahedral positions) as in the case of the cobalt and iron spinels. A comparison of the spectra of the chromium spinels to the spectra of the other spinels, may resolve this question.

For the same reason Kanno, Takeda and co-workers did not take into account possible mixing between the two different octahedral sites. It is doubtful however, whether this mixing may be detected in the infrared spectra, especially if it is as small as is the case with the cobalt and iron spinels. A complete and unambiguous assignment would be necessary before any discussion on the mixing of sites, by examination of the spectra, could be attempted.

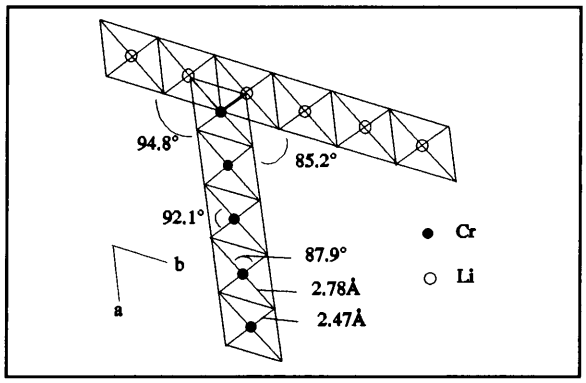

Figure 5.6: Schematic representation of the chromium spinel.

Chapter 6

Factor group correlations

In this chapter the correlation method, developed by Fateley, Dollish and co-workers [5], is used to obtain the total number and nature of the vibrational modes present in the iron and cobalt spinels. The feasibility of a line group analyses is discussed. The difficulties posed by the disorder in the arrangement of the lithium in the tetrahedral positions, are considered.

Space group information

In order to apply the correlation method suggested by Fateley, Dollish and co-workers, the information presented in Table 6.1, is needed. Some simplification of this data is necessary in order to carry out the correlation.

First, the same as in Chapter 5 (because the correlation method cannot deal with mixing between sites), the 4b site is taken as completely filled by the octahedral lithium, and the 4d site is taken as completely filled by the octahedral transition metal.

Another feature of the occupancy is the fact that only half of the 8i positions are filled by the lithium in the tetrahedral positions. This complication is dealt with in a subsequent section and only the correlation of the atoms in the octahedral positions, as well as the chlorine lattice, is given in the next section.

Imma(74)	D_{2h}^{28}	$Z^B = 2$
Atom	Wyckoff position	Occupancy (esd)
Li(1) T_d	8i	0.5
Li(2) O_h	4b	0.826(17)
Li(2) O_h	4b	0.880(13)
Co(1) O_h	4b	0.174
Fe(1) O_h	4b	0.120
Li(3) O_h	4d	0.174
Li(3) O_h	4d	0.120
Co(2) O_h	4d	0.826(17)
Fe(2) O_h	4d	0.880(13)
Cl(1)	8h	1
Cl(2)	8i	1

Table 6.1: Space group information for the cobalt and iron spinels. The shaded areas indicate the iron spinel.

Correlations of the chlorine lattice, and the atoms in the octahedral positions

Keeping the two conditions, mentioned in the precious section, in mind, a correlation can now be carried out. It is also obvious from the Table 6.1 and from the Chapter 5, that the iron and cobalt spinels are highly similar and the correlation obtained, apply to both spinels equally well. The difference will only be noticeable in the spectra, if at all.

		Site group	$C_2(y)$	Factor group						
f^y	T^y	C_{2h}	⟶	D_{2h}	C_ξ	a_ξ	=	a_{Bu}	+	a_{Au}
4	2 (T_x, T_y)	B_u		A_g	1					
2	1 (T_z)	A_u		B_{1g}	1					
				B_{2g}	1					
				B_{3g}	1					
				A_u	1	1				1
				B_{1u}	1	2		2		
				B_{2u}	1	1				1
				B_{3u}	1	2		2		
$\Gamma_{Co} = A_u + 2\,B_{1u} + B_{2u} + 2\,B_{3u}$										

Table 6.2: Correlation for the cobalt/iron in the octahedral positions (4d: C_{2h}), n = 2.

		Site group	$C_2(x)$	Factor group						
f	T^y	C_{2h}	⟶	D_{2h}	C_ξ	a_ξ	=	a_{Bu}	+	a_{Au}
4	2 (T_x, T_y)	B_u		A_g	1					
2	1 (T_z)	A_u		B_{1g}	1					
				B_{2g}	1					
				B_{3g}	1					
				A_u	1	1				1
				B_{1u}	1	2		2		
				B_{2u}	1	2		2		
				B_{3u}	1	1				1

$\Gamma_{Li} = A_u + 2\,B_{1u} + 2\,B_{2u} + B_{3u}$

Table 6.3: Correlation for the lithium in the octahedral positions (4b: C_{2h}), n = 2.

		Site group	σ_{yz}	Factor group						
f	T^y	C_s	⟶	D_{2h}	C_ξ	a_ξ	=	$a_{A'}$	+	$a_{A''}$
8	2 (T_x, T_y)	A'		A_g	1	2		2		
4	1 (T_z)	A''		B_{1g}	1	1				1
				B_{2g}	1	1				1
				B_{3g}	1	2		2		
				A_u	1	1				1
				B_{1u}	1	2		2		
				B_{2u}	1	2		2		
				B_{3u}	1	1				1

$\Gamma_{Cl(1)} = 2\,A_g + B_{1g} + B_{2g} + 2\,B_{3g} + A_u + 2\,B_{1u} + 2\,B_{2u} + B_{3u}$

Table 6.4: Correlation for the chlorine (1) (8h: C_s), n = 4.

The correlation of the transition metal in the octahedral positions, may be seen in Table 6.2. Note that the correct correlation from C_{2h} site group, to the D_{2h} factor group, for the 4d positions, is found in Fateley, Dollish and co-workers in Chapter 2. In this correlation, the axis of correlation is $C_2(y)$. This correlation axis may also be deduced from a study of the unit-cell. All the specific correlations needed to carry out the factor group correlations presented in this chapter, is obtained in the way described by Fateley, Dollish and co-workers, and need not be discussed in detail.

		Site group	σ_{xz}	Factor group						
f	T	C_s	→	D_{2h}	C_ξ	a_ξ	=	$a_{A'}$	+	$a_{A''}$
8	2 (T_x, T_y)	A'		A_g	1	2		2		
4	1 (T_z)	A''		B_{1g}	1	1				1
				B_{2g}	1	2		2		
				B_{3g}	1	1				1
				A_u	1	1				1
				B_{1u}	1	2		2		
				B_{2u}	1	1				1
				B_{3u}	1	2		2		

$\Gamma_{Co} = 2\,A_g + B_{1g} + 2\,B_{2g} + B_{3g} + A_u + 2\,B_{1u} + B_{2u} + 2\,B_{3u}$

Table 6.5: Correlation for the chlorine (2) (8i: C_s), n = 4.

The correlation for the lithium in the octahedral positions, is similar to that of the transition metal and may be seen in Table 6.3. Note that the correct correlation from the site group to the factor group, is $C_2(x)$ in this case.

Similarly, correlations for the chlorine atoms in the two different positions (8h, 8i) may be carried out and are seen in Table 6.4 and Table 6.5 respectively. Again note that the correct correlations from the site group to the factor group, are σ_{yz} and σ_{xz} respectively. A summary of all the correlations carried out in this section, is given in a later section in this chapter.

		Site group	σ_{xz}	Factor group						
f	T	C_s	⟶	D_{2h}	C_ξ	a_ξ	=	$a_{A'}$	+	$a_{A''}$
8	2 (T_x, T_y)	A'		A_g	1	2		2		
4	1 (T_z)	A''		B_{1g}	1	1				1
				B_{2g}	1	2		2		
				B_{3g}	1	1				1
				A_u	1	1				1
				B_{1u}	1	2		2		
				B_{2u}	1	1				1
				B_{3u}	1	2		2		

$\Gamma_{Li,\,8i} = 2\,A_g + B_{1g} + 2\,B_{2g} + B_{3g} + A_u + 2\,B_{1u} + B_{2u} + 2\,B_{3u}$

Table 6.6: Correlation for the lithium in the 8i (C_s) site, taken as being completely filled, n = 4.

Correlation of the lithium in the tetrahedral positions

As indicated in Table 6.1, the lithium, in what should be the tetrahedral positions, occupies only half of the 8i sites. This makes correlation difficult and sheds some doubt on the results, as the method was developed for filled sites only (a correlation with the 8i sites filled, yields twice as many modes as expected).

As indicated in the Chapter 5, the 8i site lies between the proper tetrahedral 4e, and the interstitial, octahedral 4c sites. A correlation for each of these three sites is given in Table 6.6, Table 6.7 and Table 6.8 respectively. A summary of this three correlations may be found in Table 6.9.

f	T^y	Site group C_{2v}	$C_2(z)$ →	Factor group D_{2h}	C_ξ	a_ξ	=	a_{B1}	+	a_{B2}	+	a_{A1}
2	1 (T_x)	B_1		A_g	1	1						1
2	1 (T_y)	B_2		B_{1g}	1							
2	1 (T_z)	A_1		B_{2g}	1	1		1				
				B_{3g}	1	1				1		
				A_u	1							
				B_{1u}	1	1						1
				B_{2u}	1	1				1		
				B_{3u}	1	1		1				

$\Gamma_{Li,\,4e} = A_g + B_{2g} + B_{3g} + B_{1u} + B_{2u} + B_{3u}$

Table 6.7: Correlation for the tetrahedral lithium (4e: C_{2v}), n = 2.

f	T^y	Site group C_{2h}	$C_2(y)$ →	Factor group D_{2h}	C_ξ	a_ξ	=	a_{Bu}	+	a_{Au}
4	2 (T_x, T_y)	B_u		A_g	1					
2	1 (T_z)	A_u		B_{1g}	1					
				B_{2g}	1					
				B_{3g}	1					
				A_u	1	1				1
				B_{1u}	1	2		2		
				B_{2u}	1	1				1
				B_{3u}	1	2		2		

$\Gamma_{Li,\,4c} = A_u + 2\,B_{1u} + B_{2u} + 2\,B_{3u}$

Table 6.8: Correlation for the tetrahedral lithium (4c: C_{2h}), n = 2.

Site of the lithium	Type of position	Vibrational modes							
4e	T_d	A_g		B_{2g}	B_{3g}		B_{1u}	B_{2u}	B_{3u}
8i	in between	$2\ A_g$	B_{1g}	$2\ B_{2g}$	B_{3g}	A_u	$2\ B_{1u}$	B_{2u}	$2\ B_{3u}$
4c	Interstitial O_h					A_u	$2\ B_{1u}$	B_{2u}	$2\ B_{3u}$

Table 6.9: Summary of the correlations of the tetrahedral lithium.

The question that remains to be answered is what correlation describes the actual vibrations of the lithium atoms the best. It is unlikely that both 8i positions in the same interstitial octahedron (as indicated in the previous chapter) are occupied at the same time. A far more reasonable assumption, is that the lithium is distributed singly in each interstitial octahedron, with a 4e site at its middle, and that one of the two 8i sites in each octahedron is occupied at random. As the two 8i positions are in very close contact (there is virtually no potential barrier for movement from the one position to the other) it may be expected that the lithium switches position very rapidly, and that this switch between the two 8i positions in each interstitial octahedron will be difficult to contain and should take place even at very low temperatures. In addition, the interstitial octahedra are connected to each other in chains, sharing an edge (see Chapter 5), and are therefore very closely associated, so that lithium may move between these interstitial octahedra without much difficulty, resulting in a high ionic conductivity, but the average position would be one lithium atom in each interstitial octahedron, to maintain a charge balance. If the lithium switches position between the 8i positions very rapidly, the lithium could perhaps be taken as occupying the 4c position on average, which is exactly in the centre of the two 8i positions in every interstitial octahedron. It is therefore assumed that the vibration of the lithium will resemble that of an imaginary lithium atom occupying the 4c site. This assumption will be discussed further in Chapter 9.

Summary of the correlations

A summary of all the correlations carried out in this chapter may be seen in Table 6.10. Summations with, and without, the tetrahedral lithium are given. The total without this lithium (Total II) is used in subsequent chapters and is therefore provided.

Atom type	Site	Vibrational modes								Total number of modes
Co/Fe: O_h	4d					A_u	$2B_{1u}$	B_{2u}	$2B_{3u}$	6
Li: O_h	4b					A_u	$2B_{1u}$	$2B_{2u}$	B_{3u}	6
Cl (1)	8h	$2A_g$	B_{1g}	B_{2g}	$2B_{3g}$	A_u	$2B_{1u}$	$2B_{2u}$	B_{3u}	12
Cl(2)	8i	$2A_g$	B_{1g}	$2B_{2g}$	B_{3g}	A_u	$2B_{1u}$	B_{2u}	$2B_{3u}$	12
Li: T_d (Interst. O_h)	4c					A_u	$2B_{1u}$	B_{2u}	$2B_{3u}$	6
Total I (with Li: T_d)		$4A_g$	$2B_{1g}$	$3B_{2g}$	$3B_{3g}$	$5A_u$	$10B_{1u}$	$7B_{2u}$	$8B_{3u}$	42
Total II (without Li: T_d)		$4A_g$	$2B_{1g}$	$3B_{2g}$	$3B_{3g}$	$4A_u$	$8B_{1u}$	$6B_{2u}$	$6B_{3u}$	36
Acoustical modes							B_{1u}	B_{2u}	B_{3u}	3
Librational modes			B_{1g}	B_{2g}	B_{3g}					3
Total I - Ac. modes		$4A_g$	$2B_{1g}$	$3B_{2g}$	$3B_{3g}$	$5A_u$	$9B_{1u}$	$6B_{2u}$	$7B_{3u}$	39
Total II - Ac. modes		$4A_g$	$2B_{1g}$	$3B_{2g}$	$3B_{3g}$	$4A_u$	$7B_{1u}$	$5B_{2u}$	$5B_{3u}$	33
Spectral activity		R	R	R	R	N/A	IR	IR	IR	

Table 6.10: Summary of the correlations carried out in this chapter.

Only the acoustic, and not the librational, modes are subtracted from the totals. Because there are no discrete molecular units, or chains, present, there can be no true librational modes in the crystal.

Although the results of the vibrational analysis will be discussed much more thoroughly in Chapters 8 and 9, a few observations become obvious immediately.

First, the metals in the octahedral positions, and probably the lithium in the tetrahedral positions as well, only takespart in *ungerade* vibrations. As only the *gerade* vibrations are Raman active, the metals will not take part in any vibrations visible in the Raman spectra. Because there is a centre of inversion present in the space group, there should be no non-accidental coincidences of modes between the infrared and Raman spectra, as indicated in the table. There are a lot more infrared active modes, than Raman active modes, and the infrared spectra should therefore be much more complex.

Secondly, it is expected that the octahedral lithium and the octahedral transition metal should display the same type of modes, because their arrangement is similar and only differs in the

axis of their respective alignment. Although this is not directly apparent from the correlation, it will become clear in Chapter 8. The same argument can be applied to the two symmetrically different types of chlorine atoms.

Lastly, it must be pointed out that a mere correlation does not yield a great deal of information. A mere summation of the number of modes present, in no way aids the interpretation of the actual spectra. In the next two chapters different approaches will be used to obtain more information about the actual vibrations. The correlation is not totally without value however, as it provides a convenient reference against which all other results may be checked. Although the correlation contains no information about the nature of the modes, or the size of the splitting of the modes, it does pinpoint the number and type of modes present in the crystal, exactly.

Line group analysis

Whenever there are distinct chains present in a crystal, stretching over several unit-cells, the correlation of the internal modes of this chain becomes impossible with the normal correlation method. This chains may be anything from polymers to inorganic units linked by covalent type of bonds. The problem with the normal correlation method is that it uses the crystallographic site of the centre of gravity of a molecular unit, or atom, within the unit-cell, to correlate the internal modes of the unit to the factor group of the crystal. A chain contains only a line (which may be only a few unit cells long, or indefinite in length) of gravity and the normal method fails. Fortunately a method was presented and developed by various authors (see Winston and Halford [60], Tobin [52] and Tobin [53]), employing the theory of line groups. Fateley, Dollish and co-workers also treats two examples with this method in their book.

In this method it is necessary to define a linear chain, as well as its axis of gravity, within the unit-cell. A unit-cell may contain more than one such chains, in which case each should be dealt with separately. It is also necessary to note all the symmetry elements of the space group passing through, or contained, in each chain. In order to apply the method of line groups to the crystals studied in this text, it is necessary to make two assumptions. As this

method is only used to support and clarify other methods and the results are only used with the necessary caution, these assumptions are not very critical.

First, it is assumed that the MCl_6–chains are discrete units, and not interconnected. This is definitely not the case and the results should therefore be treated with extreme caution. Under this assumption, the unit-cell contains two types of chain; the chain obtained by the repetition of the $CoCl_6$– (or $FeCl_6$–) octahedra along the a–axis, and the chain obtained by the repetition of the $LiCl_6$ octahedra along the b–axis. The line group analysis is now carried out for both chains independently.

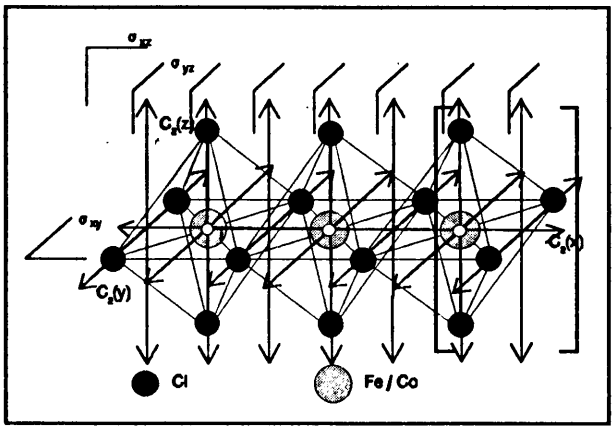

Figure 6.1: Chain of MCl_6–octahedra (M = Fe or Co), aligned along the a–axis.

Secondly, the lithium in the tetrahedral positions is considered to be bonded very weakly to the chlorine atoms connected to the two chains, and does not interfere with chain vibrations. These lithium atoms are therefore ignored. This assumption seems reasonable.

Atom type	Site symmetry	Correlation to D_{2h}
Cl (1)	C_{2v}	$C_2(y)$
Cl (2)	C_{2v}	$C_2(z)$
M (Fe, Co)	D_{2h}	—

Table 6.11: Sites of the different types of atoms and their correlation to the line group.

The chain built up of the MCl_6–octahedra (M = Fe or Co) is illustrated in Figure 6.1. All the symmetry elements present in the chain, as a separate unit, are shown in the figure. Inspection of the chain reveals a unit that builds the chain by mere translation along the chain axis. This unit is indicated in brackets in Figure 6.1. Inspection of Figure 6.1 reveals 8 different symmetry elements contained in this brackets viz. E, $C_2(x)$, $C_2(y)$, $C_2(z)$, i, σ_{xy}, σ_{xz}, and σ_{yz}, as well as a translational component along the axis of the chain. These 8 operations, with the translational part of the space group symmetry operations ignored, form a group of order 8, called the line group, and this group is isomorphic to the D_{2h} point group.

		Site group		Factor group								
f^y	T^y	C_{2v}	$C_2(y)$ →	D_{2h}	C_ξ	a_ξ	=	a_{B1}	+	a_{B2}	+	a_{A1}
2	1 (T_x)	B_1		A_g	1	1						1
2	1 (T_y)	B_2		B_{1g}	1	1				1		
2	1 (T_z)	A_1		B_{2g}	1							
				B_{3g}	1	1		1				
				A_u	1							
				B_{1u}	1	1		1				
				B_{2u}	1	1						1
				B_{3u}	1	1				1		

$\Gamma_{Cl\,(1)} = A_g + B_{1g} + B_{3g} + B_{1u} + B_{2u} + B_{3u}$

Table 6.12: Correlation of the site group to the line group for Cl (1), n=2.

		Site group		Factor group								
f^y	T^y	C_{2v}	$C_2(z)$ →	D_{2h}	C_ξ	a_ξ	=	a_{B1}	+	a_{B2}	+	a_{A1}
2	1 (T_x)	B_1		A_g	1	1						1
2	1 (T_y)	B_2		B_{1g}	1							
2	1 (T_z)	A_1		B_{2g}	1	1		1				
				B_{3g}	1	1				1		
				A_u	1							
				B_{1u}	1	1						1
				B_{2u}	1	1				1		
				B_{3u}	1	1		1				

$\Gamma_{Cl\,(2)} = A_g + B_{2g} + B_{3g} + B_{1u} + B_{2u} + B_{3u}$

Table 6.13: Correlation of the site group to the line group for Cl (2), n=2.

Each different type of atom in the line group must be inspected to obtain the symmetry element passing through that particular type of atom. This collection of symmetry elements for each type of atom, is isomorphic to one of the point groups and forms the local or site symmetry of the particular type of atom.

This site group is correlated to the line group, D_{2h} in this case. The different types of atoms are indicated in Figure 6.1, and the site group of each type of atom is given in Table 6.11. In the correlation of the site group to the line group, care must be taken to obtain the correct correlation. In this case the correct correlation is obtained by noting the axis in the line group that aligns with the z-axis of the site group.

The correlation of the site group to the line group for the two different types of chlorine atoms, may be seen in Table 6.12 and Table 6.13 respectively. Note that the site group of the transition metal is the same as the line group and no correlation is necessary. The three degrees of freedom allowed in the site group: $A_u + B_{1u} + B_{2u}$, remains the same in the line group as there is only one atom of the transition metal in the unit. A summary of the correlation of the site group to the line group may be found in Table 6.14. There is only one librational mode possible in the chain and that is around the chain-axis, B_{3g} in this case.

Atom type	Site group	Vibrational modes								Total number of modes
Cl (1)	C_{2v}	A_g	B_{1g}		B_{3g}		B_{1u}	B_{2u}	B_{3u}	6
Cl (2)	C_{2v}	A_g		B_{2g}	B_{3g}		B_{1u}	B_{2u}	B_{3u}	6
Fe/Co	D_{2h}						B_{1u}	B_{2u}	B_{3u}	3
$\Gamma_{\text{vibrational, line group}}$		$2A_g$	B_{1g}	B_{2g}	$2B_{3g}$		$3B_{1u}$	$3B_{2u}$	$3B_{3u}$	15
Spectral activity		R	R	R	R	N/A	IR	IR	IR	

Table 6.14: Summary of the correlations of the site group to the line group for the MCl_6-chain (M = Fe,Co).

The next step is to identify all the elements of the factor group that leave the chain-axis invariant. Inspection of the space group yields the following: E, i, C2(c), $C2_1$(a), $C2_1$(b), σ_{ac}, $\sigma(g)_{ab}$ and $\sigma(dg)_{bc}$. These operations, without the translational part, viz. E, C2(x), C2(y),

C2(z), i, σ_{xy}, σ_{xz} and σ_{yz} are isomorphic to the D_{2h} point group and the site group of the line group of the polymer, is therefore D_{2h}.

At this stage a double correlation is carried out: the line group is correlated to the site group and the site group is correlated to the factor group of the unit-cell, to obtain the actual symmetry of the vibrational modes. In this case all three of the above mentioned groups are the same and the correlation is trivial, as the total number of line group modes need only to multiplied by two, because there are two chains, of each type, passing through the unit-cell. There are no pure librational modes of the chain in the three-dimensional case and the acoustical modes will be subtracted after the summation of the modes of all the chains passing through the unit-cell.

Applying the line group method to the chain build up out of $LiCl_6$-octahedra, is similar to the preceding discussion and is not given. Note that the only difference is that this chain is aligned with the crystallographic b-axis, and all the correlations will therefore be different. As above, there are two chains passing through the unit-cell.

A summary of the results of the line group method may be seen in Table 6.15. These results are discussed in the next section.

Chain	Site group	Vibrational modes								Total number of modes
MCl_6-chains	D_{2h}	$4A_g$	$2B_{1g}$	$2B_{2g}$	$4B_{3g}$		$4B_{1u}$	$4B_{2u}$	$4B_{3u}$	24
$LiCl_6$-chains	D_{2h}	$4A_g$	$2B_{1g}$	$4B_{2g}$	$2B_{3g}$		$4B_{1u}$	$4B_{2u}$	$4B_{3u}$	24
Total: All chains		$8A_g$	$4B_{1g}$	$6B_{2g}$	$6B_{3g}$		$8B_{1u}$	$8B_{2u}$	$8B_{3u}$	48
Acoustic							B_{1u}	B_{2u}	B_{3u}	3
Total:		$8A_g$	$4B_{1g}$	$6B_{2g}$	$6B_{3g}$		$7B_{1u}$	$7B_{2u}$	$7B_{3u}$	45
Spectral activity		R	R	R	R	N/A	IR	IR	IR	

Table 6.15: Summary of the line group correlations of iron and cobalt spinels.

Discussion of the line group analysis

Two aspects are immediately apparent from Table 6.15, viz. the difference in the sum of the modes found by the normal correlation and the line group correlation methods; and the absence of the some modes found with the normal correlation method (for instance, there are no A_u modes) from the results of the line group correlation.

The answer to the first problem lies in the fact that the chains of different types (MCl_6– and $LiCl_6$–octahedra) share some common atoms and are therefore not completely independent units. In fact, inspection of the unit-cell reveals that all the chlorine atoms are shared between the two different types of chains, but that the chains of the same type are completely independent of each other.

If the results from the normal correlation is treated in the same way, that is doubling the number of the modes involving chlorine and adding the modes due to the octahedral lithium and transition metal, the two different results may be compared more closely. This may be seen in Table 6.16 where the sum of vibrations found by the line group method is subtracted from the sum found by the normal correlation method (ignoring the tetrahedral lithium). The result is that there are some 'missing modes', apparently missed by the application of the line group method. Interestingly enough, this 'loss of modes' only occurs amongst the *ungerade* modes, while all the *gerade* modes are found. This result sheds some doubt on the feasibility of the application of the line group method to cases where the different chains are in some way interconnected.

Type of correlation	Summ. method	Vibrational modes								Total number of modes
Normal cor.	2xCl +Li+M	$8A_g$	$4B_{1g}$	$6B_{2g}$	$6B_{3g}$	$6A_u$	$12B_{1u}$	$9B_{2u}$	$9B_{3u}$	60
Line group cor.	Total	$8A_g$	$4B_{1g}$	$6B_{2g}$	$6B_{3g}$		$8B_{1u}$	$8B_{2u}$	$8B_{3u}$	48
Difference						$6A_u$	$4B_{1u}$	$1B_{2u}$	$1B_{3u}$	12

Table 6.16: Comparison of the number of modes found by the normal correlation and the line group methods.

In the next chapters, some different methods will be developed for obtaining the vibrations present in the crystal. The aim of these methods is to obtain the method that yields results that best describes the actual vibrations present in the spinel crystals. The failure of the line group method in this case, just adds to the argument that the line group method should only be applied to chains that are completely independent and strongly bound (preferably by covalent type bonds).

Chapter 7

Stretching-mode analysis on the MCl_6-octahedra in the cobalt and iron spinels

A stretching-mode analysis can be applied to obtain the irreducible representations of the stretching-modes present in a crystal structure. This analysis is carried out in this chapter for the atoms forming the MCl_6-octahedra. Furthermore, applying the symmetry operations of the space group to certain bonds in the structure, graphical representations of the various stretching-modes can be obtained. The method used to obtain these representations, is discussed in detail. The stretching-modes are presented stereographically and are discussed.

The method of Fateley and Dollish and co-workers [5], although extremely useful, has certain severe limitations. The result of the correlation method, applied in Chapter 6, is a mere sum of irreducible representations; in the case of the iron or cobalt spinel:

$\Gamma_{tot} = 4\ A_g^{R} + 2\ B_{1g}^{R} + 3\ B_{2g}^{R} + 3\ B_{3g}^{R} + 4\ A_u^{N/A} + 7\ B_{1u}^{ir,R} + 5\ B_{2u}^{ir,R} + 5\ B_{3u}^{ir,R}$

(Only the chlorine and the metals in the octahedral positions are considered and the librational modes are not subtracted, for reasons discussed later in this chapter). It is obvious that a mere list of all the possible vibrational modes of a crystal (33 in this case) in no way aids the interpretation of the actual spectra, especially if no single crystals for a single crystal study are available. Since Fateley, Dollish and co-workers is the only text available that proceeds some way in dealing with the selection rules for the theoretical interpretation of spectra of the solid state, most authors of vibrational papers stop at a mere correlation (often with the wrong correlations from the site to the factor group), and proceeds with empirical methods, or some form of normal coordinate analysis.

It is therefore intended in this study to discuss a method for obtaining, from first principles, some more information about the vibrations active in the compounds particular to this study. Although this type of method is not new and some examples of the application of similar methods can be found in the literature [26,36,58,62,63] this text presents one of the first clear discussions of the technique.

Space group manipulations

As indicated before (Chapter 5), the space group of both the iron and cobalt spinels is the orthorhombic space group Imma. Space group information, for the Imma space group, may be seen in Table 7.1. Note that the space group is associated with the D_{2h} point group

Imma	No. 74	
I2/m2/m2/a	Orthorhombic:	mmm
D_{2h}^{28}		

Table 7.1: Space group information for the Iron and Cobalt Spinels

The first step of the method is to identify the independent symmetry operations present in the space group. Since there are 16 equivalent positions for any general position (x,y,z), it follows that there must be 16 independent symmetry operations to generate these 16 positions from the general position.

A diagram of the symmetry elements of the space group Imma, may be seen in Figure 7.1. This figure was taken directly from the Tables of Crystallography [8] (the symbolism explained in the Tables of Crystallography is used, and this reference should be consulted if any problem with the symbolism arises). If the origin is taken at the centre (one of two valid positions of the origin), the area indicated by the dotted box in the figure, contains all 16 independent symmetry operations present (in this case there is no symmetry element with more than one operation associated with it and there are therefore 16 symmetry elements as well). A complete list of the 16 independent symmetry operations may be found in Table 7.2. The second identity, at (½,½,½), arises from the fact that the positions (x,y,z) and (x+½, y+½, z+½) are equivalent in the unit-cell. It is possible to obtain a different set of 16 independent symmetry operations for the same space group by choosing, for example, a different origin. It does not matter exactly what set of operations is chosen, as long as the set is complete and the members mutually independent. It is also

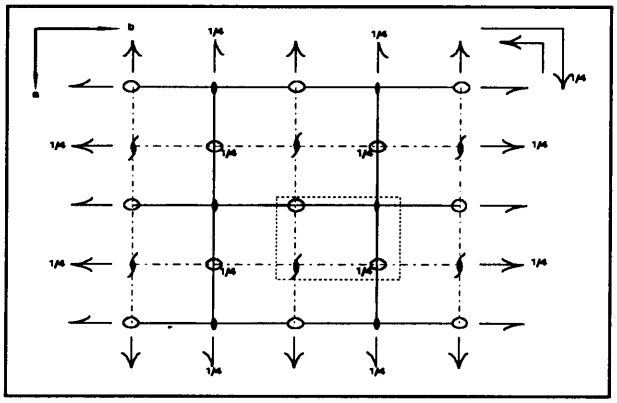

Figure 7.1: Diagram of the symmetry elements of space group Imma

obvious that each set must contain 16 members to generate the 16 equivalent positions for any chosen general position in the unit-cell.

E at (0,0,0)	E at (½,½,½)	i at (0,0,0)	i at (¼,¼,¼)
σ_{bc} at a=0	σ_{ac} at b=¼	$\sigma(dg)_{ac}$ at b=0	$\sigma(dg)_{bc}$ at a=¼
$\sigma(g)_{ab}$ at c=0	$\sigma(g)_{ab}$ at c=¼	C2 ‖ c at a=0, b=¼	C2 ‖ a at b=0, c=0
C2 ‖ b at a=¼, c=¼	$C2_1$ ‖ c a=¼, b=0	$C2_1$ ‖ b a=0, c=0	$C2_1$ ‖ a b=¼, c=¼

Table 7.2: Independent, 16, symmetry operations in the space group Imma

Every symmetry operation in a space group can be broken down into two components, viz. a pure symmetrical component, and a pure translational component (incorporating both the position of the symmetry element in the unit-cell and the translational component of glide-planes and screw-axes). The symmetrical parts of the space group operations form a group called the factor group of the space group, which in turn is associated with one of the point groups. It is therefore necessary to obtain a matrix (that incorporates the purely symmetrical part of the operation) and a vector (that incorporates the purely positional and translational part of the operation) for each of the 16 independent symmetry operations of the space group.

$$\begin{bmatrix} x' \\ y' \\ z' \end{bmatrix} = \begin{bmatrix} a_{11} & a_{12} & a_{13} \\ a_{21} & a_{22} & a_{23} \\ a_{31} & a_{32} & a_{33} \end{bmatrix} \begin{bmatrix} x \\ y \\ z \end{bmatrix} + \begin{bmatrix} t_1 \\ t_2 \\ t_3 \end{bmatrix} \qquad \text{....(7.1)}$$

$$\begin{bmatrix} x'' \\ y'' \\ z'' \end{bmatrix} = \begin{bmatrix} x' \\ y' \\ z' \end{bmatrix} + \begin{bmatrix} u_1 \\ u_2 \\ u_3 \end{bmatrix}$$

This is done by considering the effect of applying each operation to the general position (x,y,z) in the space group. The result can be seen in Eq. ....(7.1). When symmetry matrix (a_{ij}) and translational vector (t_i) are applied to a general position (x,y,z), the same position (x,y,z) or an equivalent position (x',y',z') must be obtained. In order to facilitate the representation, an additional vector (u_i) is added to insure that the equivalent position is the one within the current unit-cell (it is obvious that $u_i = \pm 1$, for only unit translations are allowed when working with equivalent positions in different unit-cells). There must

E at (0,0,0)	E at (1/2,1/2,1/2)	i at (0,0,0)	i at (1/4,1/4,1/4)
$\begin{bmatrix}1&0&0\\0&1&0\\0&0&1\end{bmatrix}+\begin{bmatrix}0\\0\\0\end{bmatrix}$	$\begin{bmatrix}1&0&0\\0&1&0\\0&0&1\end{bmatrix}+\begin{bmatrix}1/2\\1/2\\1/2\end{bmatrix}$	$\begin{bmatrix}-1&0&0\\0&-1&0\\0&0&-1\end{bmatrix}+\begin{bmatrix}0\\0\\0\end{bmatrix}$	$\begin{bmatrix}-1&0&0\\0&-1&0\\0&0&-1\end{bmatrix}+\begin{bmatrix}1/2\\1/2\\1/2\end{bmatrix}$
σ_{bc} at a=0	σ_{ac} at b=1/4	$\sigma(dg)_{ac}$ at b=0	$\sigma(dg)_{bc}$ a=1/4
$\begin{bmatrix}-1&0&0\\0&1&0\\0&0&1\end{bmatrix}+\begin{bmatrix}0\\0\\0\end{bmatrix}$	$\begin{bmatrix}1&0&0\\0&-1&0\\0&0&1\end{bmatrix}+\begin{bmatrix}0\\1/2\\0\end{bmatrix}$	$\begin{bmatrix}1&0&0\\0&-1&0\\0&0&1\end{bmatrix}+\begin{bmatrix}1/2\\0\\1/2\end{bmatrix}$	$\begin{bmatrix}-1&0&0\\0&1&0\\0&0&1\end{bmatrix}+\begin{bmatrix}1/2\\1/2\\1/2\end{bmatrix}$
$\sigma(g)_{ab}$ at c=0	$\sigma(g)_{ab}$ at c=1/4	$C_2 \parallel c$ at a=0,b=1/4	$C_2 \parallel a$ at b=0,c=0
$\begin{bmatrix}1&0&0\\0&1&0\\0&0&-1\end{bmatrix}+\begin{bmatrix}0\\1/2\\0\end{bmatrix}$	$\begin{bmatrix}1&0&0\\0&1&0\\0&0&-1\end{bmatrix}+\begin{bmatrix}1/2\\0\\1/2\end{bmatrix}$	$\begin{bmatrix}-1&0&0\\0&-1&0\\0&0&1\end{bmatrix}+\begin{bmatrix}0\\1/2\\0\end{bmatrix}$	$\begin{bmatrix}1&0&0\\0&-1&0\\0&0&-1\end{bmatrix}+\begin{bmatrix}0\\0\\0\end{bmatrix}$
$C_2 \parallel b$ at a=1/4,c=1/4	$C_{2_1} \parallel c$ at a=1/4,b=0	$C_{2_1} \parallel b$ at a=0,c=0	$C_{2_1} \parallel a$ at b=1/4,c=1/4
$\begin{bmatrix}-1&0&0\\0&1&0\\0&0&-1\end{bmatrix}+\begin{bmatrix}1/2\\0\\1/2\end{bmatrix}$	$\begin{bmatrix}-1&0&0\\0&-1&0\\0&0&1\end{bmatrix}+\begin{bmatrix}1/2\\0\\1/2\end{bmatrix}$	$\begin{bmatrix}-1&0&0\\0&1&0\\0&0&-1\end{bmatrix}+\begin{bmatrix}0\\1/2\\0\end{bmatrix}$	$\begin{bmatrix}1&0&0\\0&-1&0\\0&0&-1\end{bmatrix}+\begin{bmatrix}1/2\\1/2\\1/2\end{bmatrix}$

Table 7.3: Table of symmetry matrixes and translational vectors for each of the 16 independent symmetry operations of the space group Imma

accordingly be 16 such sets of a symmetry matrix and a translational vector (as well as a unit-translational vector) for the space group Imma. These sets may be seen in Table 7.3.

Equivalent sets of bonds

A first approximation, stretching-mode analysis may now be carried out using the following three assumptions:

First, the MCl_6 -octahedra are much more strongly defined than the MCl_4-tetrahedra. The validity of this assumption was discussed in Chapter 5 and will be discussed further in Chapters 8 and 9. At first, only the MCl_6-octahedra are considered. By subtracting the obtained modes from the modes obtained by the correlation method of the previous chapter, it should be possible to obtain the MCl_4- tetrahedral modes.

Secondly, as the chapter heading indicates, a stretching-mode analysis is carried out. However, as will become clear later in this chapter, most of the stretching-modes has some bending character as well, and a stretching-mode analysis will, in this case, identify most of

the bending modes. A simple subtraction of the pure stretching, and stretch-bending modes from the total number of modes obtained from a correlation, will indicate the pure bending modes present.

Thirdly, only symmetrical equivalent bonds are considered to interact. Thus sets of equivalent bonds transform independently under the symmetry operations of the space group. As is pointed out later in this chapter, this is a gross simplification, since there is almost certainly a large amount of interaction between symmetry modes belonging to the same irreducible representation, of the different equivalent sets. These interactions can, however, be deduced from the independent vibrational modes constructed for the different equivalent sets, and this approximation is therefore a valid one.

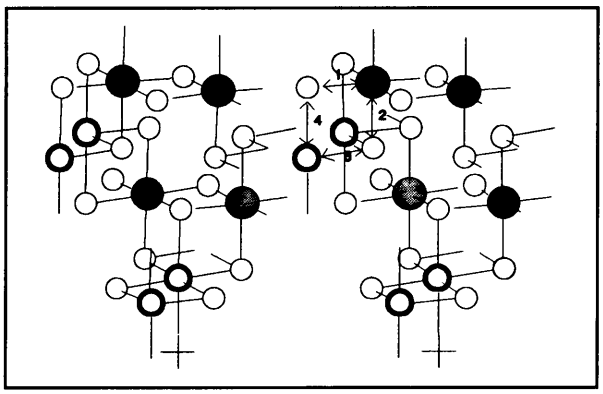

Figure 7.2: Unit-cell of the cobalt or iron spinel. The bond marked 1 represents an arbitrarily chosen bond.

Keeping these three simplifications in mind, it is now possible to identify the equivalent sets of bonds present in the unit-cell. The unit-cell of the low temperature modification of the iron and cobalt spinels may be seen in Figure 7.2. An arbitrary bond is selected (bond 1) to generate an equivalent set of bonds, set I. This is accomplished by applying each of the 16 independent symmetry operations of the space group to the bond. The easiest way of effecting this, is to construct a spreadsheet, using any commercial spreadsheet application. The results presented in this text was generated using Lotus123 [70].

Li (O_h)					
0.000	0.000	0.500	0.000	0.500	0.500
0.500	0.500	0.000	0.500	0.000	0.000
Cr (O_h)					
0.250	0.250	0.750	0.750	0.250	0.750
0.750	0.750	0.250	0.250	0.750	0.250
Cl (1)					
0.000	0.989	0.244	0.000	0.011	0.756
0.000	0.489	0.756	0.000	0.511	0.244
0.500	0.489	0.744	0.500	0.511	0.256
0.500	0.989	0.256	0.500	0.011	0.744
Cl (2)					
0.246	0.250	-0.009	0.754	0.750	0.009
0.754	0.250	-0.009	0.246	0.750	0.009
0.746	0.750	0.491	0.254	0.250	0.509
0.254	0.750	0.491	0.746	0.250	0.509

Table 7.4: Relative positions of the atoms (tetrahedral lithium excluded) in the cobalt spinel unit-cell

In the subsequent discussion the relative positions of the cobalt spinel is used (because of the similarity of the cobalt and iron spinels' unit-cells, the subsequent results apply equally well to the iron spinel). The relative positions of all the atoms, but the lithium in the tetrahedral positions, are repeated in Table 7.4.

In order to manipulate the bond mathematically, the relative positions of the two atoms, connected by the bond, are used. By applying Eq. ....(7.1) to each of these positions, using the matrix and vector associated with a particular operation, the position of an equivalent pair of atoms is obtained. The bond connecting these equivalent pair of atoms is therefore symmetrically equivalent to the original bond. By carrying out this procedure with each of the 16 independent symmetry operations of the space group, a set of 16 equivalent bonds is obtained, set I. A sample spreadsheet for this kind of calculations may be seen in Spreadsheet 7.1. Although this spreadsheet takes some time to construct, it saves considerable time when applied to subsequent bonds.

Space group:	Imma	D2h(28)	nr.74	Bond 1	Cobalt Spinel
		1st atom 0.250			2nd atom 0.000
		Position 0.250			Position 0.011
		0.750			0.756

Symmetry operation	Matrix	1st atom Position	Without Trans	Trans. vector	Final Position	Unit Trans.	Unit-cell Position	2nd atom Position	Without Trans	Trans. vector	Final Position	Unit Trans.	Unit-cell Position
E at (0,0,0)	1 0 0	0.250	0.250	0	0.250	0	0.250	0.000	0.000	0	0.000	0	0.000
(1)	0 1 0	0.250	0.250	0	0.250	0	0.250	0.011	0.011	0	0.011	0	0.011
	0 0 1	0.750	0.750	0	0.750	0	0.750	0.756	0.756	0	0.756	0	0.756
E at (½1/2,1/2,1/2)	1 0 0	0.250	0.250	0.5	0.750	0	0.750	0.000	0.000	0.5	0.500	0	0.500
(2)	0 1 0	0.250	0.250	0.5	0.750	0	0.750	0.011	0.011	0.5	0.511	0	0.511
	0 0 1	0.750	0.750	0.5	1.250	-1	0.250	0.756	0.756	0.5	1.256	-1	0.256
i at (0,0,0)	-1 0 0	0.250	-0.250	0	-0.250	1	0.750	0.000	0.000	0	0.000	1	1.000
(3)	0 -1 0	0.250	-0.250	0	-0.250	1	0.750	0.011	-0.011	0	-0.011	1	0.989
	0 0 -1	0.750	-0.750	0	-0.750	1	0.250	0.756	-0.756	0	-0.756	1	0.244
i at (1/4,1/4,1/4)	-1 0 0	0.250	-0.250	0.5	0.250	0	0.250	0.000	0.000	0.5	0.500	0	0.500
(4)	0 -1 0	0.250	-0.250	0.5	0.250	0	0.250	0.011	-0.011	0.5	0.489	0	0.489
	0 0 -1	0.750	-0.750	0.5	-0.250	1	0.750	0.756	-0.756	0.5	-0.256	1	0.744
σbc at a=0	-1 0 0	0.250	-0.250	0	-0.250	1	0.750	0.000	0.000	0	0.000	1	1.000
(5)	0 1 0	0.250	0.250	0	0.250	0	0.250	0.011	0.011	0	0.011	0	0.011
	0 0 1	0.750	0.750	0	0.750	0	0.750	0.756	0.756	0	0.756	0	0.756
σac at b=1/4	1 0 0	0.250	0.250	0	0.250	0	0.250	0.000	0.000	0	0.000	0	0.000
(6)	0 -1 0	0.250	-0.250	0.5	0.250	0	0.250	0.011	-0.011	0.5	0.489	0	0.489
	0 0 1	0.750	0.750	0	0.750	0	0.750	0.756	0.756	0	0.756	0	0.756

σ(dg)ac at b=0	1	0	0	0.250	0.250	0.5	0.750	0	0.750	0.000	0.000	0.5	0.500	0	0.500
(7)	0	-1	0	0.250	-0.250	0	-0.250	1	0.750	0.011	-0.011	0	-0.011	1	0.989
	0	0	1	0.750	0.750	0.5	1.250	-1	0.250	0.756	0.756	0.5	1.256	-1	0.256
σ(dg)bc at a=1/4	-1	0	0	0.250	-0.250	0.5	0.250	0	0.250	0.000	0.000	0.5	0.500	0	0.500
(8)	0	1	0	0.250	0.250	0.5	0.750	0	0.750	0.011	0.011	0.5	0.511	0	0.511
	0	0	1	0.750	0.750	0.5	1.250	-1	0.250	0.756	0.756	0.5	1.256	-1	0.256
σ(g)ab at c=0	1	0	0	0.250	0.250	0	0.250	0	0.250	0.000	0.000	0	0.000	0	0.000
(9)	0	1	0	0.250	0.250	0.5	0.750	0	0.750	0.011	0.011	0.5	0.511	0	0.511
	0	0	-1	0.750	-0.750	0	-0.750	1	0.250	0.756	-0.756	0	-0.756	1	0.244
σ(g)ab at c=1/4	1	0	0	0.250	0.250	0.5	0.750	0	0.750	0.000	0.000	0.5	0.500	0	0.500
(10)	0	1	0	0.250	0.250	0	0.250	0	0.250	0.011	0.011	0	0.011	0	0.011
	0	0	-1	0.750	-0.750	0.5	-0.250	1	0.750	0.756	-0.756	0.5	-0.256	1	0.744
C2||c at a=0, b=1/4	-1	0	0	0.250	-0.250	0	-0.250	1	0.750	0.000	0.000	0	0.000	1	1.000
(11)	0	-1	0	0.250	-0.250	0.5	0.250	0	0.250	0.011	-0.011	0.5	0.489	0	0.489
	0	0	1	0.750	0.750	0	0.750	0	0.750	0.756	0.756	0	0.756	0	0.756
C2||a at b=0, c=0	1	0	0	0.250	0.250	0	0.250	0	0.250	0.000	0.000	0	0.000	0	0.000
(12)	0	-1	0	0.250	-0.250	0	-0.250	1	0.750	0.011	-0.011	0	-0.011	1	0.989
	0	0	-1	0.750	-0.750	0	-0.750	1	0.250	0.756	-0.756	0	-0.756	1	0.244
C2||b at a=1/4, c=1/4	-1	0	0	0.250	-0.250	0.5	0.250	0	0.250	0.000	0.000	0.5	0.500	0	0.500
(13)	0	1	0	0.250	0.250	0	0.250	0	0.250	0.011	0.011	0	0.011	0	0.011
	0	0	-1	0.750	-0.750	0.5	-0.250	1	0.750	0.756	-0.756	0.5	-0.256	1	0.744
C21||c at a=1/4, b=0	-1	0	0	0.250	-0.250	0.5	0.250	0	0.250	0.000	0.000	0.5	0.500	0	0.500
(14)	0	-1	0	0.250	-0.250	0	-0.250	1	0.750	0.011	-0.011	0	-0.011	1	0.989
	0	0	1	0.750	0.750	0.5	1.250	-1	0.250	0.756	0.756	0.5	1.256	-1	0.256
C21||b by a=0, c=0	-1	0	0	0.250	-0.250	0	-0.250	1	0.750	0.000	0.000	0	0.000	1	1.000
(15)	0	1	0	0.250	0.250	0.5	0.750	0	0.750	0.011	0.011	0.5	0.511	0	0.511
	0	0	-1	0.750	-0.750	0	-0.750	1	0.250	0.756	-0.756	0	-0.756	1	0.244
C21||a at b=1/4, c=1/4	1	0	0	0.250	0.250	0.5	0.750	0	0.750	0.000	0.000	0.5	0.500	0	0.500
(16)	0	-1	0	0.250	-0.250	0.5	0.250	0	0.250	0.011	-0.011	0.5	0.489	0	0.489
	0	0	-1	0.750	-0.750	0.5	-0.250	1	0.750	0.756	-0.756	0.5	-0.256	1	0.744

Spreadsheet 7.1: The 16 independent operations of the unit-cell applied to the two atoms joining the chosen bond in the cobalt spinel (Bond 1 in the example).

The sixteen bonds thus obtained, form an equivalent set (all are equivalent to bond 1, the arbitrarily selected bond), and may be seen in Figure 7.3. Note that the bonds are numbered according to the number of the matrix and vector listed in Spreadsheet 7.1; thus bond 3 in Figure 7.3 is generated using i at (0,0,0), according to the number in the spreadsheet.

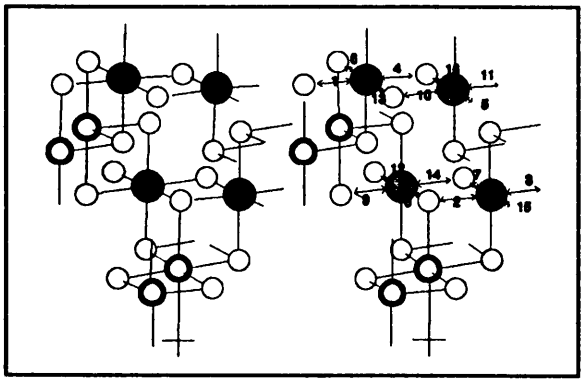

Figure 7.3: The equivalent set, set I, of bonds obtained from bond 1. Numbers indicate position in the spreadsheet

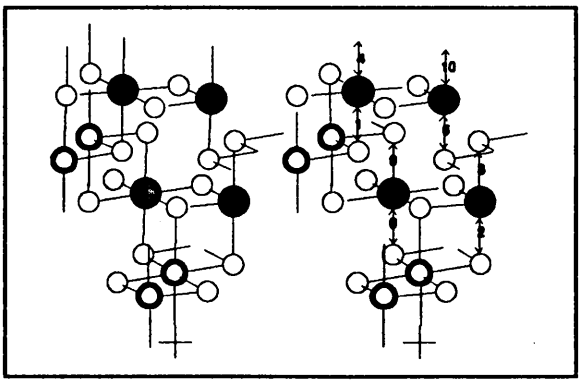

Figure 7.4: The equivalent set, set II, of bonds obtained from bond 2. Numbers indicate position in the spreadsheet.

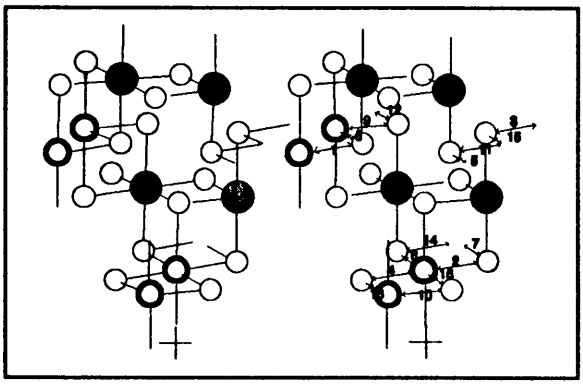

Figure 7.5: The equivalent set, set III, of bonds obtained from bond 3. Numbers indicate position in the spreadsheet.

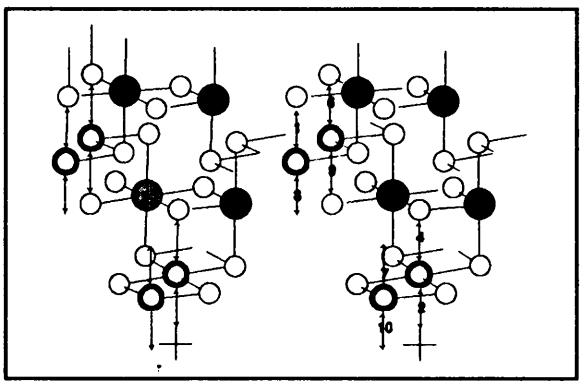

Figure 7.6: The equivalent set, set IV, of bonds obtained from bond 4. Numbers indicate position in the spreadsheet.

By selecting another bond, bond 2 in Figure 7.2, unmarked after all 16 bonds of set I have been identified, and therefore independent from set I, a second set of independent bonds, set II, may be obtained. This process is repeated until all the bonds in the unit-cell, and therefore the crystal, are marked. The first bond of each equivalent set is marked in Figure 7.2. The equivalent sets of bonds, set II, III and IV, generated from bonds 2, 3 and 4 respectively, may be seen in Figure 7.4 to Figure 7.6. Note that in the case of bond 2 and bond 4, there are only 8 equivalent bonds, rather than the 16 equivalent bonds as in the case of bond 1 and bond 3. This is due to the fact that these bonds does not fall in the general position any more, but rather on one of the special positions in the unit-cell. Note also that the numbers labelling each bond, no longer appear sequential in Figure 7.4 and Figure 7.6. This is due to the fact that the numbers indicate the position in the spreadsheet, of the symmetry operation used to generate the particular bond. The number assigned to a bond is therefore the number of the

operation that provides the first unique new position. Bonds are only numbered once, and if the same bond is generated for a second time, the number is omitted.

The method of Adams and Newton

A stretching-mode analysis can now be carried out, using the tables assembled by Adams and Newton [11]. To use the method presented by Adams and Newton, two steps are necessary. First the equivalent sets of bonds must be identified. This was dealt with in the preceding section. Secondly, it is necessary to know the crystallographic sites of the centres of these bonds. This is dealt with in this section.

The centre of each bond can easily be obtained by taking the average of the positions of the two atoms joined by the bond. This information can easily be obtained from the mentioned spreadsheet (Spreadsheet 7.1), by adding the part indicted in Spreadsheet 7.2 anywhere in Spreadsheet 7.1. By comparing the obtained centres of each of the sets of bonds with the positions indicated in the Tables for Crystallography, for the space group Imma, the special position for each set of bonds can be obtained. The position of each set of bonds may be seen in Table 7.6.

With the above information, a stretching-mode analysis, using the tables presented by Adams and Newton may be carried out. Table 3 no. 74 is used.

It should be noted, that Adams and Newton used only the asymmetric unit in assembling their tables. For the body-centred unit-cell Imma,

	1st Atom Position				2nd Atom Position		
1	0.250	0.250	0.750	--------	0.000	0.011	0.756
2	0.750	0.750	0.250	--------	0.500	0.511	0.256
3	0.750	0.750	0.250	--------	1.000	0.989	0.244
4	0.250	0.250	0.750	--------	0.500	0.489	0.744
5	0.750	0.250	0.750	--------	1.000	0.011	0.756
6	0.250	0.250	0.750	--------	0.000	0.489	0.756
7	0.750	0.750	0.250	--------	0.500	0.989	0.256
8	0.250	0.750	0.250	--------	0.500	0.511	0.256
9	0.250	0.750	0.250	--------	0.000	0.511	0.244
10	0.750	0.250	0.750	--------	0.500	0.011	0.744
11	0.750	0.250	0.750	--------	1.000	0.489	0.756
12	0.250	0.750	0.250	--------	0.000	0.989	0.244
13	0.250	0.250	0.750	--------	0.500	0.011	0.744
14	0.250	0.750	0.250	--------	0.500	0.989	0.256
15	0.750	0.750	0.250	--------	1.000	0.511	0.244
16	0.750	0.250	0.750	--------	0.500	0.489	0.744

	Bond centres		
1	0.125	0.131	0.753
2	0.625	0.631	0.253
3	0.875	0.870	0.247
4	0.375	0.370	0.747
5	0.875	0.131	0.753
6	0.125	0.370	0.753
7	0.625	0.870	0.253
8	0.375	0.631	0.253
9	0.125	0.631	0.247
10	0.625	0.131	0.747
11	0.875	0.370	0.753
12	0.125	0.870	0.247
13	0.375	0.131	0.747
14	0.375	0.870	0.253
15	0.875	0.631	0.247
16	0.625	0.370	0.747

Spreadsheet 7.2: Centres of the bonds equivalent to bond 1.

there are two asymmetric units in the unit-cell, and therefore every quantity in the unit cell must be divided by two. In fact, the asymmetric unit could have been used throughout the previous discussion, with the same results. It was found, however, that the whole unit-cell presents a clearer picture of the actual vibrations, and is therefore used. The tables of Adams and Newton yield the stretching-modes of each independent set of bonds in the asymmetric unit, and it is easy to make the mistake of doubling the number of modes obtained, to represent the full unit-cell. A bit of thought will show that the unit-cell is obtained symmetrically from the asymmetric unit (in this case by adding (½,½,½) to each coordinate) and can therefore contain no information not already present in the asymmetric unit. Consequently, doubling the number of modes, gives a false impression of the number of different vibrational modes present in the unit-cell, as each mode is only represented twice (two symmetrically equivalent vibrations). This statement can easily be verified by examination of the unit-cell, and the subsequent discussion indicates that the number of modes obtained with the aid of Adams and Newton's tables, is in fact the only unique modes possible.

By applying the tables of Adams and Newton to each of the four independent sets of bonds present in the Imma unit-cell, the stretching-modes for each of these sets may be obtained. The results of this analysis may be seen in Table 7.7. Note again, that for example set I, containing the 16 bonds equivalent to bond 1, produces only eight independent stretching-mode vibrations, because the unit-cell contains two asymmetric units.

Set of bonds	Wyckoff position
I	16 j
II	8 i
III	16 j
IV	8 i

Table 7.6: Wyckoff positions of the centres of the different sets of bonds in the unit-cell.

In the next section this information is used to obtain the physical vibrational modes in the crystal, under the three assumptions made previously.

Set of Bonds	Wyckoff position	Stretching-modes							
I	16j	A_g	B_{1g}	B_{2g}	B_{3g}	A_u	B_{1u}	B_{2u}	B_{3u}
II	8i	A_g		B_{2g}			B_{1u}		B_{3u}
III	16j	A_g	B_{1g}	B_{2g}	B_{3g}	A_u	B_{1u}	B_{2u}	B_{3u}
IV	8i	A_g			B_{3g}		B_{1u}		B_{3u}

Table 7.7: The stretching-modes obtained for each set of bonds, according to the Table 2 in Adams and Newton.

Representation of the stretching-mode vibrations

The stretching-modes can now be represented graphically, to yield a clear and informative picture of the actual behaviour of the atoms in the crystal during vibration. This is of help during the assignment of the actual spectra, and is also satisfactory intellectually. The determination of the vibrational modes is no longer a routine task performed without any insight into the actual vibrations whatsoever, but a rational visualisation of at least a realistic model of the vibrations possible in a crystal.

The characters of the irreducible representations of the point group corresponding to the factor group of the space group is used. For clarity, the character table for this point group, D_{2h}, is presented in Table 7.8.

D_{2h}	E	$C_2(z)$	$C_2(y)$	$C_2(x)$	i	$\sigma(xy)$	$\sigma(xz)$	$\sigma(yz)$		
A_g	1	1	1	1	1	1	1	1		x^2, y^2, z^2
B_{1g}	1	1	-1	-1	1	1	-1	-1	R_z	xy
B_{2g}	1	-1	1	-1	1	-1	1	-1	R_y	xz
B_{3g}	1	-1	-1	1	1	-1	-1	1	R_x	yz
A_u	1	1	1	1	-1	-1	-1	-1		
B_{1u}	1	1	-1	-1	-1	-1	1	1	z	
B_{2u}	1	-1	1	-1	-1	1	-1	1	y	
B_{3u}	1	-1	-1	1	-1	1	1	-1	x	

Table 7.8: Character table for the point group D_{2h}.

The irreducible representations of the stretching-mode vibrations, found by the method of Adams and Newton, are used to generate the stretching-modes (the modes could also be obtained by applying the irreducible representations of the group, one after the other, to the sets of bonds, and it will be found that some disappear, yielding the same amount of representations as found by the method of Adams and Newton).

To start, arrows are drawn in on every bond of an equivalent set, as if the bonds are all stretching simultaneously. Each bond in the set is generated by a specific space group operation. Each space group operation consists of a purely symmetrical and a translational part (if any), as indicated before. The factor group (obtained if all the translational parts are ignored) corresponds to one of the point groups, D_{2h} in this case. Each space group operation therefore corresponds with one of the operations of the point group. Care should be taken to insure the correct correlation between operations in the space group and in the corresponding point group, by aligning the axes and planes correctly. The correct correlation of the 16 independent space group operations to their respective point group operations, is given in Table 7.9.

For each of the irreducible representations found by the method of Adams and Newton, the characters of that representation in the point group, are applied to the bonds generated by the space group operations corresponding to the operations of the point group. If a character of +1 is applied to a bond, the bond is taken to stretch, and to contract if a character of -1 is applied. Doing this for each bond in the set, yields a picture of the contracting and expanding bonds in a particular vibration, belonging to the irreducible representation which characters are used. Thus if A_g is applied to the set I , all the bonds expand and contract in unison. Three examples of how this method is applied may be seen in Table 7.10.

Space group: Imma	Point group: D_{2h}	Space group: Imma	Point group: D_{2h}
E at (0,0,0)	E	$\sigma(g)_{ab}$ at c=0	σ_{xy}
E at (½,½,½)	E	$\sigma(g)_{ab}$ at c=¼	σ_{xy}
i at (0,0,0)	i	C2 ∥ c at a=0, b=¼	C2(z)
i at (¼,¼,¼)	i	C2 ∥ a at b=0, c=0	C2(x)
σ_{bc} at a=0	σ_{yz}	C2 ∥ b at a=¼, c=¼	C2(y)
σ_{ac} at b=¼	σ_{xz}	$C2_1$ ∥ c at a=¼, b=0	C2(z)
$\sigma(dg)_{ac}$ at b=0	σ_{xz}	$C2_1$ ∥ b at a=0, c=0	C2(y)
$\sigma(dg)_{bc}$ at a=¼	σ_{yz}	$C2_1$ ∥ a at b=¼, c=¼	C2(x)

Table 7.9: Correlation between the space group (Imma) and corresponding point group (D_{2h}).

If A_g is applied to set I, the result is Figure 7.7. Also indicated in Figure 7.7 is the movement of the chlorine atom connected to bonds 4 and 16. The outlined arrows indicate the movement forced on the chlorine if each of the two bonds is allowed to stretch independently, while the solid arrow indicates the movement of the chlorine if both bonds stretch simultaneously (the

completion of the parallelogram of which the two outlined arrows define two sides). If this method is applied to each of the atoms connected by the set of bonds the result, for A_g, may be seen in Figure 7.8. Applying each of the modes found by the method of Adams and Newton, to set I, yields the results seen in Figure 7.8 to Figure 7.15. If the method is applied to the other sets (II, III and IV) the results may be seen in Figure 7.16 to Figure 7.31.

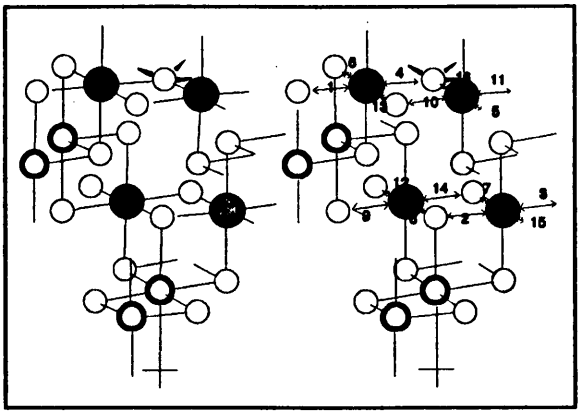

Figure 7.7: A_g applied to set I. The movement of a selected chlorine atom is indicated.

Bond	1	2	3	4	5	6	7	8	9	10	11	12	13	14	15	16
A_u	1	1	1	1	1	1	1	1	1	1	1	1	1	1	1	1
B_{1g}	1	1	1	1	-1	-1	-1	-1	1	1	1	-1	-1	1	-1	-1
B_{2g}	1	1	1	1	-1	1	1	-1	-1	-1	-1	-1	1	-1	1	-1

Table 7.10: Irreducible representations of the point group, applied to an equivalent set of bonds, set I.

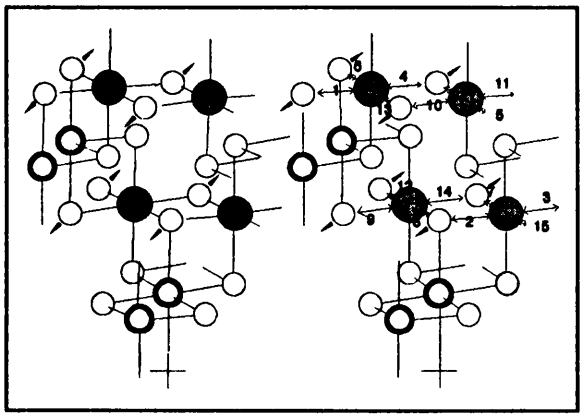

Figure 7.8: A_g applied to set I.

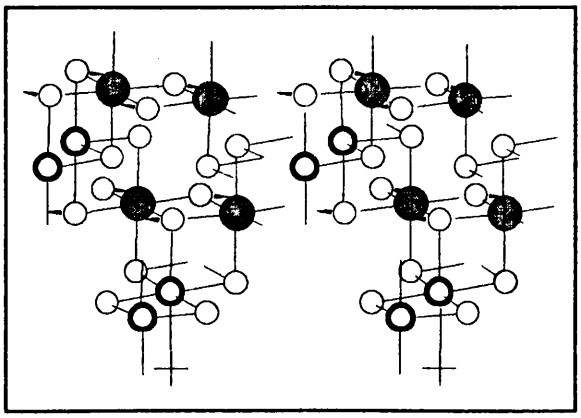

Figure 7.9: B_{1g} applied to set I.

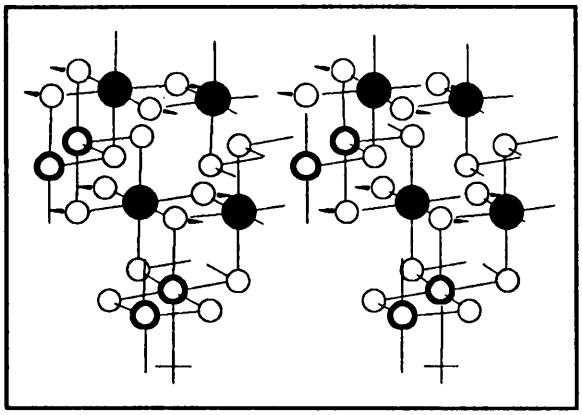

Figure 7.10: B_{2g} applied to set I.

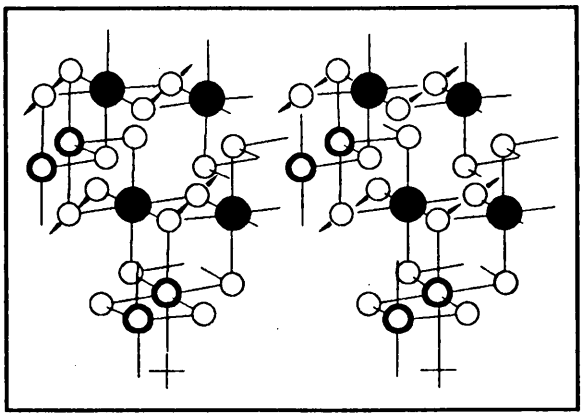

Figure 7.11: B_{3g} applied to set I.

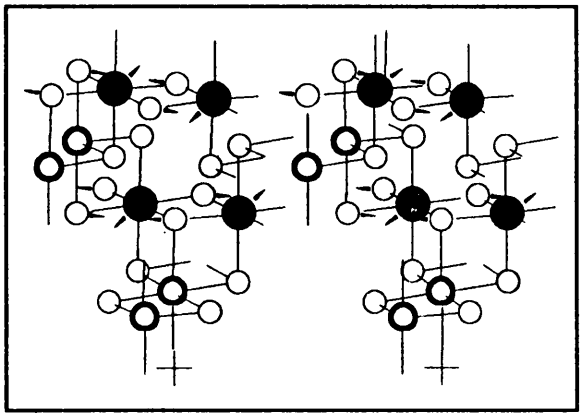

Figure 7.12: A_u applied to set I.

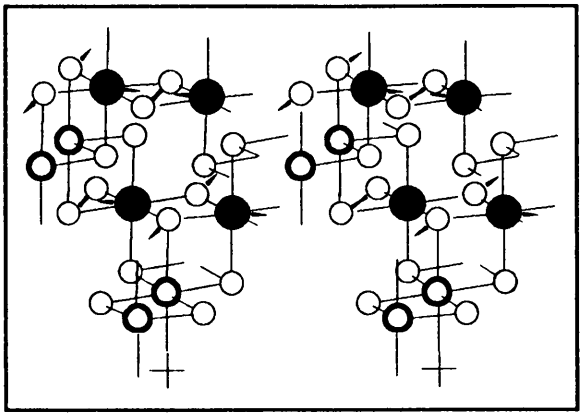

Figure 7.13: B_{1u} applied to set I.

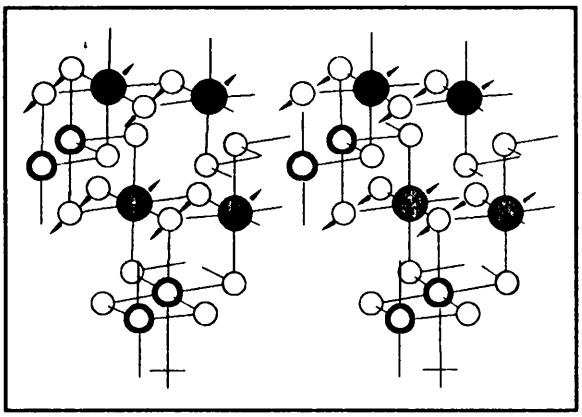

Figure 7.14: B_{2u} applied to set I.

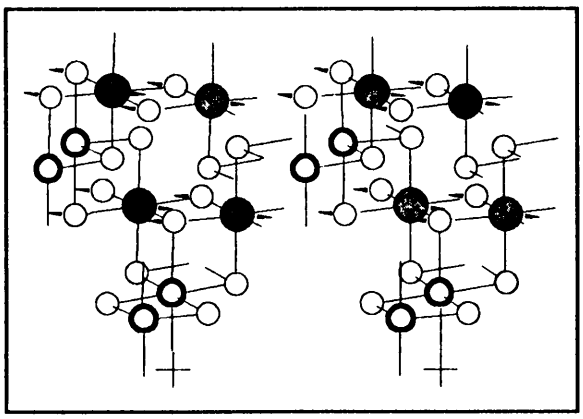

Figure 7.15: B_{3u} applied to set I.

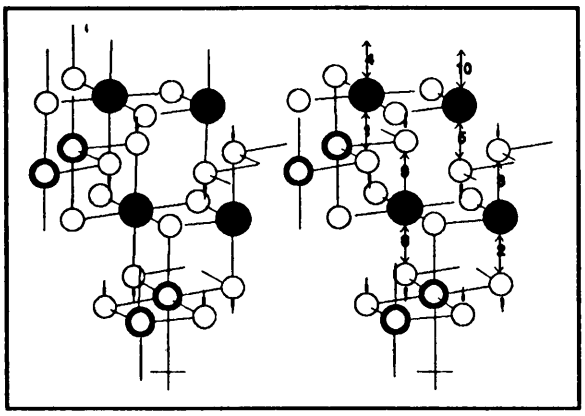

Figure 7.16: A_g applied to set II.

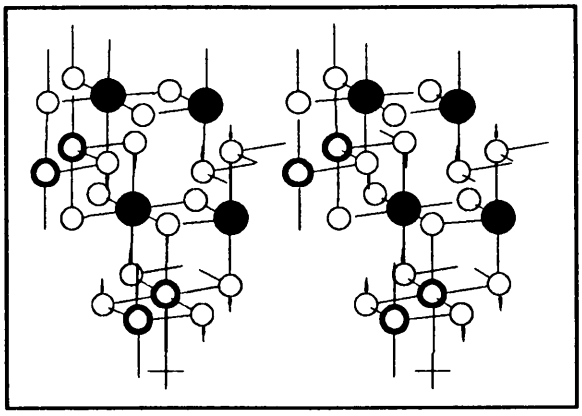

Figure 7.17: B_{2g} applied to set II.

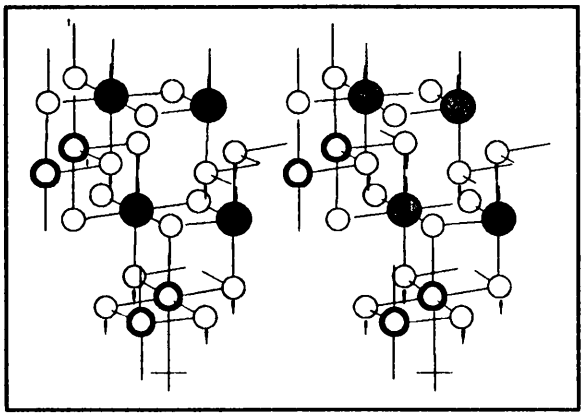

Figure 7.18: B_{1u} applied to set II.

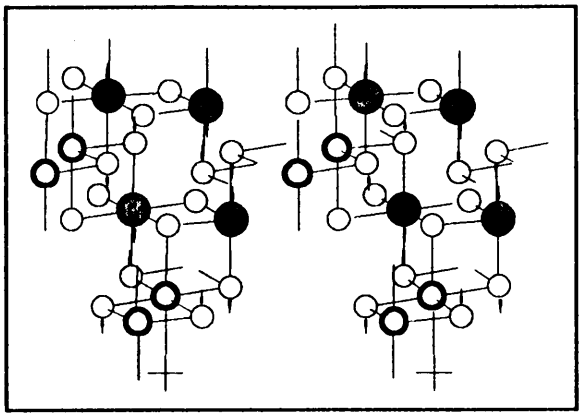

Figure 7.19: B_{3u} applied to set II.

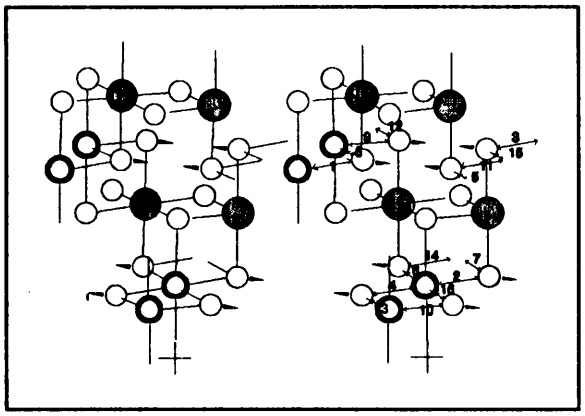

Figure 7.20: A_g applied to set III.

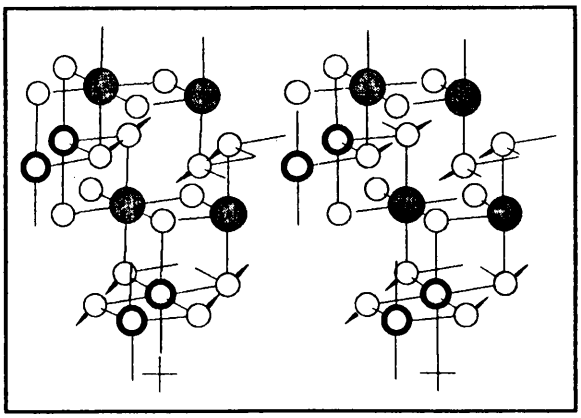

Figure 7.21: B_{1g} applied to set III.

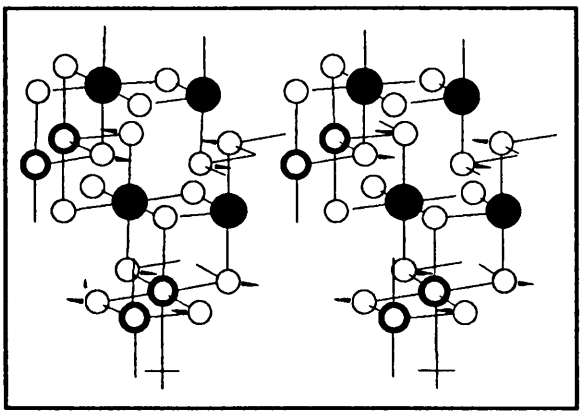

Figure 7.22: B_{2g} applied to set III.

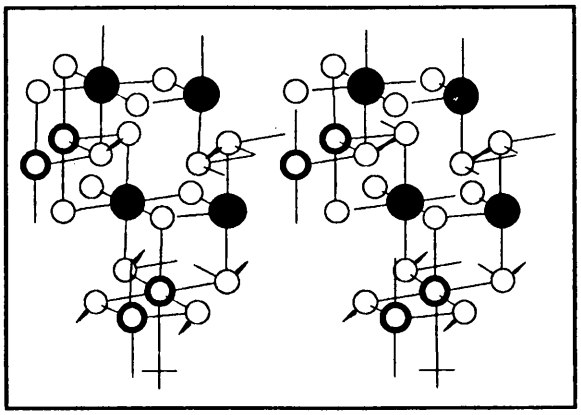

Figure 7.23: B_{3g} applied to set III.

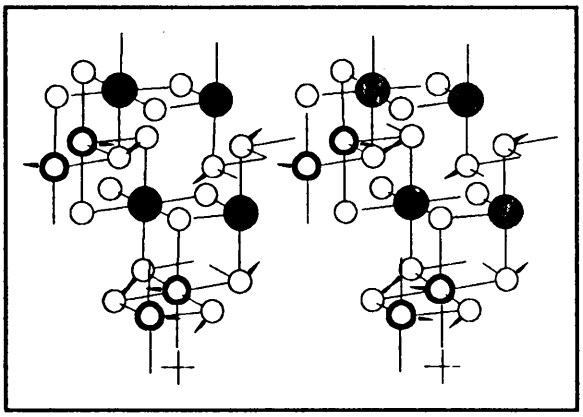

Figure 7.24: A_u applied to set III.

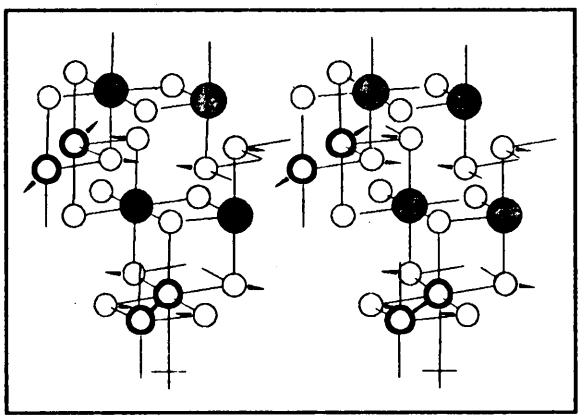

Figure 7.25: B_{1u} applied to set III.

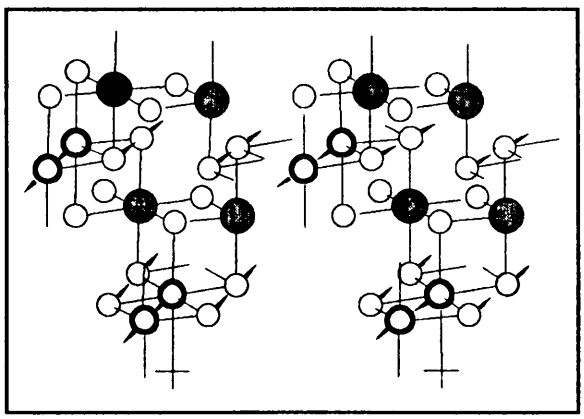

Figure 7.26: B_{2u} applied to set III.

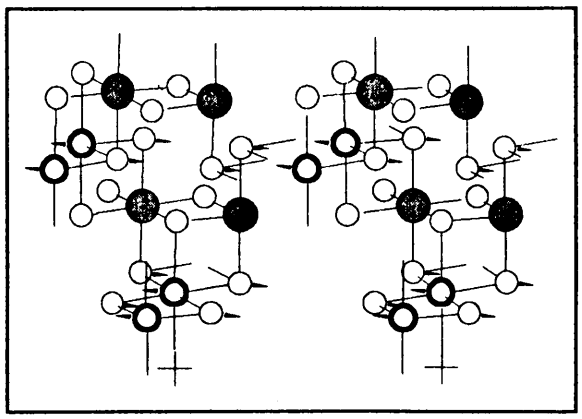

Figure 7.27: B_{3u} applied to set III.

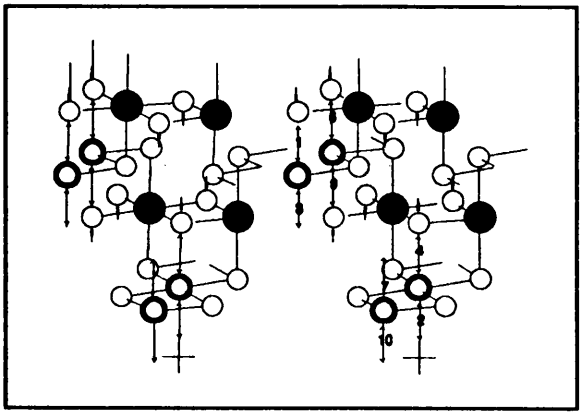

Figure 7.28: A_g applied to set IV.

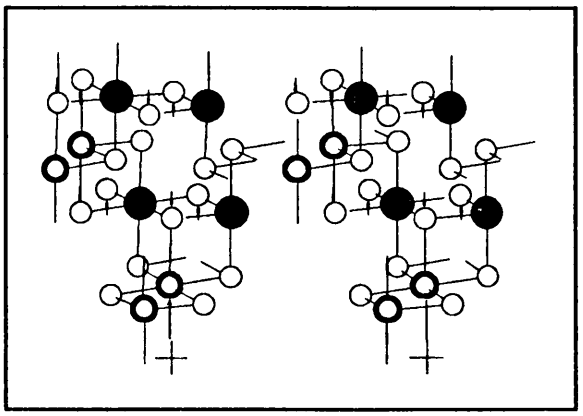

Figure 7.29: B_{3g} applied to set IV.

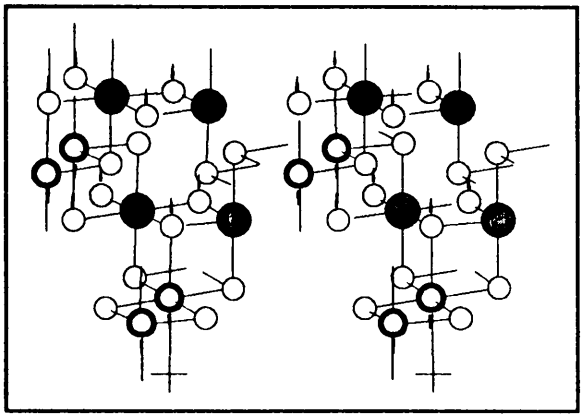

Figure 7.30: B_{1u} applied to set IV.

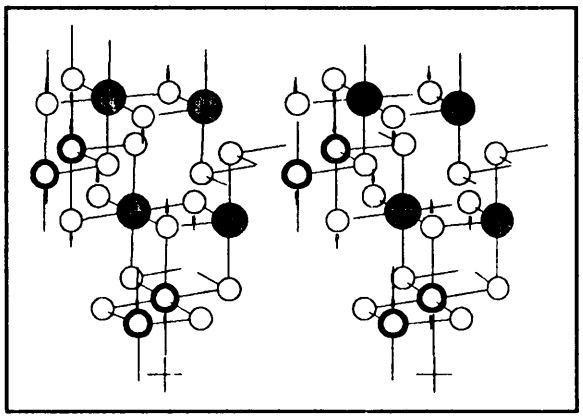

Figure 7.31: B_{2u} applied to set IV.

Discussion and comparison

Several interesting features become apparent from the development of the stretching-modes. For simplicity the results of the correlation of the previous chapter is reproduced in Table 7.11. Note that the librational and translational modes are not subtracted from the totals, and the correlation for the lithium in the tetrahedral positions is not included. A summary of the results obtained in the previous section may be seen in Table 7.12. Observe that although the interaction between the various modes has not yet been discussed, this interaction cannot yield any additional modes, as there can only be as much combinations as there are modes used for the base set. In addition, only modes of similar symmetry will interact, and this interaction can only yield a combination with the same symmetry.

The first obvious inference to be drawn is that the metal ions in the octahedral positions are only involved in infrared-active modes, while the Raman active modes involve only vibrations of the chlorine atoms. Furthermore, the stretching-mode analysis yields all the *gerade* vibrations and should give a reasonable model of the actual vibrations present in the crystal (no interaction between modes belonging to the same irreducible representation are taken into account; although such interactions should certainly be expected, as the same atoms are involved in two or more modes). The shortcomings of the stretching-mode analyses will be discussed in the next chapter and a new and more accurate method introduced.

Atom type	Wyckoff position	Vibrational modes							
Li (O_h)	4 b					A_u	$2B_{1u}$	$2B_{2u}$	B_{3u}
Co/Fe (O_h)	4 d					A_u	$2B_{1u}$	B_{2u}	$2B_{3u}$
Cl (1)	8 h	$2A_g$	B_{1g}	$2B_{2g}$	B_{3g}	A_u	$2B_{1u}$	B_{2u}	$2B_{3u}$
Cl (2)	8 i	$2A_g$	B_{1g}	B_{2g}	$2B_{3g}$	A_u	$2B_{1u}$	$2B_{2u}$	B_{3u}
Total		$4A_g$	$2B_{1g}$	$3B_{2g}$	$3B_{3g}$	$4A_u$	$8B_{1u}$	$6B_{2u}$	$6B_{3u}$
Librational			B_{1g}	B_{2g}	B_{3g}				
Translational							B_{1u}	B_{2u}	B_{3u}
Spectral Activity		R	R	R	R	N/A	IR	IR	IR

Table 7.11: Correlation results, from the previous chapter, for the iron and cobalt spinels. The lithium in the tetrahedral positions is omitted.

Atom type	Set	Vibrational modes							
Co, Cl(1)	I	A_g	B_{1g}	B_{2g}	B_{3g}	A_u	B_{1u}	B_{2u}	B_{3u}
Co, Cl(2)	II	A_g		B_{2g}			B_{1u}		B_{3u}
Li, Cl(2)	III	A_g	B_{1g}	B_{2g}	B_{3g}	A_u	B_{1u}	B_{2u}	B_{3u}
Li, Cl(1)	IV	A_g			B_{3g}		B_{1u}	B_{2u}	
Total		$4A_g$	$2B_{1g}$	$3B_{2g}$	$3B_{3g}$	$2A_u$	$4B_{1u}$	$3B_{2u}$	$3B_{3u}$
Spectral activity		R	R	R	R	N/A	IR	IR	IR

Table 7.12: Summary of the results of the stretching-mode analysis, obtained in the previous section.

Chapter 8

A vibrational analysis from first principles

It was pointed out in Chapter 6 that some of the modes predicted by the correlation method are missing from the results of the stretching-mode analysis. In this chapter reasons for this absence are discussed. Another method is explored, whereby all the vibrational modes present in the crystal can be obtained by starting from first principles, viz. allowing each atom three degrees of vibrational freedom. This method is applied and stereographic representations of the normal modes are obtained. An attempt is made to describe the vibration of the tetrahedral lithium, under some assumptions. This chapter concludes with some discussion of the vibrational modes found, and the difficulties encountered while examining the mixing of modes of similar symmetry, are presented.

Failure of the stretching-mode analysis

A bit of reflection will reveal a reason for the failure of a mere stretching-mode analysis. An inspection of the *ungerade* vibrations obtained by the stretching-mode analysis, reveals that both one of the sets of metals and one of the two different types of chlorine atoms, are taking part in every vibrational mode obtained. Knowledge of the symmetry of crystals indicates that atoms of two crystallographically different positions, cannot take part in the same normal mode. Yet it appears as if the stretching-mode analysis implies exactly this. This is not the case however, as the results of the stretching-mode analysis already contain some mixing of the normal modes belonging to the same irreducible representation. This mixing of modes is undoubtably present in this case (and in all cases where the same atoms are taking part in two different vibrations of the same symmetry). There must consequently be ways of mixing the normal modes not predicted by the stretching-mode analysis alone. This mixing of normal modes is discussed at the end of the chapter.

It is interesting to note that in the case of the *gerade* vibrations, all the modes predicted by the correlation method are found by a stretching-mode analysis. This is due to a number of reasons. First, all the chlorine atoms are considered in the stretching-mode analysis. Secondly, every mode obtained involves only symmetrically equivalent chlorine atoms and there are therefore no implied mixing of modes. Thirdly, there are no pure bending modes possible in this case, as every bend in angle must imply some stretch in some of the bonds chosen for the stretching-mode analysis. The bonds selected, are therefore a good enough description of the unit-cell to yield all the *gerade* vibrations, during a stretching-mode analysis, but not in the case of the *ungerade* vibrations.

Preparing for the vibrational analysis

The basic assumption underlying the vibrational analysis, is that each atom in the crystal is allowed three degrees of vibrational freedom. These three degrees of freedom are taken as movement along the axes of the Cartesian coordinate system. The analysis is started by aligning vectors along the Cartesian axes of any atom chosen from, and therefore representing, an equivalent set (atoms occupying one crystallographic site in the unit-cell). In the case of the D_{2h} point group, there are no degeneration of the axes (i.e. there are only one-dimensional irreducible representations in this group) and therefore, the vibrational analysis on any equivalent set of atoms, divides into three separate problems, one for each of the three independent axes of the Cartesian coordinate system. If a vector is aligned with one of the axes of an atom representing an equivalent set, it is transformed into a vector aligned in the positive or negative direction of the same axes, on the same, or another atom of the equivalent set, under any operation present in the space group Imma.

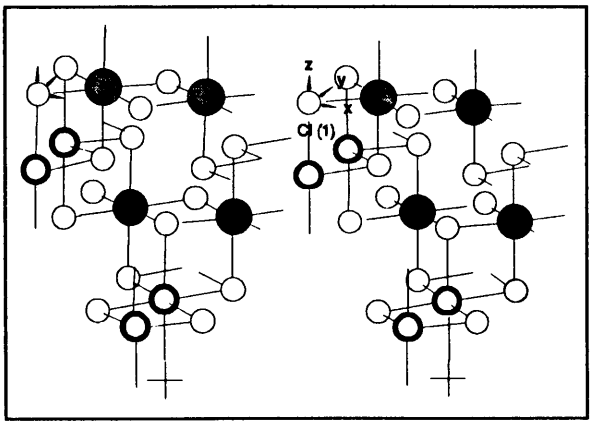

Figure 8.1: A vector aligned with each of the three Cartesian axes on a chlorine atom representing the Cl(1) equivalent set.

Thus, vectors representing the movement of the atom, are placed on a selected atom from each equivalent set present in the crystal and aligned with each of the three axes. If one atom of the Cl (1) equivalent set is chosen, the three vectors placed on this atom and aligned with the three Cartesian axes may be seen Figure 8.1.

In order to manipulate this vector mathematically, in the same way as in the previous chapter, it is necessary to place a 'dummy atom' at the other end of the vector. If the vector along the x-axis is taken to have a 0.1 fractional length (a purely arbitrary choice, as no quantification of movement of the atoms is involved), the two ends of the vector on the Cl (1) atom indicated in the figure lie at (0.000; 0.011; 0.756) and (0.100; 0.011; 0.756) respectively.

The spreadsheet constructed in the previous chapter, Spreadsheet 7.1, may now be applied to this 'pair of atoms' and the result is an equivalent set of 'atom pairs' that define an equivalent set of vectors. This equivalent set of vectors may be seen in Figure 8.2. Again the numbers indicate the position, in the spreadsheet, of the symmetry operation of the space group, yielding the particular vector designated in the figure.

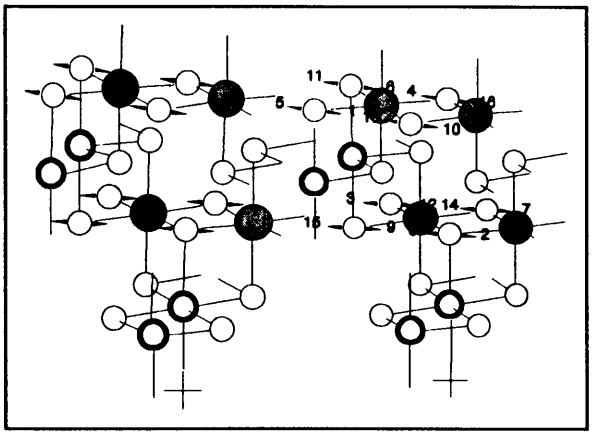

Figure 8.2: The result of applying Spreadsheet 7.1 to a vector aligned with the x-axis on an atom of the Cl(1) equivalent set.

As in the previous chapter, the character of the symmetry operation of the point group, associated with the symmetrical part of the space group operation, under a specific irreducible representation, is applied to the vector obtained by the particular operation. A negative character implies that the vector must be

Cl_1 (x)	A_g	B_{1g}	B_{2g}	B_{3g}	A_u	B_{1u}	B_{2u}	B_{3u}
1, -5	+ -	+ +	+ +	+ -	+ +	+ -	+ -	+ +
2, -8	+ -	+ +	+ +	+ -	+ +	+ -	+ -	+ +
6, -11	+ -	- -	+ +	- +	- -	+ -	- +	+ +
7, -14	+ -	- -	+ +	- +	- -	+ -	- +	+ +
9, -15	+ -	+ +	- -	- +	- -	- +	+ -	+ +
10, -13	+ -	+ +	- -	- +	- -	- +	+ -	+ +
12, -3	+ -	- -	- -	- +	+ +	+ -	+ -	+ +
16, -4	+ -	- -	- -	- +	+ +	+ -	+ -	+ +

Table 8.1: Application of the D_{2h} point group to the vectors obtained from one aligned with the x-axis on one of the Cl(1) atoms.

aligned in opposite direction to the direction indicated in Figure 8.1 (i.e. the original alignment). The characters of each of the irreducible representations of the D_{2h} point group are applied, in turn, to the set of vectors obtained by the space group operations. If the characters of the A_g irreducible representation are applied to the vector aligned with the x-axis of the atom, indicated in Figure 8.1, from the Cl (1) set, the result is vectors on all the other atoms of the set, aligned with either the positive or negative x-axis direction. In this way, all the possible combinations are obtained. Note that more than one operation in Spreadsheet 7.1, map a vector to the same atom, and that different operations may map vectors of opposite direction to the same atom, thus cancelling each other out. It is immediately clear from Figure 8.2 that there is no A_g mode possible with the vectors aligned along the x-axis, because every atom contains two equal vectors in opposite directions. This procedure is carried out for each irreducible representation of the D_{2h} point group and the process is repeated for each direction on the chosen atom of each set and subsequently for a representative atom of each independent set of atoms, present in the unit-cell.

The easiest way of obtaining the desired results, is to construct a table in stead of drawing all the possible combinations. An example of such a table, for a vector aligned along the x-axis of a Cl (1) atom, as depicted in Figure 8.2, may be seen in Table 8.1. This table is obtained, by noting the direction of the vector obtained by each of the 16 independent operations of Spreadsheet 7.1. If the vector, generated by each operation, is aligned with the negative axis, a negative sign is inserted before the vector number (the same number as the number of the operation that generated it, in the spreadsheet) in the first column of the table. All numbers of operations that generated vectors on the same atom, are grouped together in the first column.

For each of the irreducible representations of the point group, the character, associated with the purely symmetrical part of an operation, is applied to the appropriate vector. Thus, if a negative character of the point group is applied to a vector aligned with the negative axis (i.e. the vector has a negative number in the first column of the table), the resulting vector is aligned with the positive axis on the same atom, and a positive sign is inserted in the column added for the particular irreducible representation.

The result (as may be seen in Table 8.1) is a column of two signs (one for each of two vectors obtained on each atom of set I), for every irreducible representation of the point group. Furthermore, if the two signs in each cell are opposite in nature, it means that the result is a vector pointing in the negative, as well as a vector pointing in the positive direction of the axis, and therefore cancelling each other. If the signs are of the same nature, it means that the two vectors are aligned in the same direction and therefore enhance each other, indicating a vibrational movement.

Atom Type	Axis	Vibrational modes							
Cl (1)	x		B_{1g}	B_{2g}		A_u			B_{3u}
	y	A_g			B_{3g}		B_{1u}	B_{2u}	
	z	A_g			B_{3g}		B_{1u}	B_{2u}	
Total Cl (1):		$2A_g$	B_{1g}	B_{2g}	$2B_{3g}$	A_u	$2B_{1u}$	$2B_{2u}$	B_{3u}
Cl (2)	x	A_g		B_{2g}			B_{1u}		B_{3u}
	y		B_{1g}		B_{3g}	A_u		B_{2u}	
	z	A_g		B_{2g}			B_{1u}		B_{3u}
Total Cl (2):		$2A_g$	B_{1g}	$2B_{2g}$	B_{3g}	A_u	$2B_{1u}$	B_{2u}	$2B_{3u}$
Li: O_h	x					A_u			B_{3u}
	y						B_{1u}	B_{2u}	
	z						B_{1u}	B_{2u}	
Total Li: O_h:						A_u	$2B_{1u}$	$2B_{2u}$	B_{3u}
M: O_h	x						B_{1u}		B_{3u}
	x					A_u		B_{2u}	
	y						B_{1u}		B_{3u}
Total M: O_h:						A_u	$2B_{1u}$	B_{2u}	$2B_{3u}$
Total modes:		$4A_g$	$2B_{1g}$	$3B_{2g}$	$3B_{3g}$	$4A_u$	$8B_{1u}$	$6B_{2u}$	$6B_{3u}$
Spectral activity:		R	R	R	R	N/A	IR	IR	IR

Table 8.2: Summary of the modes found in the application of the method discussed in the text.

From Table 8.1 it is obvious that the vibrational modes associated with the Cl (1) atoms, in the x-direction, is: $B_{1g} + B_{2g} + A_u + B_{3u}$. These modes are shaded in the table. Note that there are four modes for Cl (1) in the x-direction. This is expected, because there are four

equivalent Cl (1) atoms in the asymmetric unit and, as pointed out in the previous chapter, the asymmetric unit contains all the information needed to generate the unit-cell and must therefore contain all the possible vibrations as well.

This process may now be carried out for all of the other types of atoms present in the unit-cell (i.e. the Cl(2), Li(O_h) and M(O_h) atoms, M = Co or Fe). The results will contain the same number and type of modes as found by the correlation method. That this is indeed the case, may be seen in Table 8.2, where a summary of this method, applied to the cobalt or iron spinels, can be found.

The question that may be asked at this stage, is why all this work is necessary to obtain the same results as found by a simple correlation, only taking a few minutes, needing virtually no study of the unit-cell at all. The answer is that the results can be used, not only to obtain the number and nature of vibrational modes present, but to construct graphical representations of each of the normal modes found, as well. This is an enormous advantage over a mere correlation as it allows an intimate knowledge of each vibration present in the crystal.

Construction of graphical representations of the vibrational modes

As was mentioned at the end of the previous section, it is possible to construct graphical representations of the vibrational modes found by this method. This is quite easily done, by using the tables similar to Table 8.1.

The table (similar to Table 8.1) for each direction of each set, is examined to obtain the representations of the modes that do not cancel out. Each mode is drawn by determining the direction of the vector on every atom of the set. The vector for each atom is simply added to the atom with the same number as the first number found in the first column of each row of the table. The direction is obtained by multiplying the sign of this number with the sign of the number in the appropriate column of the representation under consideration, and aligning the vector in the opposite or same direction as the vector yielded by the space group operation, with the same number in the spreadsheet. Thus, in the case of the Cl (1) atom's

vibration in the x-direction (depicted in Table 8.1), the first vector of the B_{2g} mode should be drawn in the positive x-axis direction.

The results, for the octahedral metals and chlorine lattice, of the cobalt or iron spinel, may be seen in Figure 8.3 to Figure 8.38. As indicated at the beginning of this chapter, a lot of the modes found by this method (all the *gerade* modes for instance) are similar to the modes found by the stretching-mode analysis. The reasons why these similar modes are repeated in this chapter are twofold. The first is that it allows comparison (mode for mode) with the results found by the stretching-mode analysis. Secondly, all the normal modes are now grouped together and this eases the understanding of the interaction of modes, as discussed at the end of this chapter, significantly.

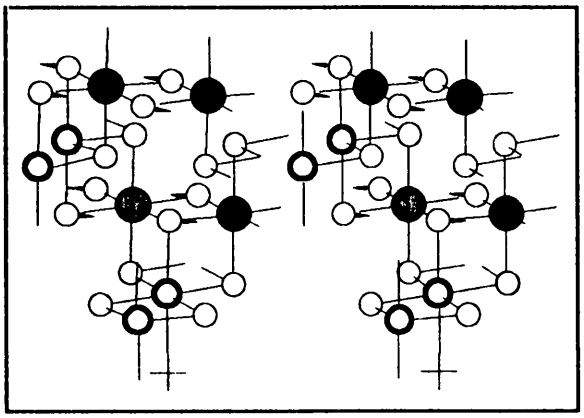

Figure 8.3: Cl (1), x-axis, B_{1g}.

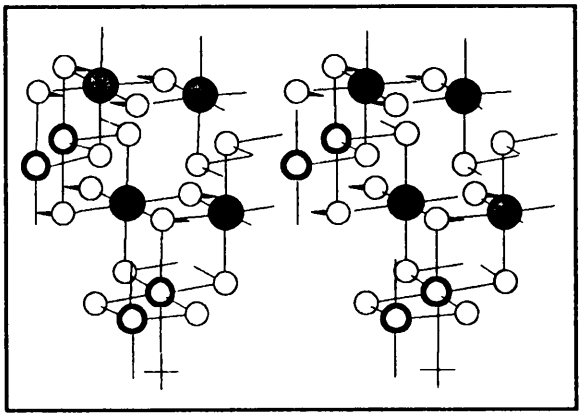

Figure 8.4: Cl (1), x-axis, B_{2g}.

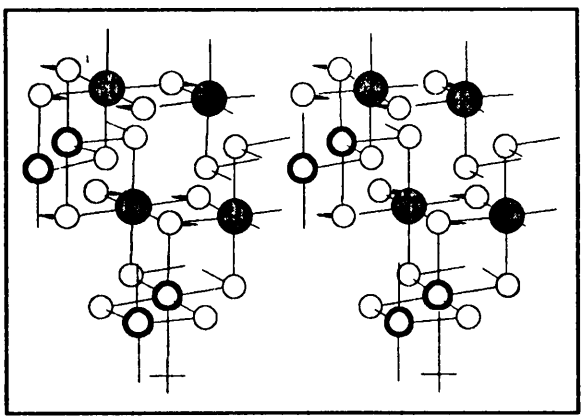

Figure 8.5: Cl (1), x-axis, A_u.

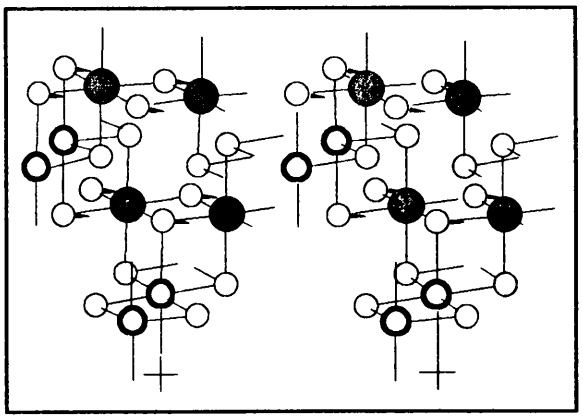

Figure 8.6: Cl (1), x-axis, B_{3u}.

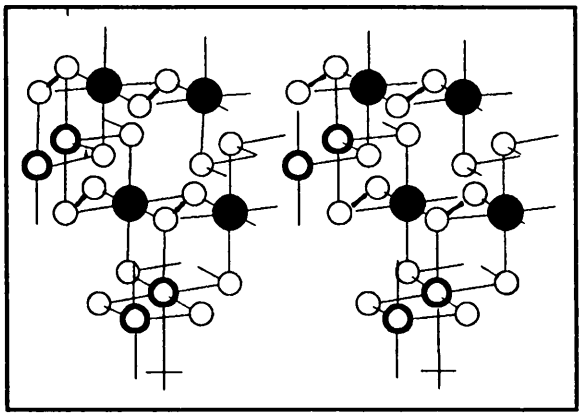

Figure 8.7: Cl (1), y-axis, A_g.

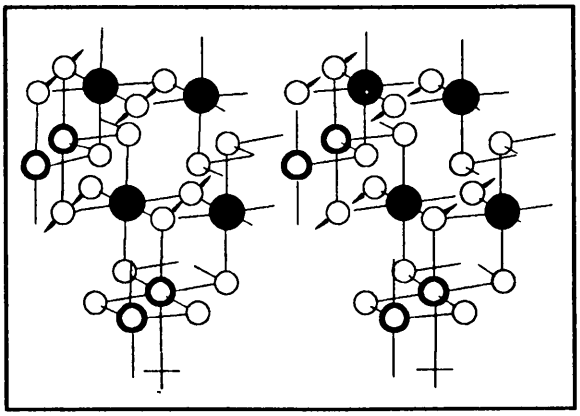

Figure 8.8: Cl (1), y-axis, B_{3g}.

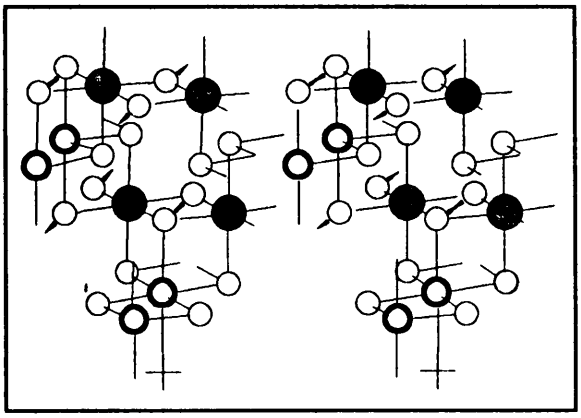

Figure 8.9: Cl (1), y-axis, B_{1u} .

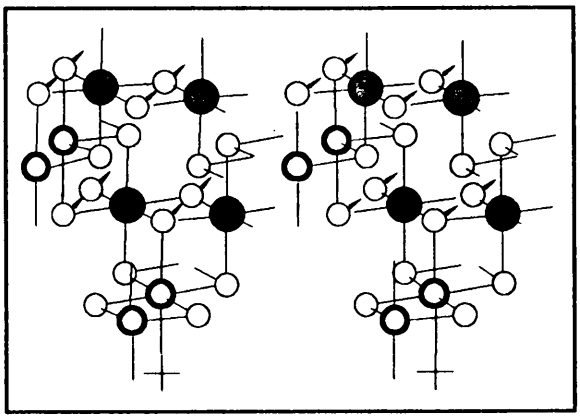

Figure 8.10: Cl (1), y-axis, B_{2u}.

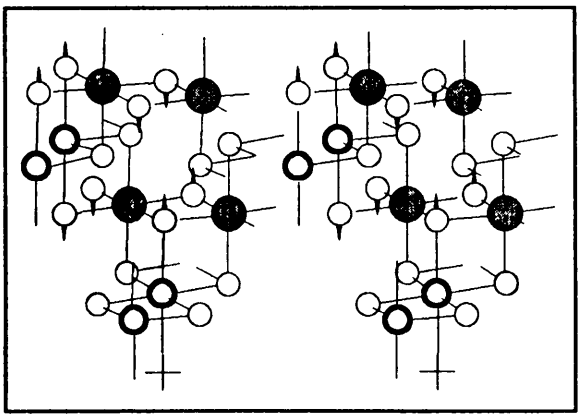

Figure 8.11: Cl (1), z-axis, A_g.

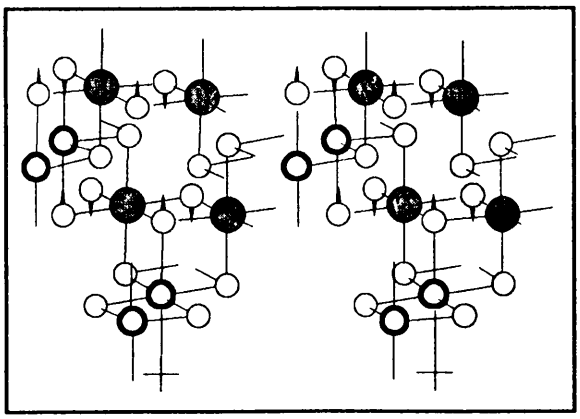

Figure 8.12: Cl (1), z-axis, B_{3g}.

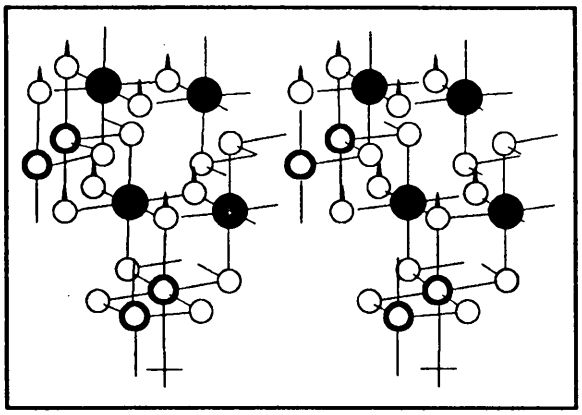

Figure 8.13: Cl (1), z-axis, B_{1u}.

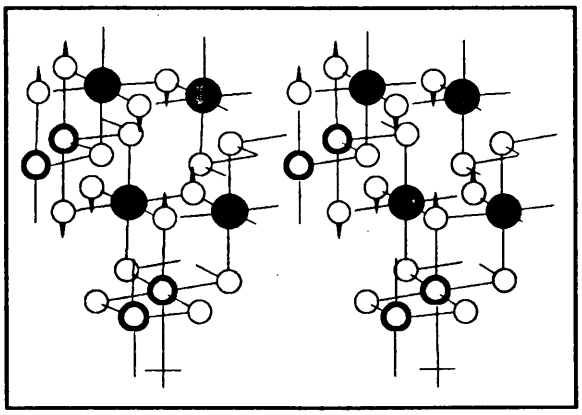

Figure 8.14: Cl (1), z-axis, B_{2u}.

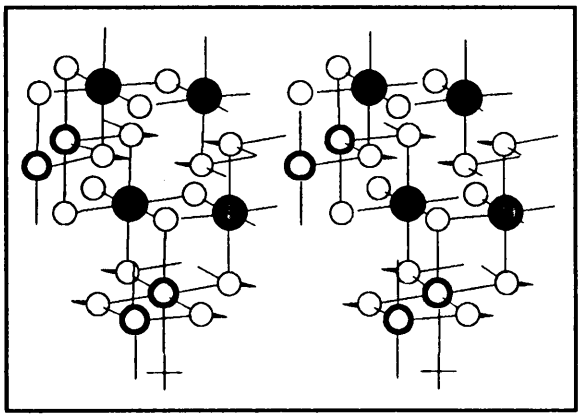

Figure 8.15: Cl (2), x-axis, A_g.

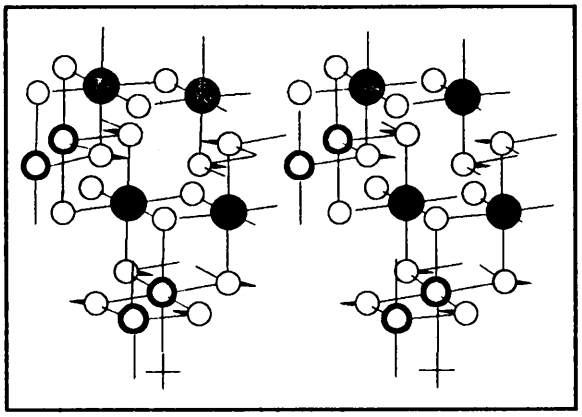

Figure 8.16: Cl (2), x-axis, B_{2g}.

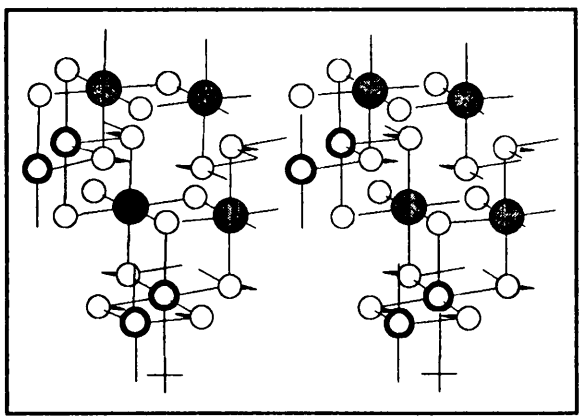

Figure 8.17: Cl (2), x-axis, B_{1u}.

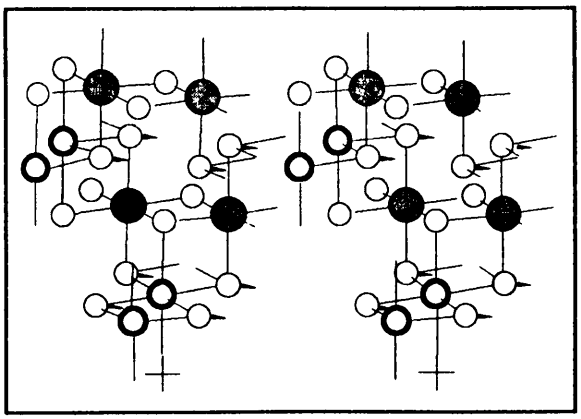

Figure 8.18: Cl (2), x-axis, B_{3u}.

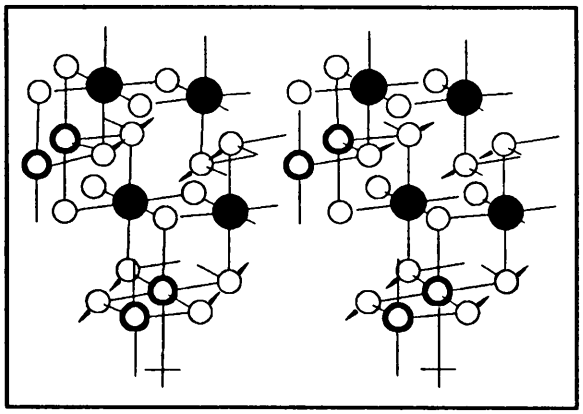

Figure 8.19: Cl (2), y-axis, B_{1g}.

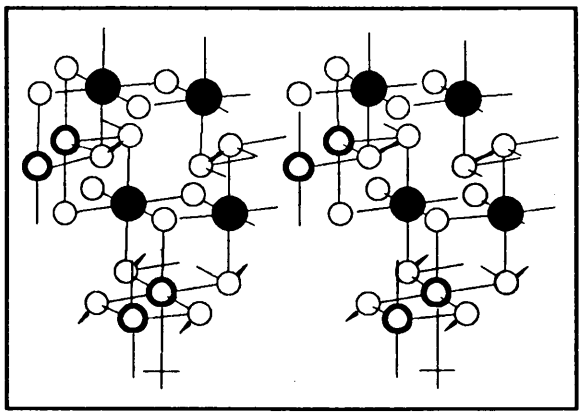

Figure 8.20: Cl (2), y-axis, B_{3g}.

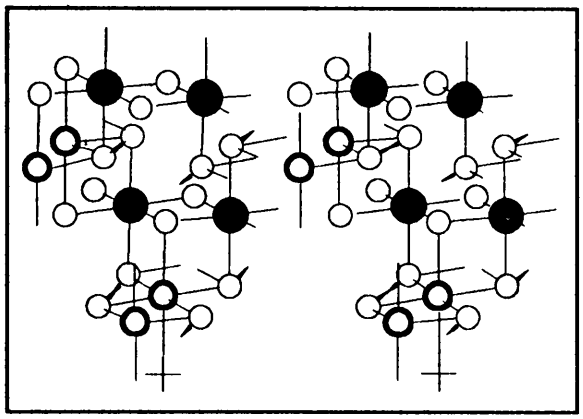

Figure 8.21: Cl (2), y-axis, A_u.

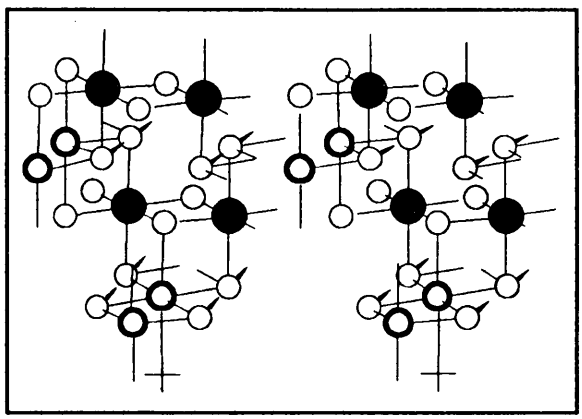

Figure 8.22: Cl (2), y-axis, B_{2u}.

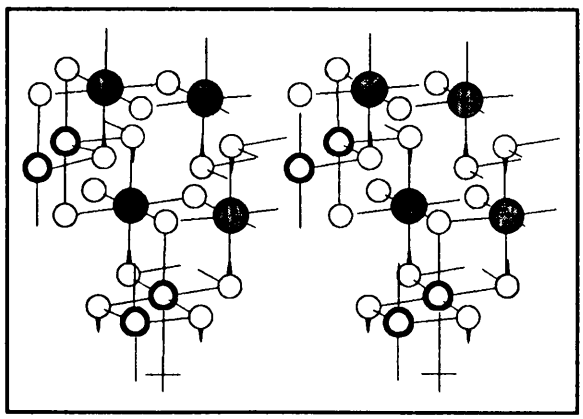

Figure 8.23: Cl (2), z-axis, A_g.

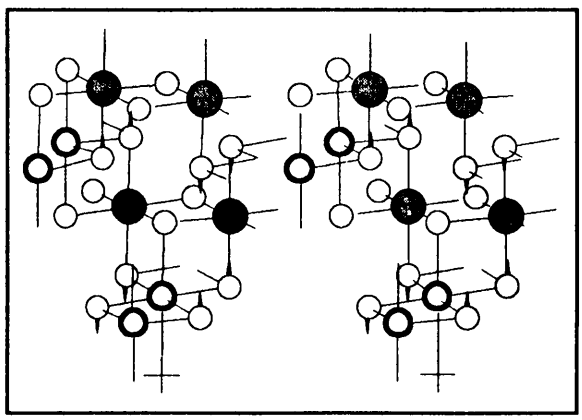

Figure 8.24: Cl (2), z-axis, B_{2g}.

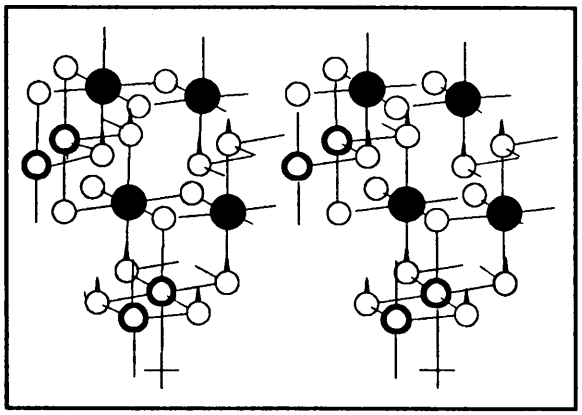

Figure 8.25: Cl (2), z-axis, B_{1u}.

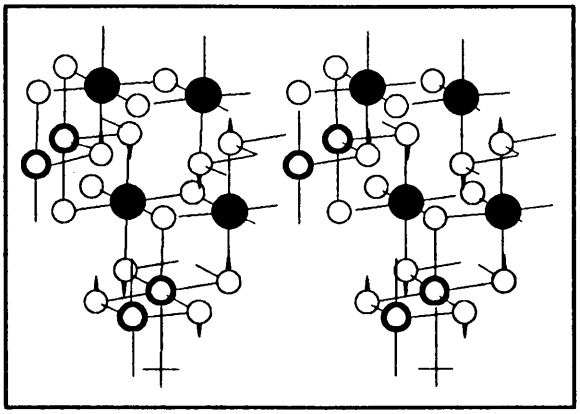

Figure 8.26: Cl (2), z-axis, B_{3u}.

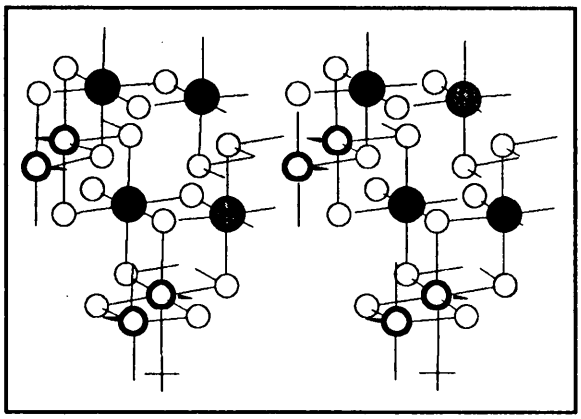

Figure 8.27: Li: O_h, x-axis, A_u.

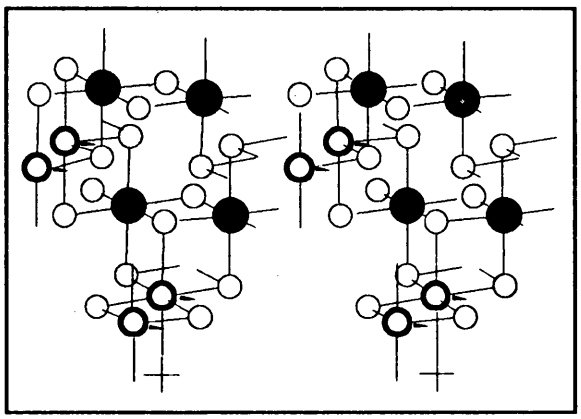

Figure 8.28: Li: O_h, x-axis, B_{3u}.

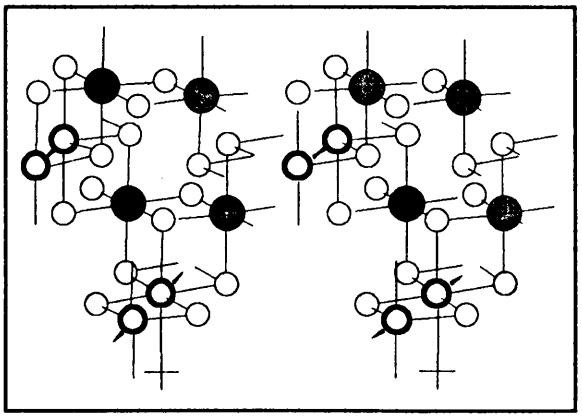

Figure 8.29: Li: O_h, y-axis, B_{1u}.

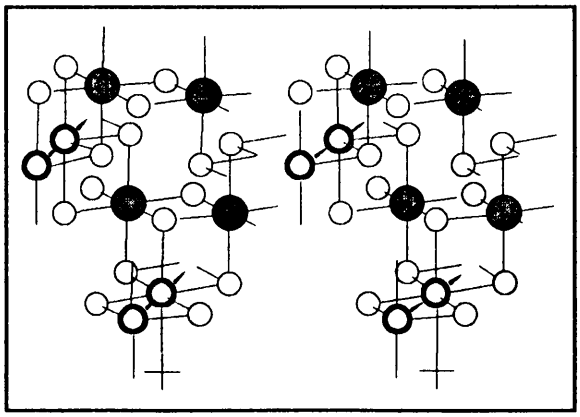

Figure 8.30: Li: O_h, y-axis, B_{2u}.

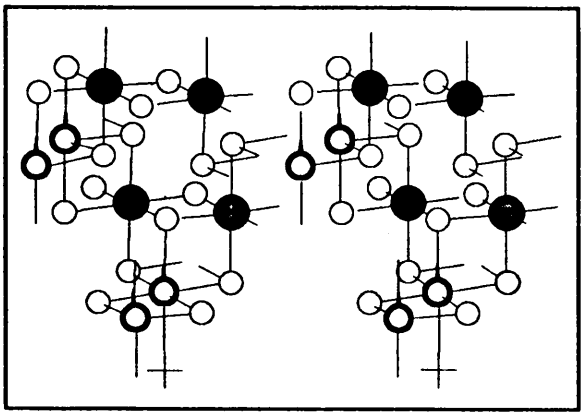

Figure 8.31: Li: O_h, z-axis, B_{1u}.

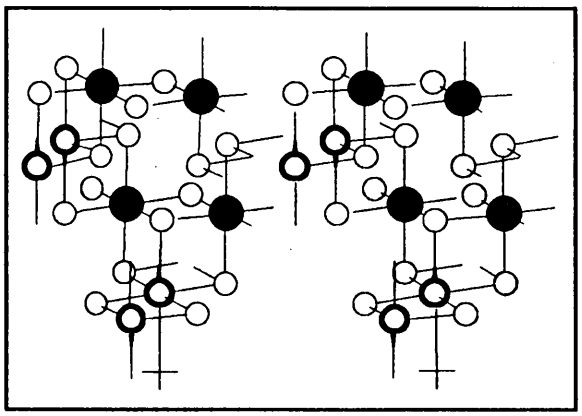

Figure 8.32: Li: O_h, z-axis, B_{2u}.

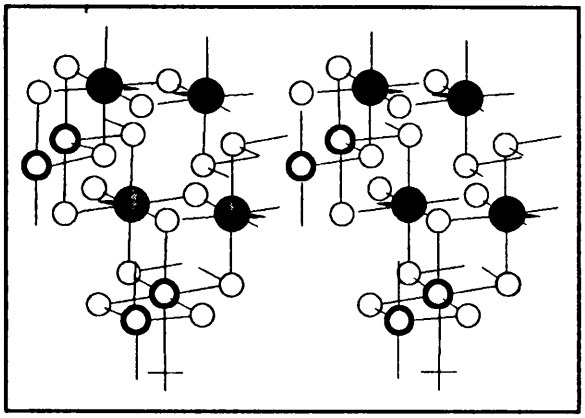

Figure 8.33: M: O_h, x-axis, B_{1u}.

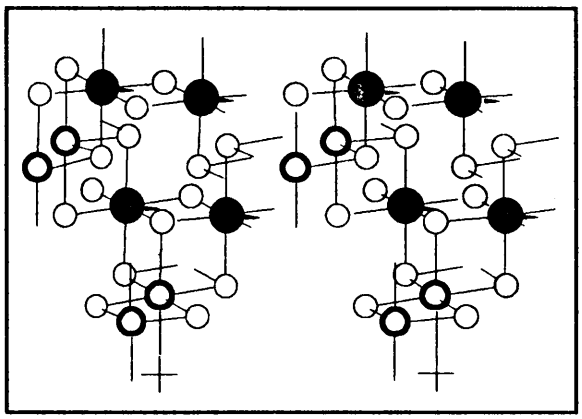

Figure 8.34: M: O_h, x-axis, B_{3u}.

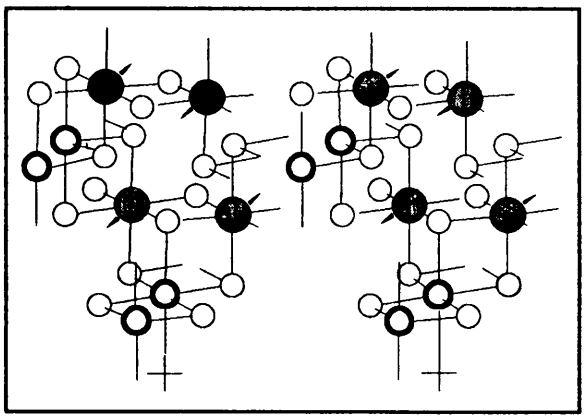

Figure 8.35: M: O_h, y-axis, A_u.

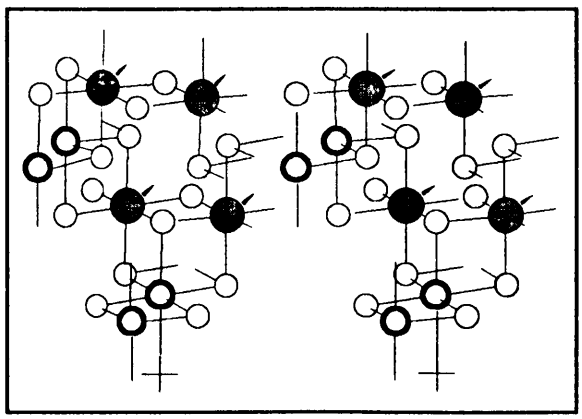

Figure 8.36: M: O_h, y-axis, B_{2u}.

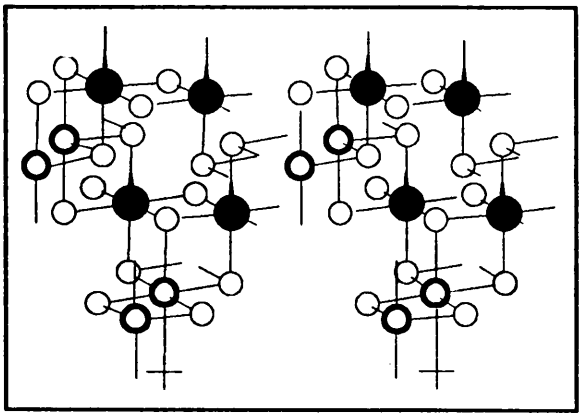

Figure 8.37: M: O_h, z-axis, B_{1u}.

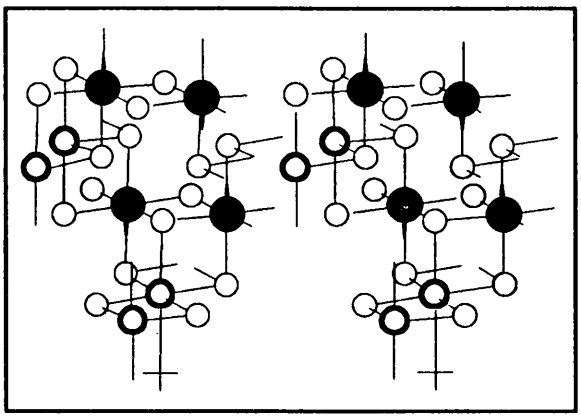

Figure 8.38: M: O_h, z-axis, B_{3u}.

Discussion of the results of the vibrational analysis

Comparison of the results found by the discussed method and by the correlation method, reveals that all the modes predicted by the correlation method were found by the method discussed in this chapter. This must be the case, as a similar approach is present in both methods. In the correlation method each atom is allowed three degrees of vibrational freedom as well, but this fact is somewhat obscured by the method (the irreducible representation of each degree of freedom in the site group, is correlated to the factor group, to determine the way in which the various atoms in an equivalent set may interact). In the discussed method, no correlation is carried out, but the interactions of each degree of freedom of the atoms of an equivalent set, are systematically inspected, thus yielding the same results.

Inspection of the vibrational modes found, yields an observation that may have been noticed by inspection of the unit-cell alone. This observations is that the Cl(1) and the Cl(2) sets yield exactly the same type of vibrations, only differing in their alignment along the axes. This is seen, by noting that the vibrations in the x-direction of Cl(1) (Figure 8.3 to Figure 8.6) are exactly the same as the vibrations of Cl(2) in the y-direction (Figure 8.19 to Figure 8.22). Because the direction is different, the vibrations of each set, although similar in nature, belong to different irreducible representations. In this way, the B_{2g} vibration of Figure 8.4, is the same as the B_{3g} vibration of Figure 8.20. The same similarity exists between the vibrations of Cl(1) in the y-direction (Figure 8.7 to Figure 8.10) and the

vibrations of Cl(2) in the x-direction (Figure 8.15 to Figure 8.18). In the case of vibrations in the z-direction, an analogous similarity exists. Keeping the different alignment along the x- and y-axes of the two sets of chlorine in mind, it is not difficult to see that the vibrations in the z-direction for Cl(1) (Figure 8.11 to Figure 8.14) is exactly the same as the vibrations in the z-direction for Cl(2) (Figure 8.23 to Figure 8.26). Because of the 1:1 ordering of the of the octahedral metals along the a- and b-axes of the crystal, the energy of the vibrations should be different, however.

The same holds true for the vibrations of the metal ions in the octahedral positions (Figure 8.27 to Figure 8.38). Again the vibrations of the octahedral lithium in the x-direction, are similar to that of the transition metal in the y-direction and visa versa. The same argument also applies to the vibration of the metals in the z-direction.

This graphical representation of the vibrational modes, should be a good representation of the actual normal modes present in the crystal. They do not, however, represent accurately what is really happening in the unit-cell during vibration. The reason for this is simply that there must be interaction between modes of similar symmetry, containing the same, or some of the same atoms. These interactions will be discussed in more detail at the end of this chapter and it is sufficient to mention at this stage that the representations given above, although representing the normal modes, must be treated with due caution.

Vibration of the lithium in the tetrahedral positions

As was discussed before, the lithium that are supposed to be in the tetrahedral positions, present some problems, because the site they occupy (the 8i site) is only half filled and a normal correlation is therefore not possible. As indicated in Chapters 5 and 6, the 8i site is between the true tetrahedral 4e site and the interstitial octahedral 4c site, although it lies closer to the 4c site.

In order to aid the understanding of the actual vibrations of these lithium atoms, the method, described in this chapter, is applied to all three these positions. During the analysis, the 8i site is taken as filled, otherwise the application of the method is impossible. As was the case

in the application of this method in the previous section, the same total and type of modes must be obtained as found by the correlation method. The results of the application of this method to the lithium, may be seen in Figure 8.39 to Figure 8.50 for lithium in the 8i positions, in Figure 8.51 to Figure 8.56 for the 4c positions and in Figure 8.57 to Figure 8.62 for the 4e positions.

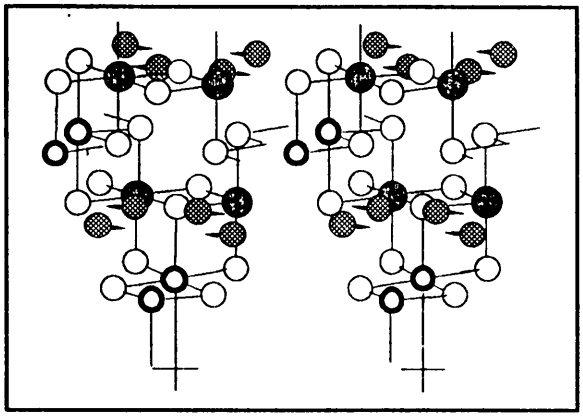

Figure 8.39: Li in the 8i site, x-axis, A_g.

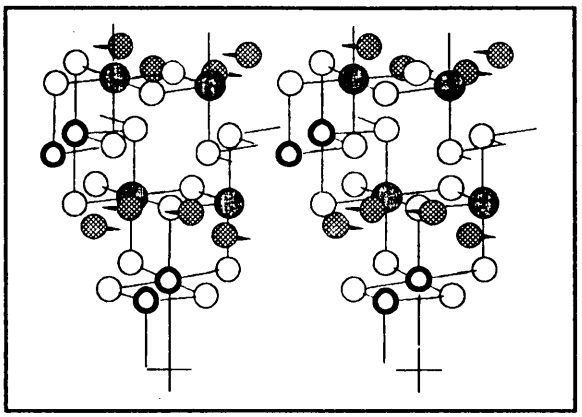

Figure 8.40: Li in the 8i site, x-axis, B_{2g}.

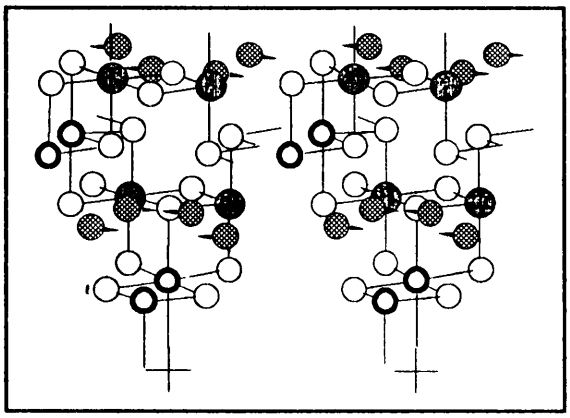

Figure 8.41: Li in the 8i site, x-axis, B_{1u}.

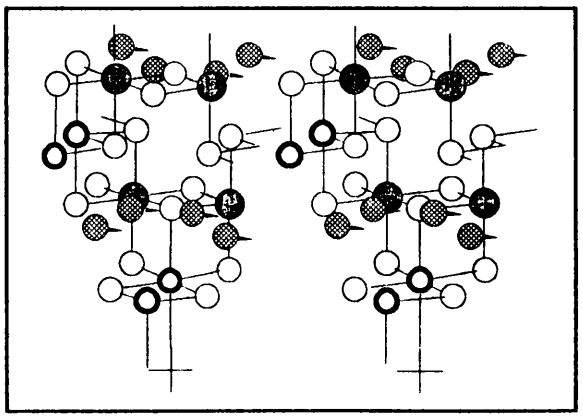

Figure 8.42: Li in the 8i site, x-axis, B_{3u}.

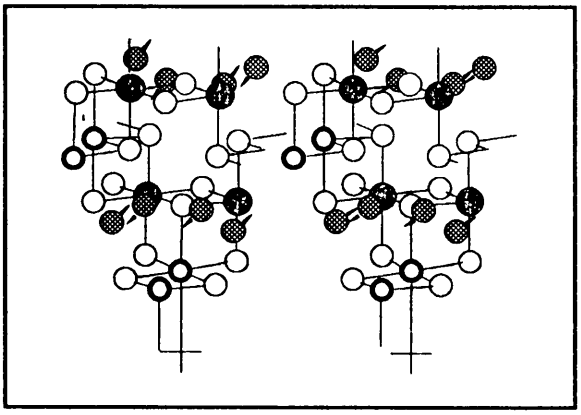

Figure 8.43: Li in the 8i site, y-axis, B_{1g}.

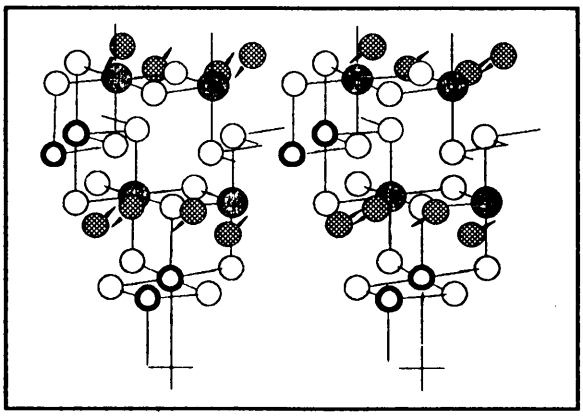

Figure 8.44: Li in the 8i site, y-axis, B_{3g}.

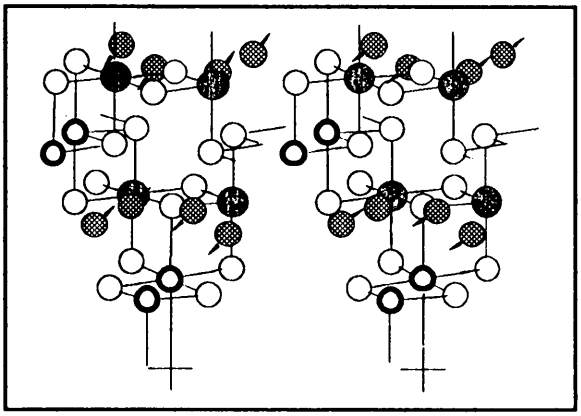

Figure 8.45: Li in the 8i site, y-axis, A_u.

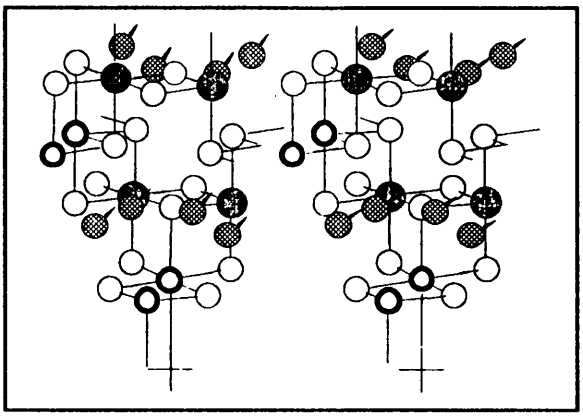

Figure 8.46: Li in the 8i site, y-axis, B_{2u}.

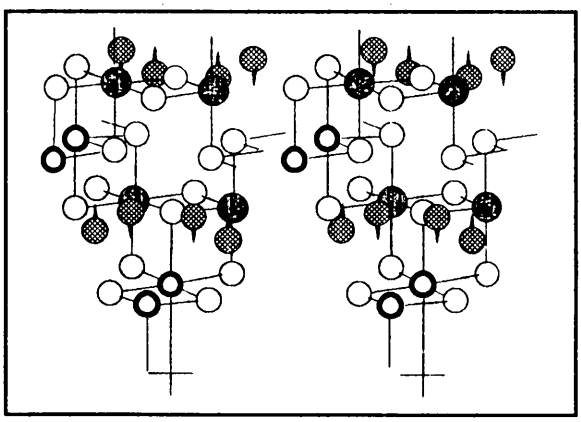

Figure 8.47: Li in the 8i site, z-axis, A_g.

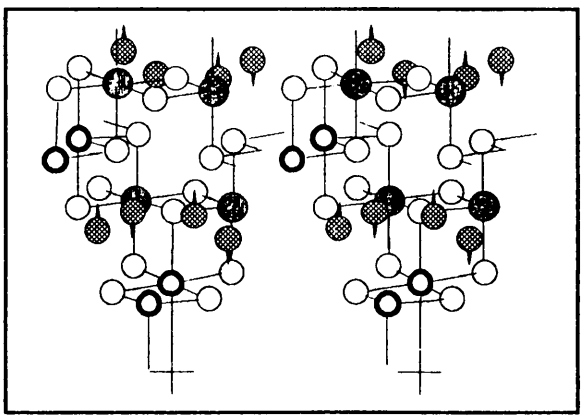

Figure 8.48: Li in the 8i site, z-axis, B_{2g}.

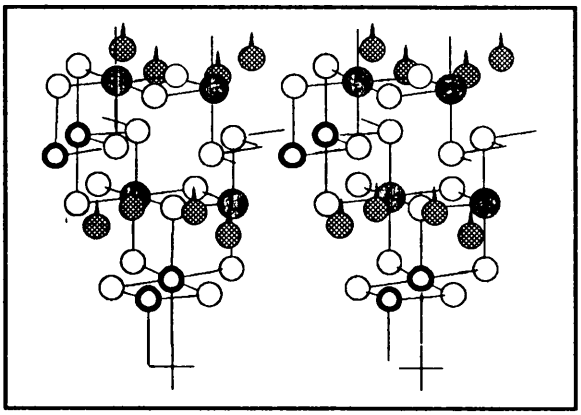

Figure 8.49: Li in the 8i site, z-axis, B_{1u}.

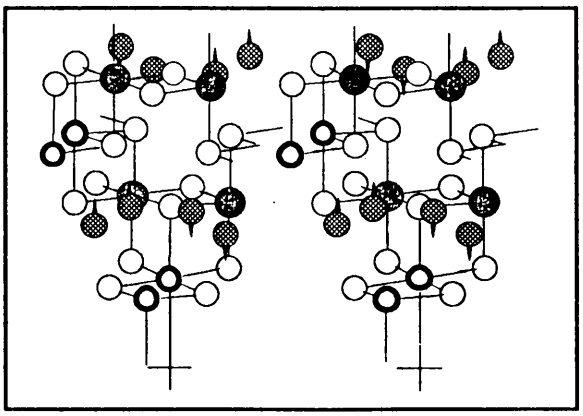

Figure 8.50: Li in the 8i site, z-axis, B_{3u}.

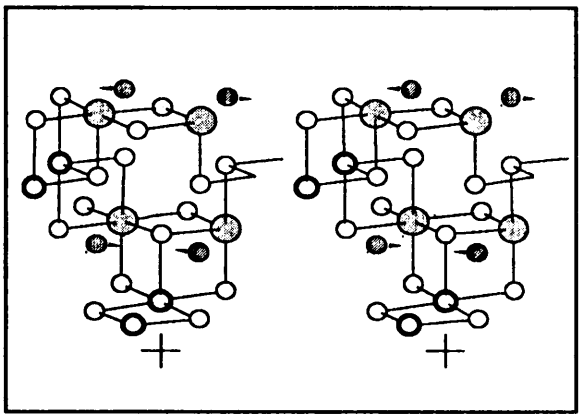

Figure 8.51: Li in the 4c site, x-axis, B_{1u}.

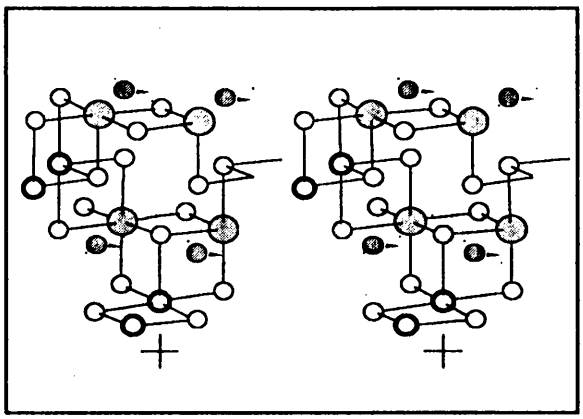

Figure 8.52: Li in the 4c site, x-axis, B_{3u}.

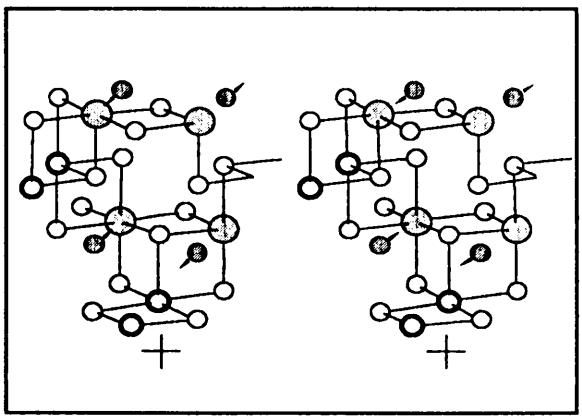

Figure 8.53: Li in the 4c site, y-axis, A_u.

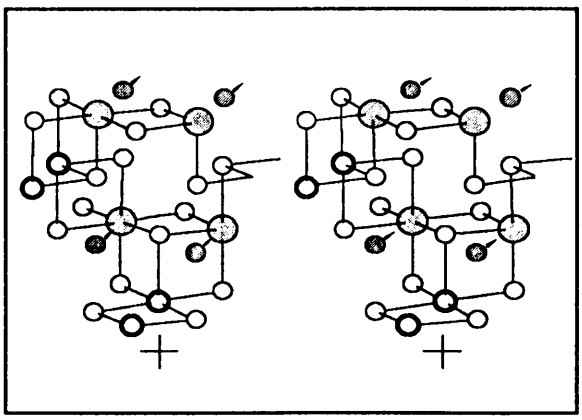

Figure 8.54: Li in the 4c site, y-axis, B_{2u}.

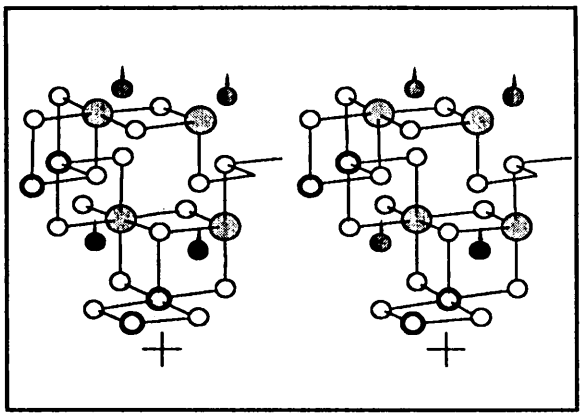

Figure 8.55: Li in the 4c site, z-axis, B_{1u}.

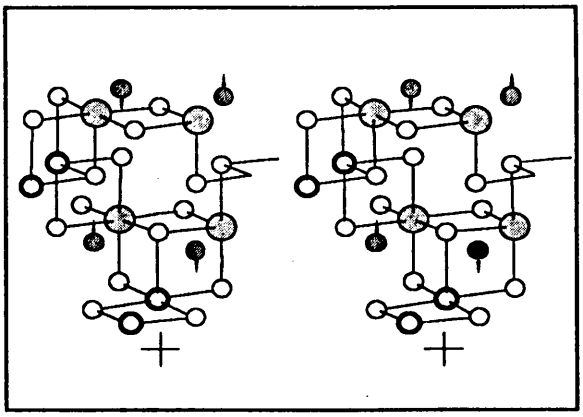

Figure 8.56: Li in the 4c site, z-axis, B_{3u}.

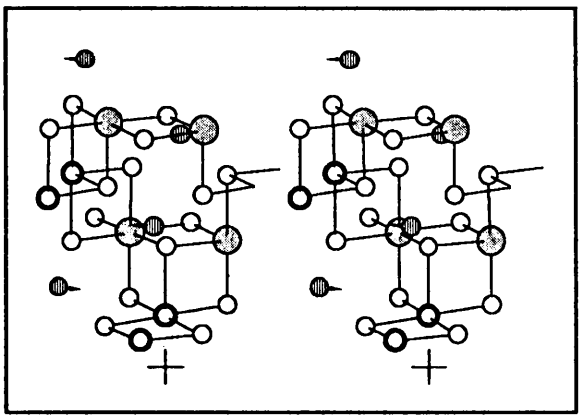

Figure 8.57: Li in the 4e site, x-axis, B_{2g}.

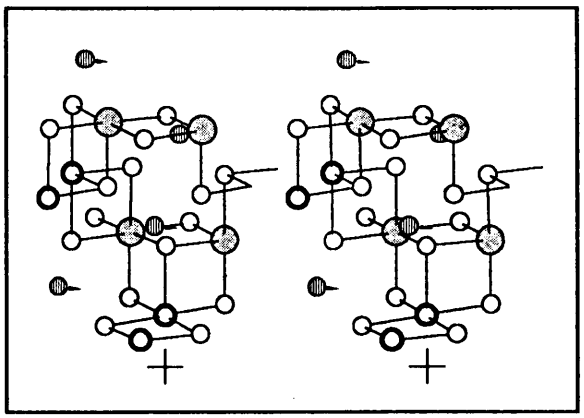

Figure 8.58: Li in the 4e site, x-axis, B_{3u}.

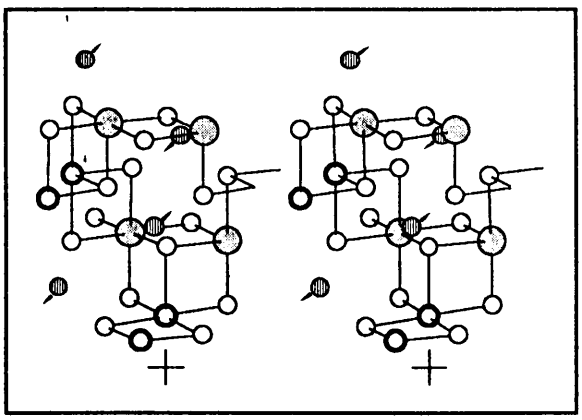

Figure 8.59: Li in the 4e site, y-axis, B_{3g}.

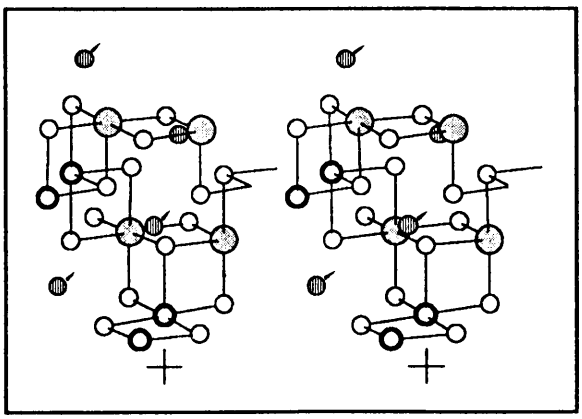

Figure 8.60: Li in the 4e site, y-axis, B_{2u}.

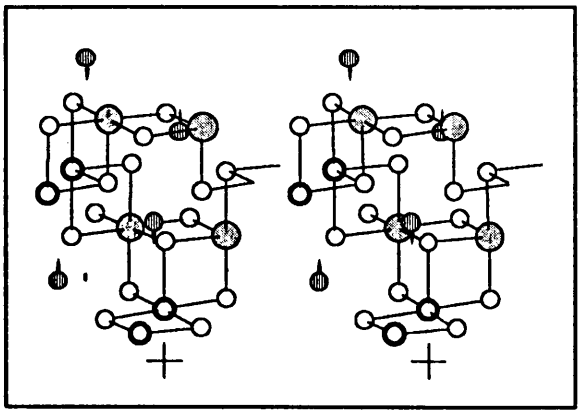

Figure 8.61: Li in the 4e site, z-axis, A_g.

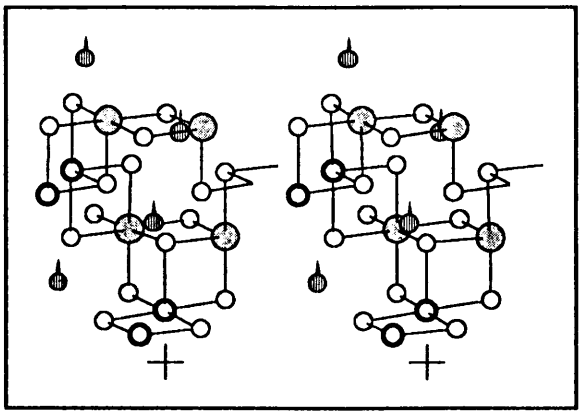

Figure 8.62: Li in the 4e site, z-axis, B_{1u}.

Discussion of the lithium in the tetrahedral positions

If the results for the 4e and the 4c positions are compared an interesting aspect comes to the fore: Although the modes have totally different symmetry, there are some similarity present. In each case the two modes for each direction consists of a acoustical type of mode, where all the atoms of a set move along the axis in unison, and a mode where pairs of atoms in a chain vibrate against each other (see for example Figure 8.52 (4c(x): B_{3u}) and Figure 8.58 (4e(x): B_{3u}) for an example of the acoustical type of mode, or Figure 1.51 (4c(x): B_{1u}) and Figure 8.57 (4e(x): B_{2g}) for an example of the mode where the atoms move against each other). The difference in symmetry arises mainly from the specific alignment of the positions in the unit-cell.

A better discussion may be found in Chapter 9, but a brief explanation of the supposed vibrations of the tetrahedral lithium is necessary. The structure of the cobalt and iron (and the chromium as well) spinels is a distortion of the inverse spinel (as discussed in Chapter 5). The distortion creates a large shift in the position of the tetrahedral lithium (from the tetrahedral positions to the 8i positions within the interstitial octahedron), while the octahedral lithium (and the transition metal) remains in the octahedral positions, with an octahedral surrounding that is hardly distorted at all. It may therefore be safely assumed that the $LiCl_4$-tetrahedron is much more weakly defined, than the Li/MCl_6-octahedron. In fact, the surrounding of the tetrahedral lithium may be taken as a distorted octahedron. Because of this

reason and the fact that lithium is so light as compared to a chlorine atom, any vibration of the tetrahedral lithium will hardly excite any movement from the surrounding chlorine lattice at all. As a result lithium atoms in one chain, connected to other lithium atoms in another chain via chlorine atoms, will hardly couple at all, and may in all probability be taken to vibrate independently.

A very interesting comparison can be drawn between the vibrational modes found for the 4c positions and the filled 8i positions. Inspection of the unit-cell, as well as representations given in Chapter 5, reveals one very interesting feature. In both the 8i and 4c cases, the tetrahedral lithium lies in chains directed along the x-axis. Two chains pass through the unit-cell in the x-direction, and the two chains do not share any common atoms. In the case of the 4c positions, the chains consist of $LiCl_6$-octahedra sharing an edge in the x-direction. In the case of the 8i positions, the chain is exactly the same, except that the one 4c position in the middle of the interstitial octahedron is substituted with two 8i positions, one above and to the one side, and the other below and to the other side of the middle of the interstitial octahedron, in the x-direction. These two chains are not interconnected in any way and the interaction between their vibrations should therefore be negligible. If the movement of the chlorine atoms is taken as minimal in the vibrations concerning the tetrahedral lithium, the vibration of the two chains will be almost independent.

Keeping these considerations in mind, some interesting features of the vibration of the tetrahedral lithium becomes apparent.If the vibration of the 4c positions is considered first, it is clear that all are *ungerade* and therefore infrared, but not Raman, active. It is clear that there are six modes, two for each direction. If the acoustical type of mode is taken to be close to zero in energy (not an unreasonable assumption), three infrared active bands should be observed, if interactions with other modes are ignored. In the case of the 4e positions however, the non-acoustical modes are *gerade*, and therefore Raman active, and no infrared active vibrations should be observed.

In the case of the 8i positions however, a larger variety of modes, both *gerade* and *ungerade*, are present. If the approximation discussed Chapter 6 about the 8i and 4c sites, holds true, some interesting characteristics become apparent. This approximation requires that there is only one lithium atom present in each of the interstitial octahedra over an average of time.

If the two chains are taken to vibrate in isolation as an additional approximation, the four modes found for each direction breaks down into two, viz. a acoustical type of mode, where the atoms in each chain moves in unison along the axes, and a mode where the atoms in each chain moves against each other. If the lower chain in Figure 8.39 is considered, and the upper lithium atom is picked in each interstitial octahedron (i.e. the two lithium atoms with the bigger z-coordinates), the result is a mode where the atoms move against each other, nearly the same as the mode found for the 4c position (Figure 8.51, 4c(x): B_{1u}). If a combination of one upper and one lower lithium in each interstitial octahedron is taken, the result is an acoustical type of mode where the atoms move in unison along the axis, the same as for the 4c position (Figure 8.52, (4c(x): B_{3u}). Although the resulting vibrations are not of exactly the same type as the modes found for the 4c positions, the vibrations of the 4c positions does give a approximation of the vibrations present in the crystal, if the assumptions mentioned above, hold true.

Exactly what implications these findings hold for the actual spectra will be discussed in Chapter 9. It is sufficient at this stage, to point at the advantage of constructing graphical (especially stereographical) representations of the vibrational modes. Without these drawings it would have been impossible to draw any comparisons between the vibrations of the 8i and 4c positions.

Interaction of modes

Unfortunately it seems impossible to predict the nature and size of the interaction of modes of similar symmetry theoretically from symmetry considerations alone. Most people try to overcome this problem by a normal coordinate analysis, but it is often difficult to chose parameters that describe the structure adequately and yet can be calculated with the data available.

Consider for example the four A_g modes in which the chlorine atoms take part (Figure 8.7, Figure 8.11, Figure 8.15 and Figure 8.17). It is certain the two A_g modes of each set will interact and almost as certain that the modes in the different sets will interact with eac other as well, because they contain atoms that are nearest neighbours. The logical way to combine

these modes is by a simple binary method (i.e. adding and subtracting the modes in all possible combinations). Each of the A_g modes can be added or subtracted, yielding a total number of combinations: $2^4 = 16$. For the A_g modes this is summarized in Table 8.3. Note that only the first eight are unique, from combination nine onwards (shaded in the table), the negative of the previous eight combinations are obtained (no. 9 is the negative of no. 8, in the table) and the negative of a vibration is exactly the same as the vibration itself, only taken halfway through the vibration.

1	+ A_g:Cl(1)$_y$ + A_g:Cl(1)$_z$ + A_g:Cl(2)$_x$ + A_g:Cl(2)$_z$
2	+ A_g:Cl(1)$_y$ + A_g:Cl(1)$_z$ + A_g:Cl(2)$_x$ - A_g:Cl(2)$_z$
3	+ A_g:Cl(1)$_y$ + A_g:Cl(1)$_z$ - A_g:Cl(2)$_x$ + A_g:Cl(2)$_z$
4	+ A_g:Cl(1)$_y$ + A_g:Cl(1)$_z$ - A_g:Cl(2)$_x$ - A_g:Cl(2)$_z$
5	+ A_g:Cl(1)$_y$ - A_g:Cl(1)$_z$ + A_g:Cl(2)$_x$ + A_g:Cl(2)$_z$
6	+ A_g:Cl(1)$_y$ - A_g:Cl(1)$_z$ + A_g:Cl(2)$_x$ - A_g:Cl(2)$_z$
7	+ A_g:Cl(1)$_y$ - A_g:Cl(1)$_z$ - A_g:Cl(2)$_x$ + A_g:Cl(2)$_z$
8	+ A_g:Cl(1)$_y$ - A_g:Cl(1)$_z$ - A_g:Cl(2)$_x$ - A_g:Cl(2)$_z$
9	- A_g:Cl(1)$_y$ + A_g:Cl(1)$_z$ + A_g:Cl(2)$_x$ + A_g:Cl(2)$_z$
⋮	⋮ ⋮ ⋮

Table 8.3: Possible combinations of the four A_g modes present.

These combinations may be represented graphically, in a similar way to which the stretching-modes were drawn in Chapter 7 (the vectors of the chorine atoms of different A_g modes, are combined to give one resulting vector each atom). The representations for the first two combinations in the table, may be seen in Figure 8.63 and Figure 8.64 respectively. All the other modes of the same symmetry can be combined in a simmilar way.

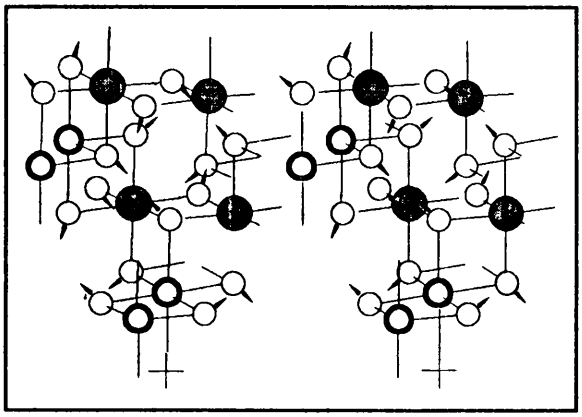

Figure 8.63: Representation of the first combination of A_g modes from Table 8.3.

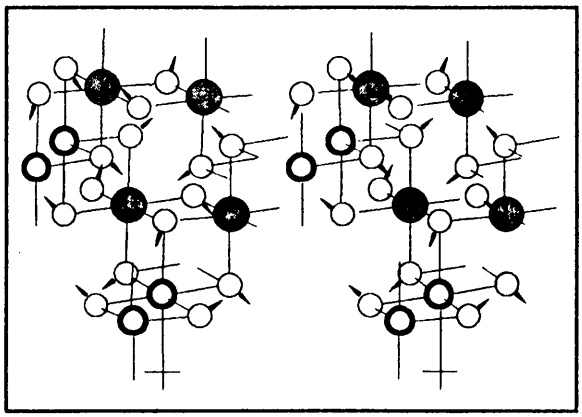

Figure 8.64: Representation of the second combination of A_g modes from Table 8.3.

The big problem with these combinations, is that there are eight, apparently different, combinations of the A_g modes possible. This is impossible, because with a base set of four modes, only four unique combinations must be obtained. Apparently, four of the combinations are not independent. It is not known to the author by what method independent combinations may be obtained. As the symmetrical properties of the positions of the atoms had already been used to obtain the component modes, and as all the components are of the same symmetry, and therefore the combinations are of the same symmetry too, it seems impossible to separate the combinations by some method involving symmetry (the projection operator method does not seem to apply).

Maybe it is possible to determine the relative energies of the different combinations with the aid of a normal coordinate analyses, on this subset of the unit-cell; thus obtaining the combinations that have the same energy (inspection of all these combination reveals that they must be very close in energy) and choosing a representative example. This however, falls beyond the scope of this study and is guaranteed to be an enormous amount of work.

The theoretical interpretation seems to have come to a dead end, just before really interesting results have been obtained. In the next chapter the practical assignment of the spectra is attempted, keeping the theoretical considerations in mind.

PART 4

Practical Interpretations

Chapter 9

Interpretation of spectra

After all the manipulations of the space group on the basis of crystal data, assignment of the actual spectra is attempted. Although an unambiguous assignment seems impossible with the data available, some interesting observations on the nature of the tetrahedral lithium vibrations can be made. The suggestions are, that in disagreement with the oxide spinels, the $LiCl_4$–tetrahedra are much more weakly defined than the $LiCl_6$–octahedra. Some doubt exists in the structure determination of the Li_2CrCl_4, because the position of the tetrahedral lithium has not been resolved unambiguously (see the discussion in Chapter 5). With the aid of the spectra, it is possible to resolve some of that doubt.

Assignment of the tetrahedral lithium

This assignment is attempted first, because it seems to be the easiest. During various chapters (Chapters 5, 6, 7 and 8) the positions (8i positions that may be approximated by the 4c positions) of the lithium in the tetrahedral positions had been discussed. These discussions can be summarized as follows:

First, the lithium does not occupy the true tetrahedral positions (4e) predicted by the inverse spinel structure, but half of the 8i positions (between the 4e sites and the interstitial octahedral 4c sites).

Secondly, the fact that the 8i sites are only half filled and that no real potential barrier exists between the two sites in an interstitial octahedron, indicates that a very fast exchanging of position between these sites is taking place, that may be difficult to restrain, even at very low temperatures. Furthermore, the interstitial octahedra share an edge and exchange of the lithium between different interstitial octahedra is possible, but this movement may be slowed, or excluded, at low temperatures, as there is a potential barrier between different octahedral sites.

Thirdly, although the transition metal obviously prefers the octahedral positions in these chloride spinels (the structure is inverse, with half the lithium in the octahedral and the other half in the tetrahedral positions), the $LiCl_6$-octahedra must be more strongly defined than the $LiCl_4$-tetrahedra. Support for this statement comes from the fact that the octahedral lithium are highly ordered and arranged along the b-axes of the unit-cell with virtually no distortion of the octahedra at all. In contrast, the $LiCl_4$-tetrahedra are highly distorted. So much so, that the lithium really occupies a position in the interstitial octahedron, and its environment may be taken as a slightly distorted octahedron. It does not seem unreasonable to assume that the lithium in the tetrahedral positions are much more loosely associated with the chlorine lattice, than is the case of the true octahedral lithium. The vibrations concerning this tetrahedral lithium should therefore be of much lower energy than that of the octahedral lithium and transition metals. This is in opposition to the results for oxide spinels of similar composition (Tartre [51]), in which the LiO_4-tetrahedra are much more strongly defined than the LiO_6-octahedra. The nature of the anion involved, however, is completely.

Fourthly, the lithium is very much lighter than the chlorine atoms of the lattice and, as said, the tetrahedral lithium is only very loosely associated with the surrounding chlorine lattice, so that any vibrations involving the tetrahedral lithium, must consist mainly of movement by the lithium, with very little vibration of the surrounding lattice. This is an additional reason why the vibration of the tetrahedral lithium must be of low energy.

Fifthly, as the vibration of the tetrahedral lithium was not considered in the chapter on the stretching-mode analysis (Chapter 7) no information can be obtained from this chapter. In addition it would be impractical to apply a stretching-mode analysis to the tetrahedral lithium, as no strongly defined lithium—chlorine type of bond, for the tetrahedral lithium, exists.

Sixthly, if the possible vibrations of all three positions (8i, 4c and 4e), under consideration for the tetrahedral lithium, are considered, the assumption can be made (as discussed in Chapter 8) that the vibration of the lithium, occupying half of the 8i sites, very closely resembles the vibration of an imaginary lithium in the 4e site. As was summarised in Chapter 8, both sites have two types of vibrations for each of the three independent directions; an acoustical type of vibration, where all the lithium atoms move in unison along the axis, and a vibration where the lithium move against each other (The optical vibrations

are B_{1u} along the x-axis, A_u along the y-axes and B_{3u} along the z-axis). To be consistent with the normal splitting of acoustical and optical modes, the former movement should result in a vibration very close to 0 cm^{-1} and should not be observed. The other three vibrations should have a higher energy associated with them, but could not be too much different in energy from each other, because all three movements are essentially of the same type, and may be only slightly affected by the different arrangement of other cations in the various directions. A normal coordinate analyses of this subset may perhaps predict the order of energies of these three modes, but falls beyond the scope of this study. In the case of the true tetrahedral positions, 4e, the picture is completely different. There are an acoustical and a optical type of mode along each axes too, but the symmetry is *gerade* for the optical vibrations and the lithium in this positions, should not show up in the infrared spectra at all, while three extra bands must appear in the Raman spectra.

Seventhly, because the tetrahedral lithium is so loosely contained in the interstitial octahedra, no great coupling is expected with other modes of the same symmetry. If any mixing is observed at all, it should merely be a slight broadening of all bands.

A rough assignment of the bands involving the vibration of the tetrahedral lithium, should be possible on the above observations. If the low energy regions of the far-infrared spectra of the iron, cobalt and chromium spinels (Chapter 4) are inspected in the region 300 cm^{-1} to 100 cm^{-1} a broad band, that shows some splitting, is observed for al three compounds. The spectra of the iron and chromium spinels can be resolved clearly, but the spectra for the cobalt spinel is difficult due to a lot of noise in the low-energy region 150 cm^{-1} to 0 cm^{-1}. A summary of the spectra for this region is repeated in Table 9.1 (the same symbolism as in Chapter 4 is used).

Li_2FeCl_4	Li_2CoCl_4	Li_2CrCl_4
~154sh↓	~155sh↓	~ 140sh↓
182	172	175
207	?202sh↑	~~185sh↑
231	238	230sh↑

Table 9.1: Infrared band associated with the tetrahedral lithium (energy in cm^{-1}).

What is immediately obvious, is that there are three bands in this region of the far-infrared spectrum, for all three compounds. It seems reasonable to assign these bands to the vibration

of the tetrahedral lithium (found in the interstitial octahedra) for which three modes were predicted. Three main bands with a shoulder at lower energy of the lowest energy band were observed. A better assignment in which each band is associated with a particular vibrational mode, is impossible on the spectral and theoretical data. A normal coordinate analysis of this subset of the structure may reveal the order of energies of the three modes, and permit a better assignment.

Three features of these bands are apparent. First, there is a lot of noise associated with the bands, especially at room temperature. Secondly, the bands are very broad and not clearly resolved. Thirdly, cooling the compounds to 80 K does not improve the quality of the spectra significantly, nor are the bands any sharper. Apart from the normal problems with noise associated with this part of the far-infrared spectrum, one conclusion for these features may be that the movement of the lithium is responsible. The fact that the 80 K spectra do not show any improvement indicates that the movement of the lithium is not restricted to any great extent. It may be that the movement between the octahedra are restricted, but the movement within each interstitial octahedron is unaffected.

A final but important conclusion may be drawn from the spectra of the chromium spinel. As stated in Chapter 5, Kanno, Takeda and co-workers were unable to resolve the position of the tetrahedral lithium clearly, due to a lack of data. The similarity between the spectra of the chromium spinel on the one hand, and the cobalt and iron spinels on the other, definitely indicates that the lithium occupies a similar position in the chromium spinels, as in the other two spinels. Because there is no great difference between the two types of compounds, except for a small distortion of the lattice, it seems safe to assume that the tetrahedral lithium occupies a position in the interstitial octahedron, in the chromium spinel as well. The only difference between the spectra of the chromium spinel an the other two spinels, lies in the fact that the bands in the chromium spinel are less resolved and show up as shoulders. This may be due to the lower symmetry of the chromium spinel space group, resulting in greater similarity between the modes. Unfortunately there seems to be an error in the positions reported by Kanno, Takeda and co-workers for the chromium spinel. As discussed in Chapter 5, the positions reported, do not fit in with the data obtained from the Tables for Crystallography, for the C2/c space group. This prevented the author from obtaining the

symmetry of the interstitial octahedral site, or a site associated with the 8i positions, to carry out a correlation to obtain the expected modes.

Vibration of the octahedral metals and the chlorine lattice

All the pure lattice vibrations (the vibrations involving only the chlorine atoms) are *gerade* (see Chapter 8) and therefore not visible in the infrared spectra. These lattice modes will be of relatively low energy, and may fall in the same aria as the vibrations of the tetrahedral lithium, discussed in the previous section. All the *ungerade* modes, and therefore visible in the infrared, involve some movement by a metal.

If the spectra of the three spinels (Chapter 4) are examined in the region 1000 cm^{-1} to 250 cm^{-1} seven bands are observed for the cobalt and iron spinels and nine or ten for the chromium spinel. This is much less than the expected 24 modes. Some reasons for this may be as follows:

First, the correlation method, as well as the method developed in Chapter 8, only predicts the number and nature of the modes and not the size of the splitting between them. If the splitting is small between a large number of similar bands, the bands will not be resolved in the spectra. In this case most of the observed bands are broad and may perhaps be associated with more than one mode.

Secondly, a lot of the modes shown in Chapter 8 appear to be similar and are expected to have similar energies (a normal coordinate analysis may go some way to clear this doubt). Furthermore the amount and type of interaction between the modes are not known, and due to the absence of clear spectral evidence unlikely to be resolved empirically.

Thirdly, the spectra are not of sufficient quality to identify bands and their position to such an extend as to be unambiguous and no precise measurements of shift of bands between the three compounds can be made.

A further assignment of the octahedral modes seems impossible, and without further knowledge as to the strength of the Li—Cl and Cr/Fe/Co—Cl bonds, bands can not be associated with one or the other. The best that can be said is that the bands in the region 1000 cm^{-1} to 250 cm^{-1} is associated with vibration of the metals in the octahedral positions.

No pure lattice modes are observed in the infrared spectra, because all these modes are only active in the Raman spectra (Chapter 6). The energy of the bands in the Raman spectra should therefore be lower than most of the bands in the infrared spectra.

A great similarity exists between the spectra of the iron and cobalt spinels on the one hand, and the spectra of the chromium spinel on the other (there are some more modes present). The difference between the two types of compounds can therefore be not very great and, as discussed in Chapter 5, they must have similar structures.

PART 5

Critical Assessment

Chapter 10

Critical assessment

In this chapter, the methods tried in this study are evaluated critically, with the conclusion that they do not totally predict vibrational behaviour. The choice of the spinel compounds of this text, for a vibrational analysis, is considered and although a satisfactory assignment seems impossible, some interpretation of the behaviour of the tetrahedral lithium is possible. This discussion is concluded by answering the questions posed at the end of the introduction.

Assessment of the theoretical interpretations

If the correlation method (as suggested by Fateley, Dollish and co-workers [5], and carried out in Chapter 6) is considered critically, with special attention to its application in this text, some observations can be made. First, as stressed extensively during this text, this method fail to give an understanding of the vibrational modes present in a crystal, beyond the symmetry and number of normal modes present. Other serious drawbacks are the method's inability to cope with disorder in sites, and sites that are only partially occupied. In this study, the inability to cope with disorder in sites (e.g. the mixing of the octahedral lithium and the transition metal in the 4b site) does not present too great a problem, as the amount of mixing is small and may be taken as a slight perturbation of the ideal case. In cases where substantial mixing takes place, the method will not provide an accurate prediction of the modes present. Due to the statistical nature of this mixing, it seems unlikely that a theoretical method, for predicting vibrational behaviour from symmetry considerations alone, is possible. The second drawback, that of the inability to cope with partially filled sites, is more serious, because the only possible correlation (with the site taken as filled) yields a completely false picture. The disorder, because of the distribution amongst the sites, will result in a substantial difference from the modes predicted. Approximation of these sites, with sites of lower symmetry, as attempted in this text for the tetrahedral lithium, seems the only alternative, but then some information about the distribution is necessary, and some assumptions must be made.

A critical evaluation of the line group approach is desperately needed. This evaluation will have to include an investigation into the bond types and strengths needed to be able to define a chain. Just as important is an investigation into the role of interconnection between chains, as crystals where chains are completely isolated, without any possibility of interaction, are very rare. It was optimistic to apply the line group method to the spinels of this text (Chapter 6), because the chains are clearly not bonded strongly enough. The amount of interaction between the different chains, contribute largely to render the results of this line group analysis almost useless. Still, an understanding of these 'supposed' chains, aids the understanding of the crystal structure.

A stretching-mode analysis is always useful as an approximation, because it often yields very useful results and is usually not too difficult in its application. It is of special importance in cases where a crystal consists of discrete molecular units, where the internal vibrations of each of these units, are much stronger than the vibrations of the crystal lattice, build up by these units. The main problem with a stretching-mode analysis, is often the difficulty with the associated bending-mode analysis. It is often very difficult to assign the appropriate amount and types of bonding and torsion interactions necessary, and most assignments remains ambiguous. In the case of an inorganic crystal, such as the examples of this text, no clearly defined bonds exist, and some interactions between atoms, are only marginally stronger than others. Secondly, because of the constrained nature of the crystal, all bending interactions must have a stretching component between some atoms, and vice versa. If a crystal structure is accurately represented by a set of 'imaginary' bonds, the symmetrical manipulations of these bonds, should result in all the modes being found, and give an acceptable representation of the vibrations present in the crystal. It is not always easy to select these bonds, and some doubt as to the applicability of a specific selection will always remain. In the stretching-mode analysis attempted in this text, a logical set of bonds, to define octahedra (a structural element present in many crystal structures), has been chosen. As was discussed in Chapter 7, this representation does not yield all the modes in the case of the octahedral metal vibrations. It seems that the bonds selected do not describe this part of the structure accurately enough to yield all the modes (although the lattice is clearly, well described). Any other selection of bonds however, will not be as logic, and will at best be acceptable, but not unambiguous.

A vibrational analysis, from the first principles described in Chapter 8, yields all the modes predicted by the correlation and, as such, is useful. It also allows the construction of graphical representations of the normal modes present in the crystal. This is of aid in the interpretation of spectra, as was discussed for the tetrahedral lithium (Chapter 9). A true picture of the vibrations is still unreachable, because of the difficulty with interaction between modes of similar symmetry, discussed in Chapter 9.

The bridge between the structure and the vibrational spectra is still not completed. Just at the critical part, the developed theory fails. It is probably naive to expect a method based on symmetrical qualities only, to explain the vibrational spectra fully. A more integrated approach to vibrational spectroscopy is called for. Every aspect of structure (e.g. bond types and strengths, electronic and ionic behaviour etc.) needs to be considered, before any accurate prediction can be made. This text falls short in this aspect as only symmetrical methods were considered, and perhaps the failure of these methods in this text, stresses the need for consideration of other factors involved. Hopefully a clearer picture of matter in the solid state will evolve eventually, with all the structural traits considered interactively. Vibrational analyses will form an important part of this picture and it is hoped that a method will be evolved eventually, whereby vibrational spectra can be explained and predicted theoretically.

Assessment of the practical interpretations

As discussed in Chapter 9, a complete assignment of the chloride spinels is impossible. An inspection of the spectra in Chapter 4, reveals that they are of insufficient quality to make a complete assignment. Perhaps future researchers may obtain better infrared spectra, as well as Raman spectra, to complete the assignment.

Keeping the above mentioned reservations in mind, the chloride spinels, studied in this text, do not lend themselves well to vibrational analysis. This does not mean that all difficult examples should be discarded, and further attempts to overcome the problems will certainly be interesting. But, in order to develop the theoretical methods further, a clearer and easier example should be selected.

The assignment of the vibrations of the tetrahedral lithium is satisfactory, especially as it confirms the positions found by Kanno, Takeda and co-workers. Furthermore, a prediction about the position of the tetrahedral lithium in the chromium compound, could be made, thus stressing the importance of vibrational spectroscopy in cases where X-ray methods fail (especially in cases where a small and light atom is reasonably close to a big atom in the structure). Not many of these types of structure clarifications of spinel structures, with the aid of vibrational spectroscopy, have been attempted, and one of the best examples is the study by Tartre [51].

Attempts to assign the rest of the spectra, failed, an unsatisfactory result, but the gap between theory and practice is stressed by this failure.

Conclusions

The vibrational methods developed in this text does not bridge the gap between structure and spectra completely, although they proceed a substantial amount from a mere correlation, and do ease the interpretation somewhat.

It was not possible to assign the spectra of the spinel compounds unambiguously and completely. Some interesting observations on the vibrational behaviour of the tetrahedral lithium was possible however, and the vibrational study was not completely unsuccessful.

Appendixes

Appendix A

Obtaining and viewing the stereographic representations

In order to make use of the stereographic projections used extensively in this text, instructions for viewing are provided. A motivation for the use of stereographic representations is given. The mechanism behind these stereographic pictures is discussed briefly and a brief overview of the construction of these representations, is given.

Motivation for the use of stereographic representations

Many people have difficulty visualising three-dimensional molecular and crystal structures. The obvious solution to this problem, is the use of molecular models and building sets. One of the main drawbacks of these sets however, is that they do not allow the construction of many of the crystal structures particular to solid state, inorganic chemistry. Although the use of models is certainly recommended, this text will contain another form of three-dimensional representation. The use of stereographic representations, although difficult to produce at times, is an enormous aid in understanding crystal structures, as it offer a true three-dimensional view, and does not rely on plane projections as many other representations do.

Mechanism behind the stereographic representations

This stereographic technique uses the brain's way of judging distance. Without going into extensive biological detail, the principle is as follows: One eye (usually the right eye in right-handed people) looks straight at an object. The other eye, being on the other side of the nose, is slightly offset, and therefore looks at the object at an angle. From this angle, the

objects will appear to have depth, because of the different distances to different parts of the object (this is not the only way of perceiving depth however, at greater distances, the brain uses the size of an object and other principles of perspective, to judge distance).

The brain can be fooled into believing an object three-dimensional, by presenting each eye with a slightly different view of the object. The view presented to the left eye, is rotated by a slight amount, around the vertical axis, from the view presented to the right eye. The brain interprets this rotation angle as depth and the image is seen in three dimensions.

Method of viewing the stereographic representations

An example of the type of stereographic images used in this text, may be seen in Figure A.1. There are two methods of viewing the image in three dimensions. The first is as follows: Hold the figure about twenty centimetres away from the eyes. Try to focus on an object about two to three meters behind the paper while looking at the paper. After about two or three minutes of practice, the structure will stand out in three dimensions. If the three-dimensional effect is obtained once, it is usually easier thereafter. The other method is to use the two crosses at the bottom of the two images in the stereographic projection. While looking at the two crosses on the picture at a distance of about twenty centimetres, extend the focus of the eyes slowly as if looking at an object moving away. The two crosses will appear to be moving closer to each other. Once the crosses overlap exactly, look slowly upwards at the image, while maintaining the same focus, and the figure should appear in three dimensions. As before, practise makes perfect. In both the aforementioned methods, it is essential to keep the head and the paper, with the figure on it, exactly horizontal. These projections are called normal-eyed or relaxed-eyed representations.

Some people, cannot view the projections in this way and use a different method. These people look at the left image with their right eyes, and at the right image with their left eyes. This is called the cross-eyed method. A bit of thought about the processes involved will explain the phenomenon, that these people see the image with those parts that should appear

at the front, at the back, and visa versa. By exchanging the two sides of the projection however, the three-dimensional image will appear normal to these people.

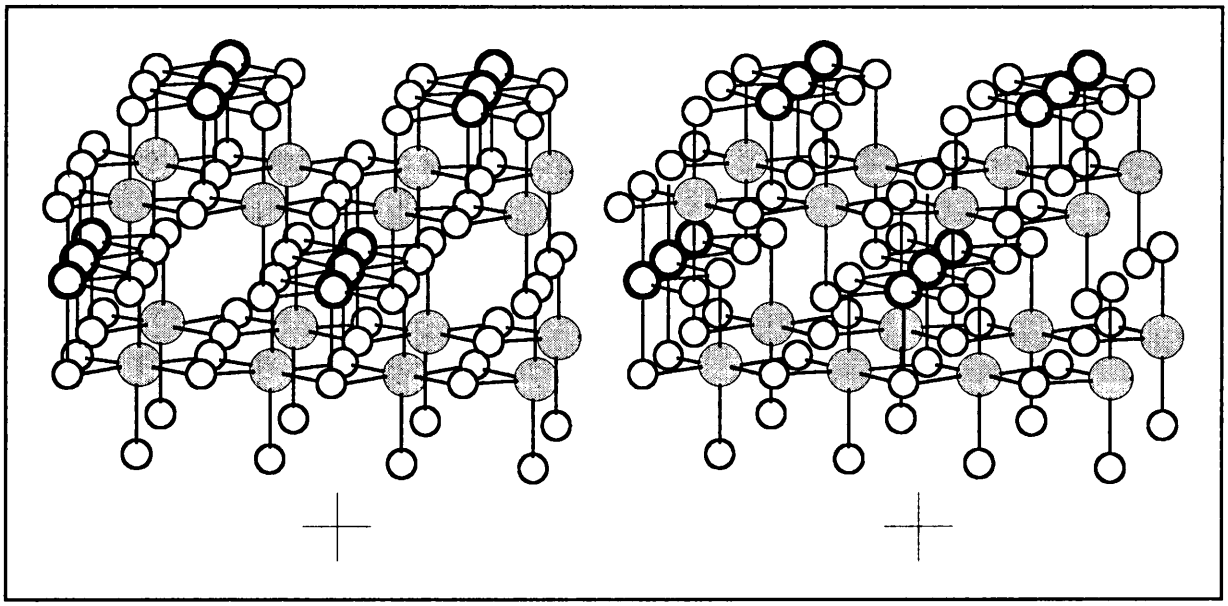

Figure A.1: Example of a normal-eyed projection.

An example of this type of projection appears in Figure A.2. Many people find it easier to use this projection. The best way of viewing the projection is to look at the two crosses at the bottom of the two images in the projection, while holding the paper about twenty centimetres away from the eyes. By squinting slightly (like looking at the tip of one's nose), there should appear four crosses. Variate the squint slightly, until the two inside crosses appear to overlap. By looking slowly up at the image, the three-dimensional picture should be seen. This process may be aided by looking at a finger right in front of the nose. Slowly move the finger towards the page, until in front of the page under the crosses. The two crosses in the middle should now appear to overlap and the image should be seen in three dimensions. This projection is called a cross-eyed projection, because the eyes look across each other at oposite immages.

Because most people use the normal projection, this is the projection that is used throughout the text. For those people that have trouble with this projection, the cross-eyed versions of all the stereographic projections in the text, are assembled in Appendix B. The figures are

sorted according to chapters, and the original figure number and the caption are repeated for clarity.

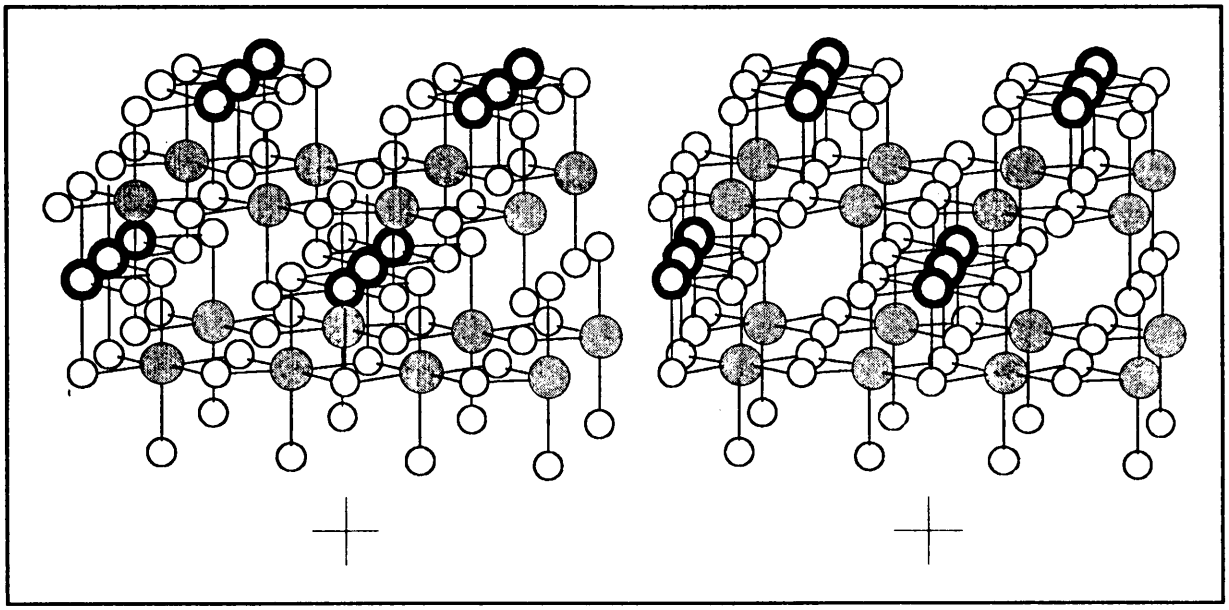

Figure A.2: Example of a cross-eyed representation.

Creation of the stereographic representations

Unfortunately, there is no computer package available (to the author's knowledge) that enables easy construction of these stereographic representations, and several packages were used by the author to obtain one representation.

The package that produced the original stereographic representations, used throughout, is the Alchemy II program [64] (see the discussion later on, about Alchemy III). As input this program needs an input file in a specific format, containing the lattice constants and fractional coordinates of the atoms to be represented (a .CRY file). Refer to the Alchemy documentation for a description of the operation of the program, as well as for the format of the input file. It is also necessary to update the Alchemy files ATOMDEF.TAB and BNDINFO.TAB as the program is designed for organic chemists (e.g. the program does not

recognise an octahedral oxygen or chlorine atom). This is very easy and explained in the appendixes of the documentation.

The alchemy input file must contain the fractional coordinates of all the atoms to be represented, so all the positions in the unit-cell should be generated and entered, with any MS-DOS text editor (beware of Windows text editors, as these editors produce ANSI text, that are somewhat different from ASCII text used by Alchemy). If more than one unit-cell is to be represented, the generation of the coordinates for the additional unit-cells, by hand, can be tedious and a simple Turbo Pascal [71] program may be used to generate the positions in additional unit-cells. A sample program may be found in the next section. This program is documented to be self-explanatory.

Once the correct viewing perspective has been obtained in Alchemy II, the 'Ball and Stick to File' option is used to produce a HPGL (Hewlet Packard graphic language) file. This file may be directly used by a word processor (such as Wordperfect [72] used for this text), or edited by a vector graphics package (such as DrawPerfect [68]). The problem with these images is that they are wire-frame (no filling of objects) pictures, and very difficult to interpret, if not outputted to a colour graphics device (such as a plotter). An example of such an image may be seen in Figure A.3. Alchemy is also unable to draw the vibrational modes and various other enhancements of figures, produced in this text.

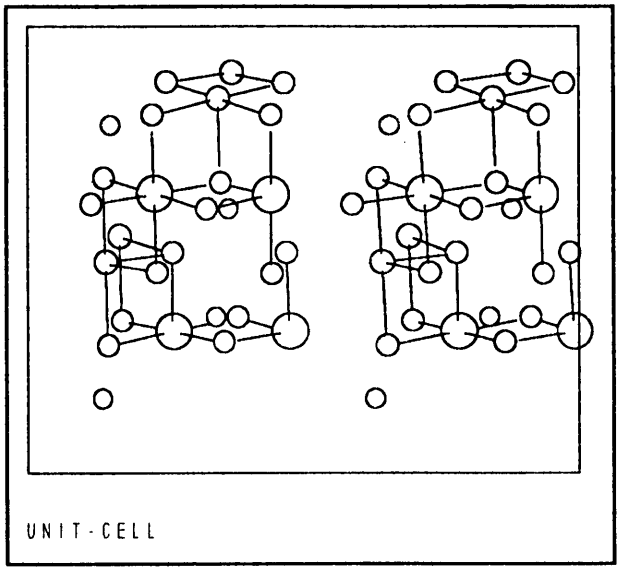

Figure A.3: Example of an output fule produced by Alchemy II.

In order to make the graphics more presentable, a vector graphics package, DrawPerfect, was used (a far more advanced package that offer a large amount of effects, as well as better manipulation tools than DrawPerfect, is CorelDRAW! [66]). This package was used to substitute filled circles for empty circles, representing atoms. Additional lines and vibrational directions were drawn in. The trouble with the stereographic representations, is that any

object must be drawn in the right direction in each of the two images in each representation, in order to obtain the desired three-dimensional position. This requires some care, as it often necessitates the use of guide lines (stored as a template, to be removed later) to orientate arrows and other objects, correctly. An example of a figure with these guide lines, may be seen in Figure A.4. The result is a figure in a format that can be handled by a word processor like WordPerfect.

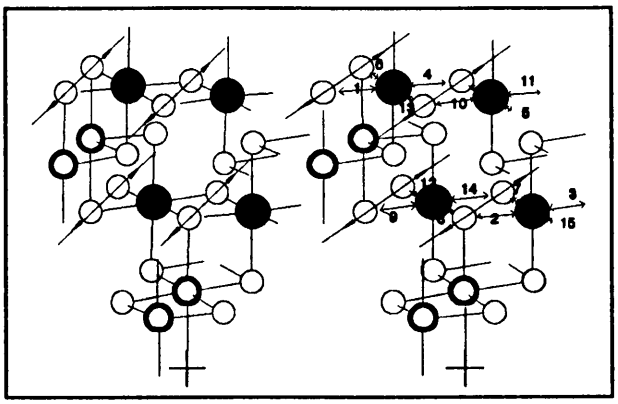

Figure A.4: An example of the guide lines represent a vibration.

A newer version of Alchemy, Alchemy III [65], is available. The problem with this package, is that it cannot produce output of 'ball and stick' and 'spacefill' models to a vector format available to graphics packages (it may be worth mentioning that this program contains some serious bugs, and is very slow when compared to Alchemy II, for the same operations). In stead, it produces output in Hewlet Packard Laserjet Printer language (PCL5), that can be printed on a laser printer. If really necessary, this format can be transformed to a format available to graphics packages, by a conversion program like Image Alchemy [69] (not to be confused with the Alchemy discussed before). The problem with this conversion is that it produces a file in bitmap format, that cannot be manipulated, in the usual way, by vector graphics packages. If the situation is desperate however, these bitmapped graphics may be converted to vector graphics, by a program like CorelTRACE! [67], although this conversion is not always very successful, and needs a lot of subsequent editing.

Program for the extension of unit-cell coordinates to other unit-cells

```
program convert;
{*****************************************************************************
 * Conversion program to add additional unit-cells to Alchemy II *.CRY      *
 *   files. This is accomplished by bits of code added to the program       *
 *   by the user to generate specific adjacent unit-cells.                  *
 * E.g. a segment containing the code:                                      *
 *      XposReal := XposReal + 1                                            *
 *   will ad the coordinates of the unit-cell adjacent in the positive      *
 *   x-axis direction to the input file.                                    *
```

```
*                                                                              *
* InTxtFile must be assigned to a valid Alchemy II *.CRY file                  *
*   (no error checking is done!)                                               *
* OutTxtFile may be assigned to any name (remember the .CRY extension)         *
*   and will be a valid Alchemy II *.CRY file                                  *
*                                                                              *
* Alchemy II *.CRY files are ASCII files that have the following               *
*   structure which must be adhered to:                                        *
*                                                                              *
* Atomtype Xpos      Ypos      Zpos                                            *
*          1         2         3         4                                    *
* 12345678901234567890123456789012345678901234567890                          *
* ------------------------------------------------------------------           *
* 7.1772 7.2478 10.2785 90 90 90                                               *
* Li0      0.000     0.000     0.500                                           *
* Co0      0.250     0.250     0.750                                           *
* Cl2      0.246     0.250    -0.009                                           *
*  .                                                                           *
*  .                                                                           *
*  .                                                                           *
* Cl2      0.746     0.250     0.509                                           *
* ------------------------------------------------------------------           *
* Atomtype must be a valid Alchemy II Atom Type or one added by the user       *
* The first line contains the unit-cell data in the following format:          *
*   a(Å) b(Å) c(Å) α(°) β(°) γ(°)                                              *
* Columns must be set up using spaces and not tabstops                         *
*                                                                              *
*                                        G C van Rooyen                        *
*                                        7 September 1992                      *
********************************************************************************}

Uses Crt;

Var
  CodeInt                   : Integer;     { Not used, required by Val     }

  XposReal, YposReal,
  ZposReal                  : Real;        { Unit-cell fractional coordi-
                                             nates                           }
  AtomtypeSt                : String[8];   { String for Alchemy II Atom
                                             type from LineSt                }
  FirstLineSt               : String[50];  { String for Unit-cell parama-
                                             ters from the first line of
                                             InTxtFile                       }
  LineSt                    : String[50];  { String for each line except
                                             first from InTxtFile            }
  XposSt, YposSt, ZposSt    : String[6];   { Strings for pos. from LineSt  }

  InTxtFile                 : Text;        { Input Text file, must be as-
                                             signed to a valid Alchemy II
                                             *.CRY with a valid DOS path    }
  OutTxtFile                : Text         { Output Text file, in Alchemy
                                             II *.CRY format, must be as-
                                             signed to a valid DOS filename
                                             and path                        }
{end Var};



begin {program convert}
                                         { Program message                 }
  Crt.ClrScr;
  WriteLn('Program Convert executing...');

                                         { Assign the Input and Output
                                           text files and prepares them
                                           for reading and writing re-
                                           spectively                      }
  Assign(InTxtFile, 'path:infile.CRY');
  Assign(OutTxtFile, 'path:outfile.CRY');
  Reset(InTxtFile);
  Rewrite(OutTxtFile);
                                         { Read the first line, contai-
                                           ning unit-cell information
                                           from InTextFile and write it
```

```
                                        to OutTextFile                  }
  ReadLn(InTxtFile, FirstLineSt);
  WriteLn(OutTxtFile, FirstLineSt);

  While NOT Eof(InTxtFile) do           { Continue untill all the lines }
  begin                                 { are read from InTextFile      }


    ReadLn(InTxtFile, LineSt);          { Read a line from InTextFile   }

                                        { Break up the line in the Atom
                                          definition and the fractional
                                          coordinates                   }
    AtomtypeSt := Copy(LineSt,  1, 8);
    XposSt     := Copy(LineSt,  9, 6);
    YposSt     := Copy(LineSt, 19, 6);
    ZposSt     := Copy(LineSt, 29, 6);

                                        { Convert the positions, which
                                          are in strings to numbers so
                                          that they may be manipulated  }
    Val(XposSt, XposReal, CodeInt);
    Val(YposSt, YposReal, CodeInt);
    Val(ZposSt, ZposReal, CodeInt);

                                        { Write the orriginal position
                                          to OutTxtFile                 }
    WriteLn(OutTxtFile, AtomtypeSt, XposReal:6:3, '    ',
                                    YposReal:6:3, '    ',
                                    ZposReal:6:3);

                                        { Generate coordinates in an
                                          adjacent unit-cell for the
                                          specific atom whose line is
                                          currently being manipulated
                                          and write the new position
                                          to OutTxtFile                 }
    XposReal := XposReal + 1;
    WriteLn(OutTxtFile, AtomtypeSt, XposReal:6:3, '    ',
                                    YposReal:6:3, '    ',
                                    ZposReal:6:3);
    XposReal := Xposreal - 1;           { Reset the position            }

                                        { Do the same for another
                                          adjacent unit-cell            }
    YposReal := YposReal + 1;
    WriteLn(OutTxtFile, AtomtypeSt, XposReal:6:3, '    ',
                                    YposReal:6:3, '    ',
                                    ZposReal:6:3);
    YposReal := YposReal - 1;           { Reset the position            }


   {************************************************************************
    * Any other unit-cell may be generated in the same way, by incremen-   *
    *   ting or decrementing XposReal, YposReal and ZposReal respectively  *
    *   or in combinations. The line beginning with WriteLn(OutFile...     *
    *   must be included in each part. It must be remembered to reset the  *
    *   values of XposReal, YposReal and ZposReal after each part in order *
    *   that another unit-cell may be generated.                           *
    ************************************************************************}

  end
  {end While};
                                        { Close the files used in this
                                          program                       }
  Close(InTxtFile);
  Close(OutTxtFile);

                                        { End message                   }
  WriteLn('Program Convert completed.');
  Write('Press any key to continue..');
  repeat until Crt.KeyPressed;

end
{end program convert}.
```

Appendix B

Collection of the cross-eyed stereographic representations

In this appendix, all the cross-eyed versions of the normal- (or relaxed-) eyed stereographic representations used in this text, are collected. These representations are given, because people using the cross-eyed method, are often unable to use the normal-eyed method. The representations are listed under their respective chapter headings, but sub-headings are not given. All captions are repeated.

Chapter 5

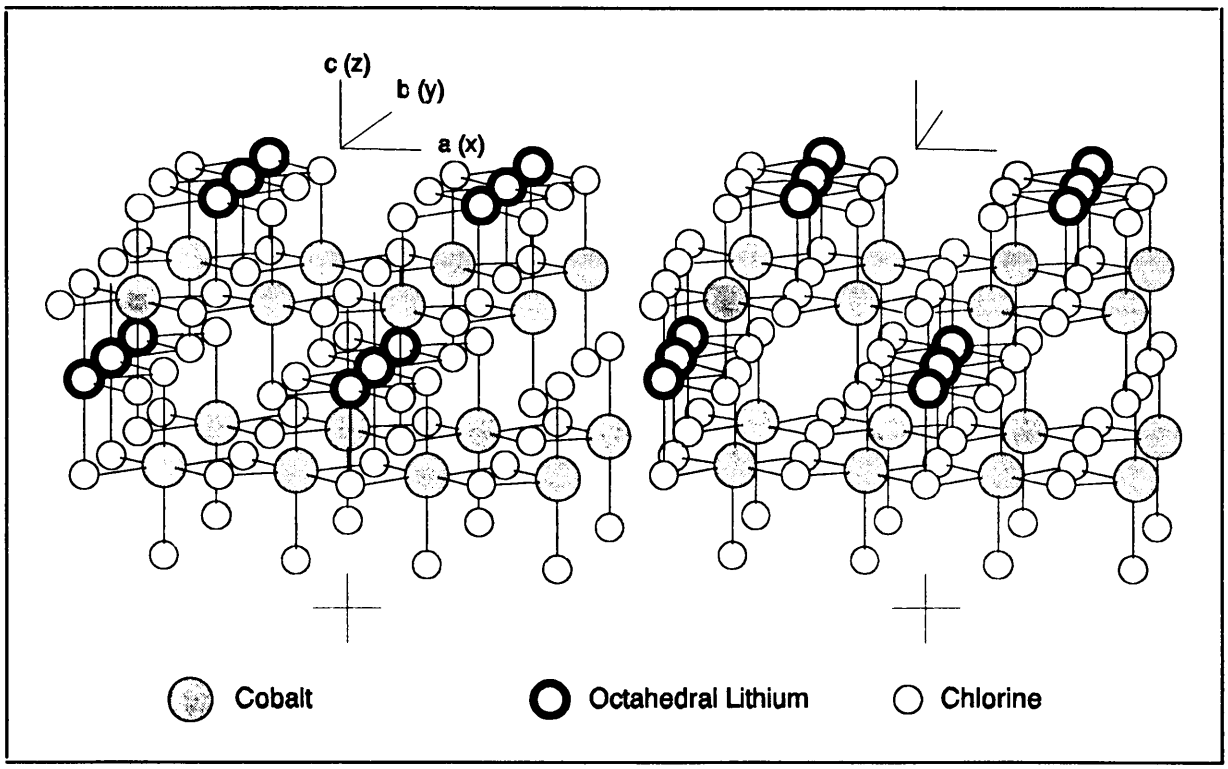

Figure 5.1: Stereographic representation of three adjacent unit-cells for the cobalt spinel, without the tetrahedral lithium.

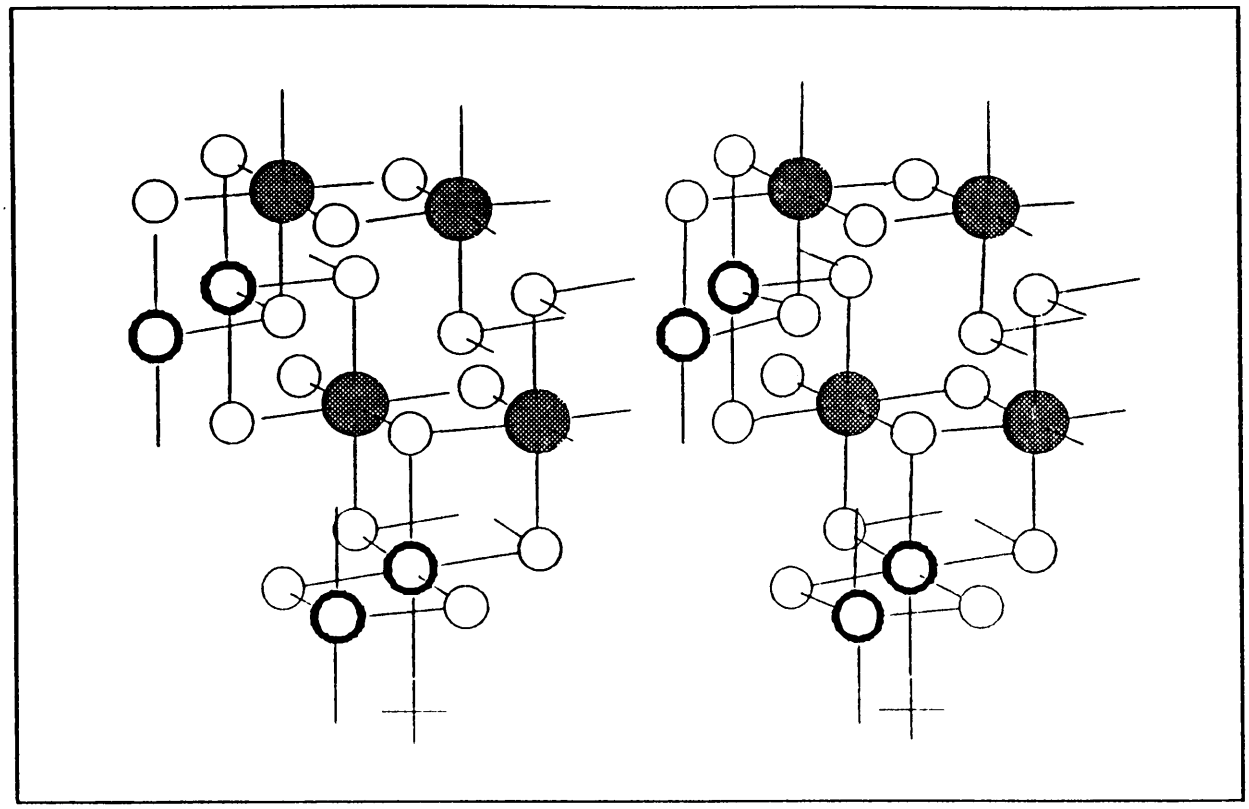

Figure 5.2: Stereographic projection of the unit-cell of the iron and cobalt spinels.

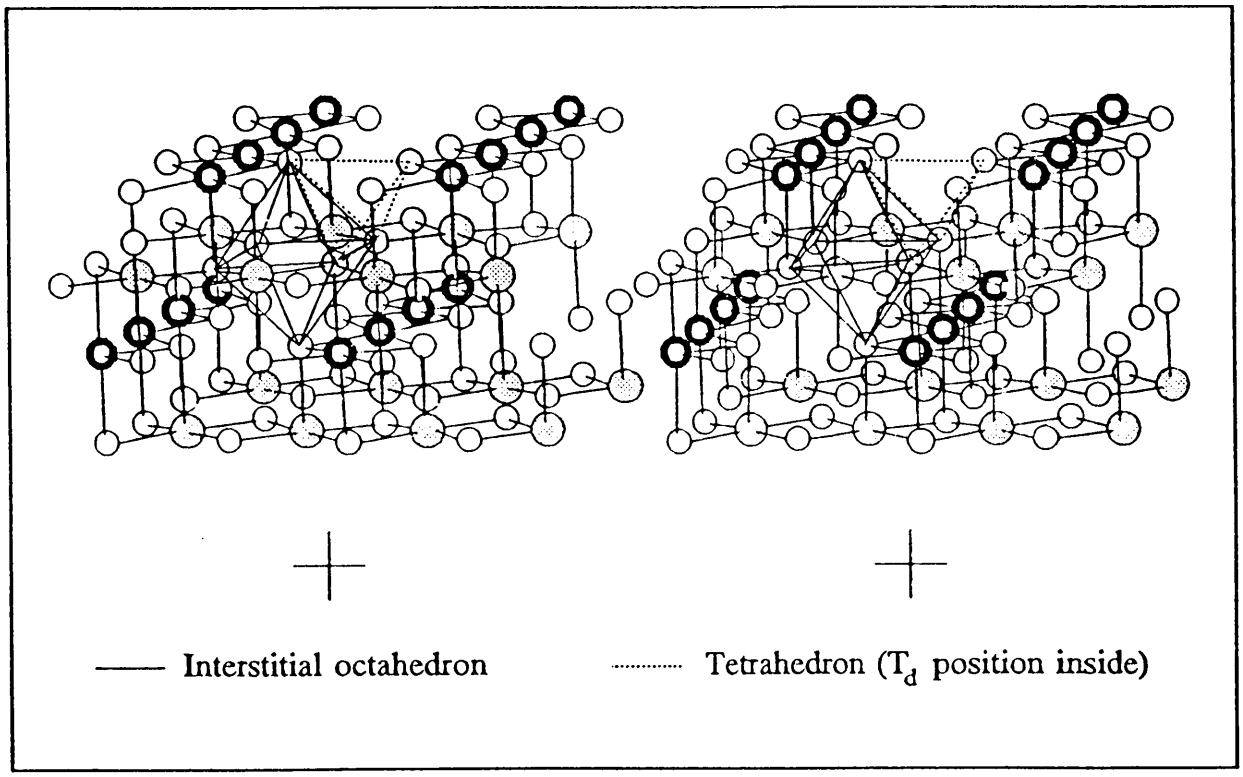

Figure 5.3: Representation of the cobalt spinel, with the interstitial octahedron and tetrahedron containing the tetrahedral position, indicated.

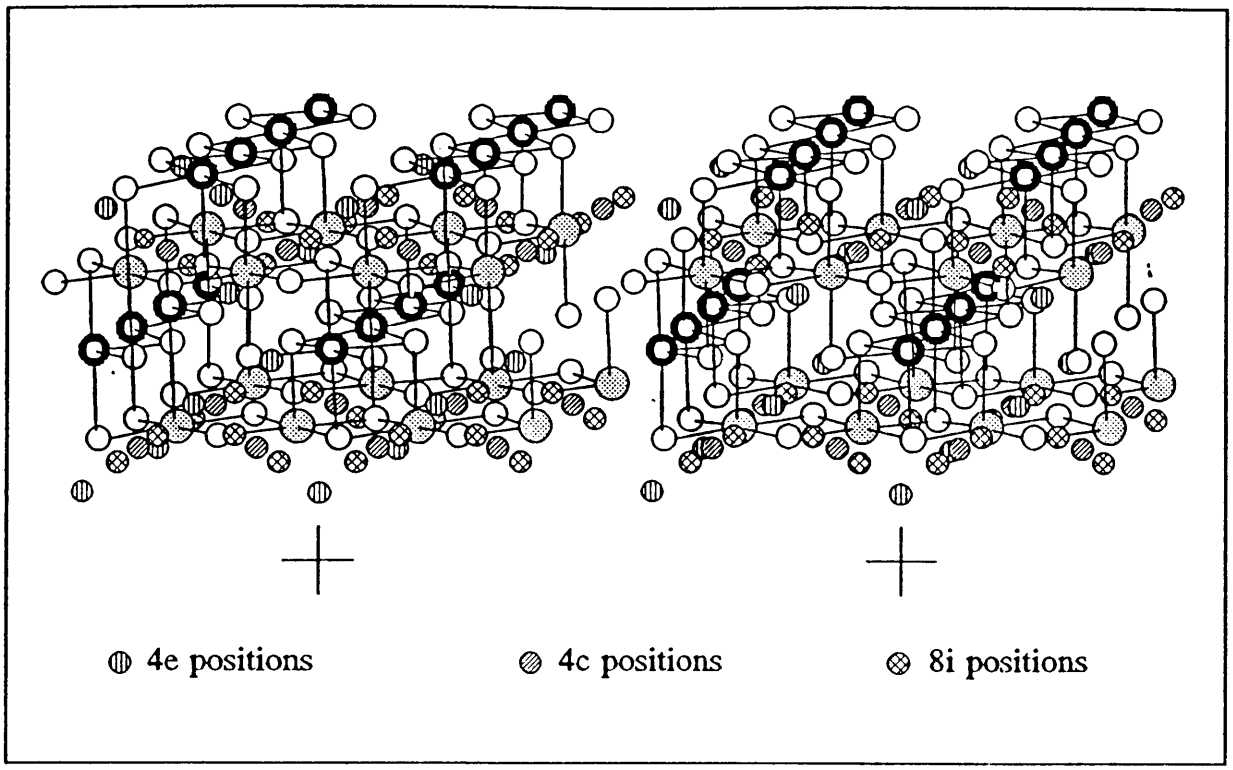

Figure 5.4: Representation of the cobalt spinel, with the 4c, 4e and 8i positions indicated.

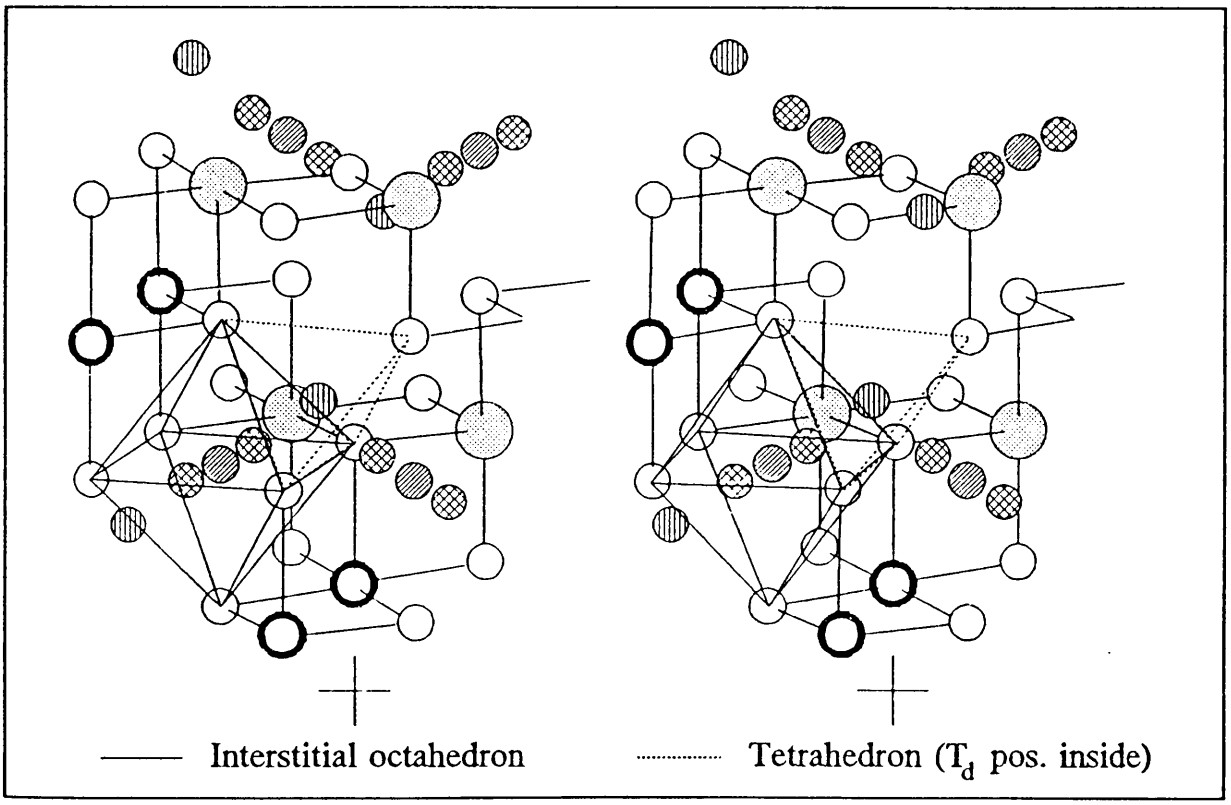

Figure 5.5: Unit-cell of the cobalt spinel, with the interstitial octahedron, tetrahedron, 4c, 4e and 8i positions indicated.

Chapter 7

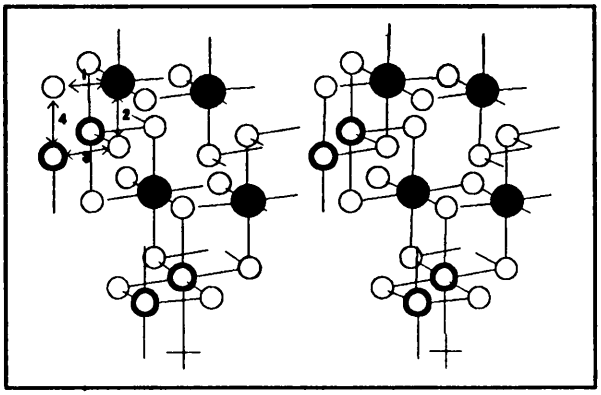

Figure 7.2: Unit-cell of the cobalt or iron spinel. The bond marked 1 represents an arbitrarily chosen bond.

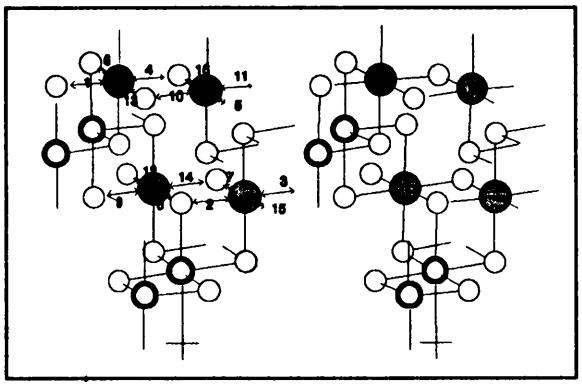

Figure 7.3: The equivalent set, set I, of bonds obtained from bond 1. Numbers indicate position in the spreadsheet.

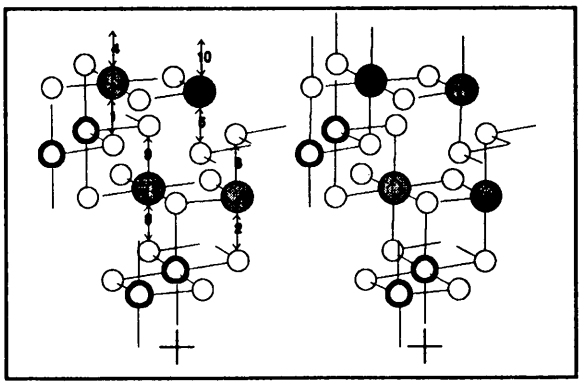

Figure 7.4: The equivalent set, set II, of bonds obtained from bond 2. Numbers indicate position in the spreadsheet.

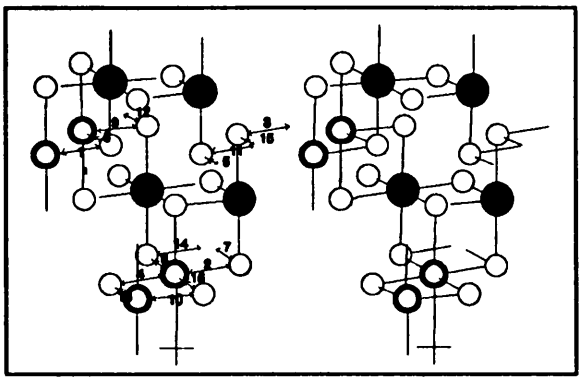

Figure 7.5: The equivalent set, set III, of bonds obtained from bond 3. Numbers indicate position in the spreadsheet.

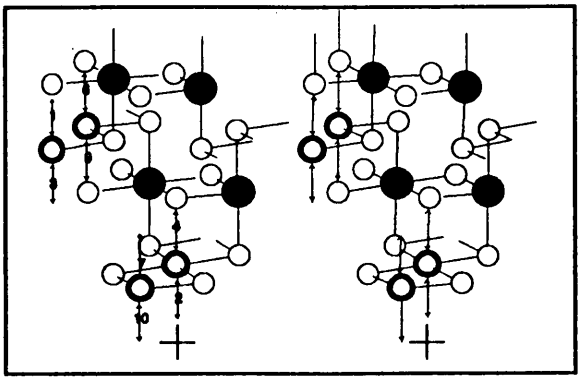

Figure 7.6: The equivalent set, set IV, of bonds obtained from bond 4. Numbers indicate position in the spreadsheet.

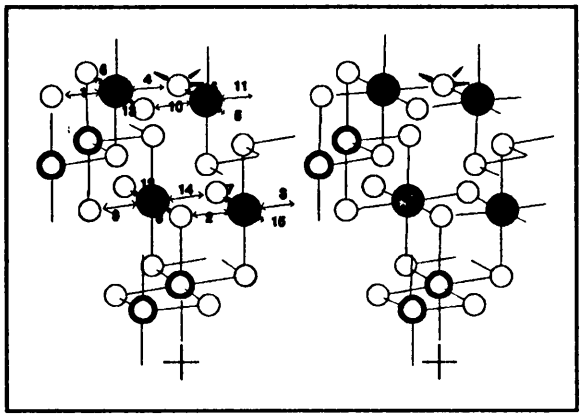

Figure 7.7: A_g applied to set I. The movement of a selected chlorine atom is indicated.

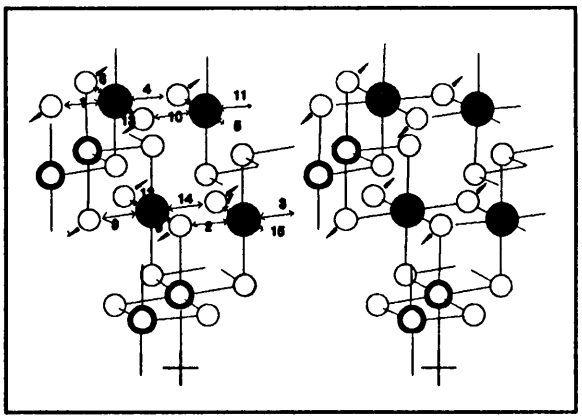

Figure 7.8: A_g applied to set I.

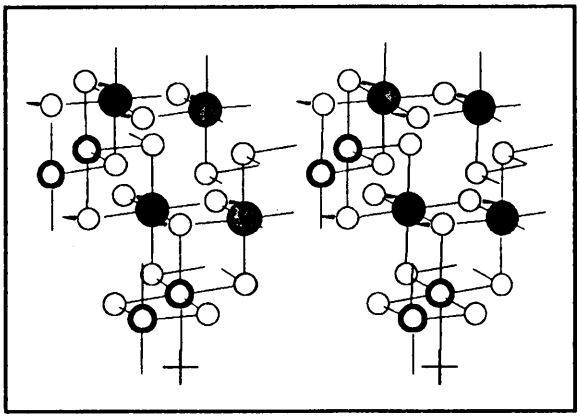

Figure 7.9: B_{1g} applied to set I.

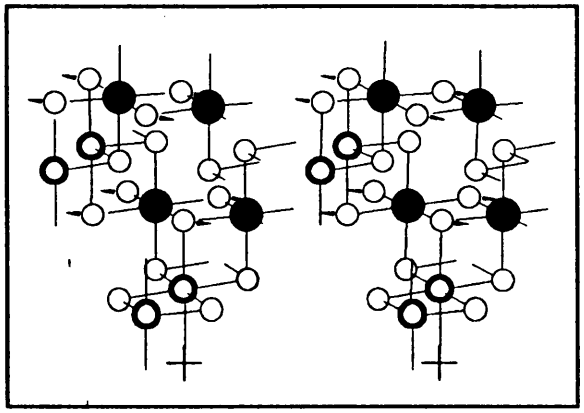

Figure 7.10: B_{2g} applied to set I.

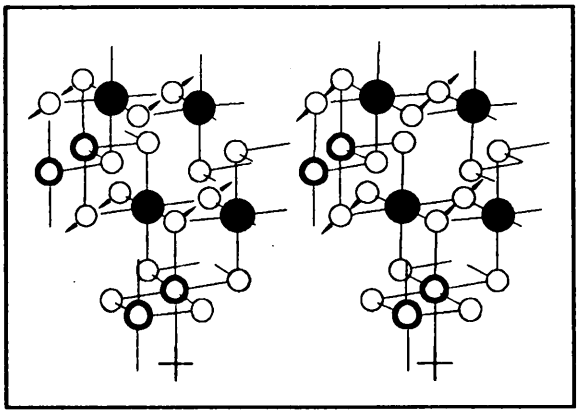

Figure 7.11: B_{3g} applied to set I.

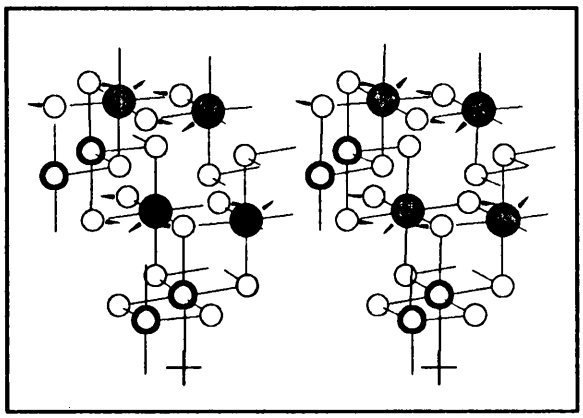

Figure 7.12: A_u applied to set I.

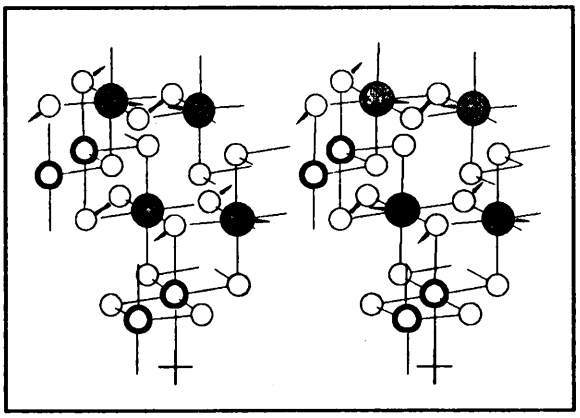

Figure 7.13: B_{1u} applied to set I.

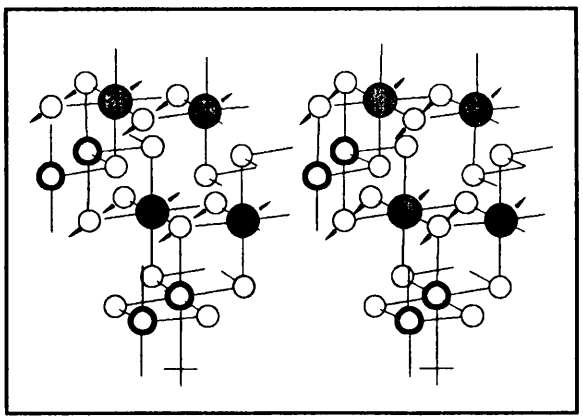

Figure 7.14: B_{2u} applied to set I.

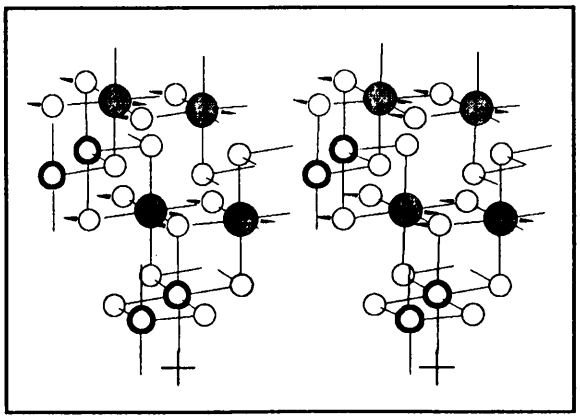

Figure 7.15: B_{3u} applied to set I.

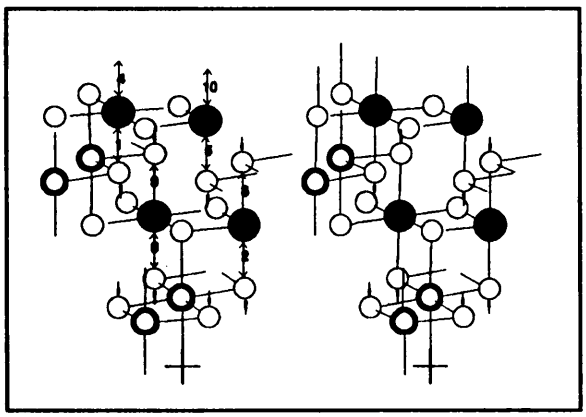

Figure 7.16: A_g applied to set II.

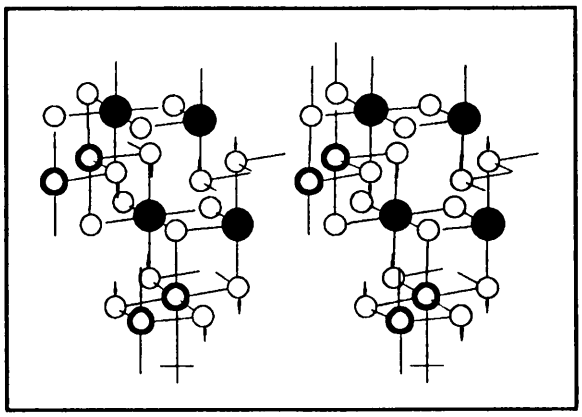

Figure 7.17: B_{2g} applied to set II.

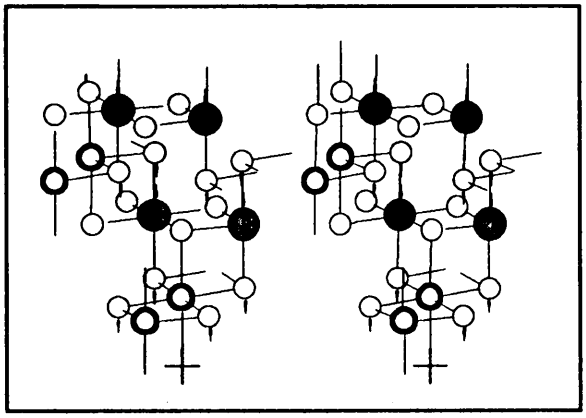

Figure 7.18: B_{1u} applied to set II.

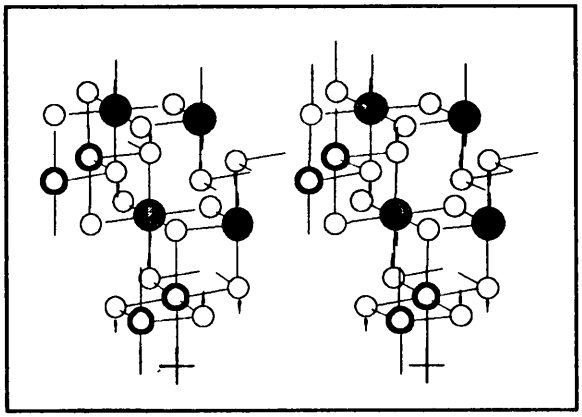

Figure 7.19: B_{3u} applied to set II.

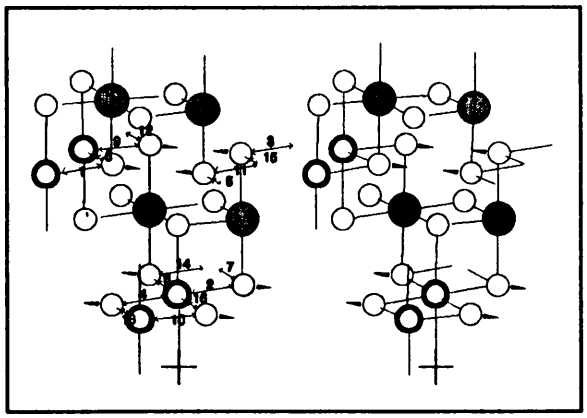

Figure 7.20: A_g applied to set III.

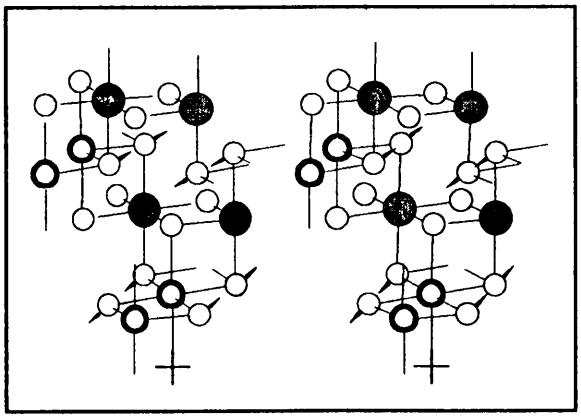

Figure 7.21: B_{1g} applied to set III.

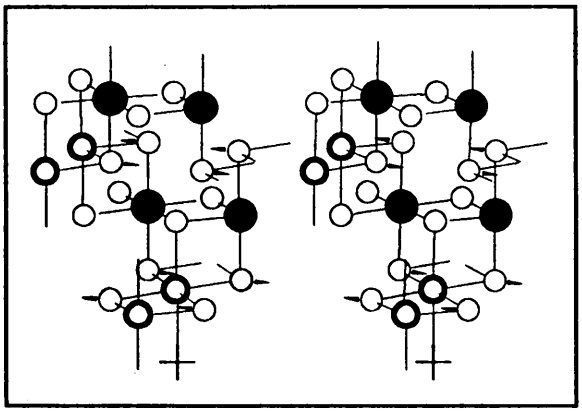

Figure 7.22: B_{2g} applied to set III.

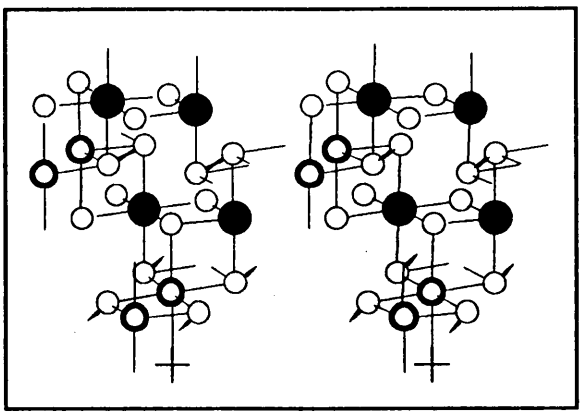

Figure 7.23: B_{3g} applied to set III.

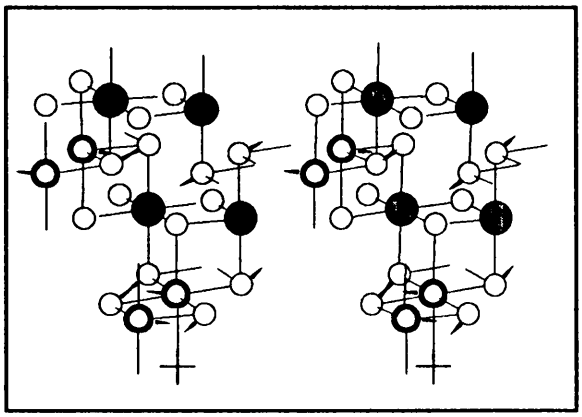

Figure 7.24: A_u applied to set III.

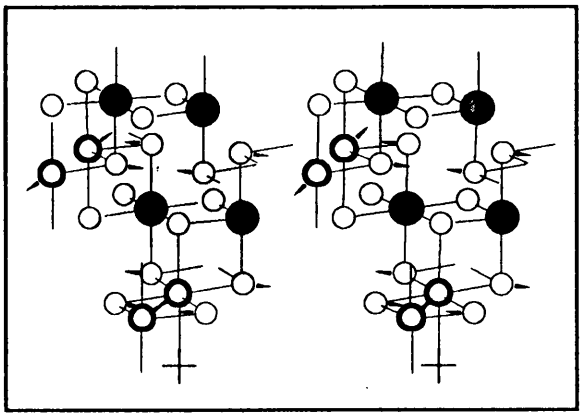

Figure 7.25: B_{1u} applied to set III.

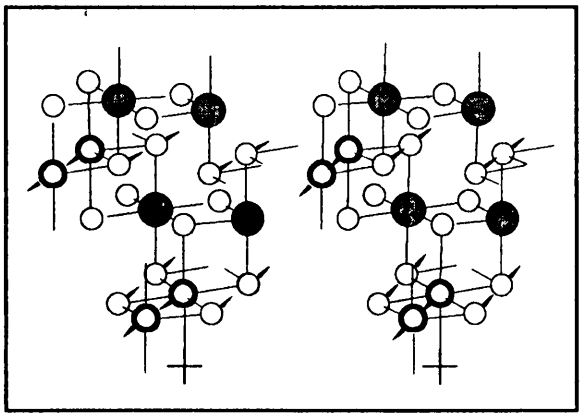

Figure 7.26: B_{2u} applied to set III.

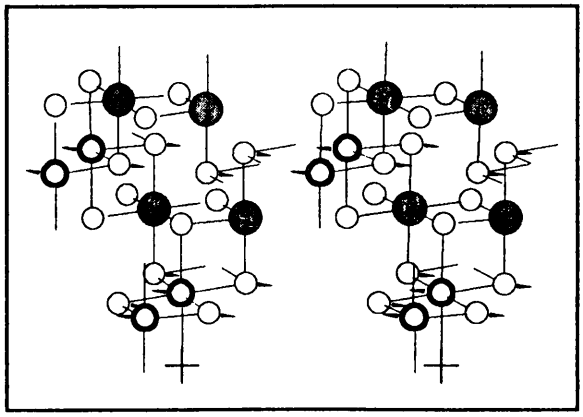

Figure 7.27: B_{3u} applied to set III.

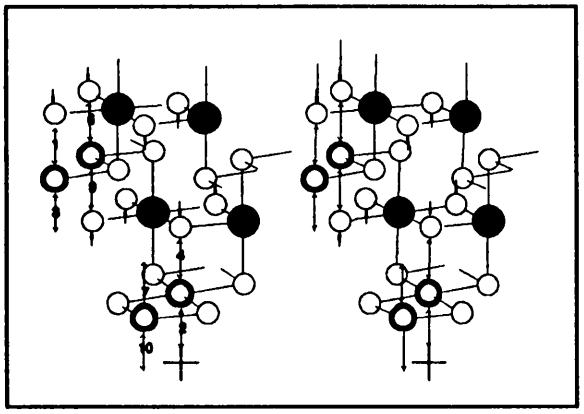

Figure 7.28: A_g applied to set IV.

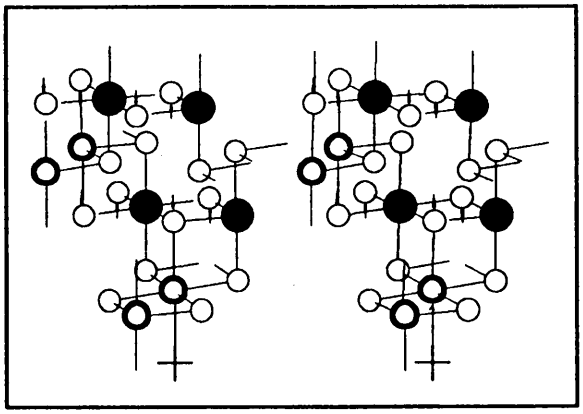

Figure 7.29: B_{3g} applied to set IV.

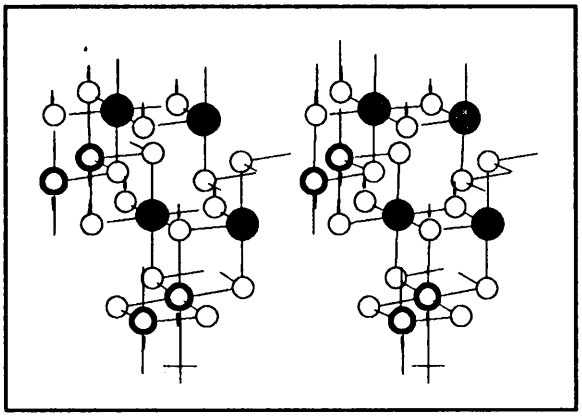

Figure 7.30: B_{1u} applied to set IV.

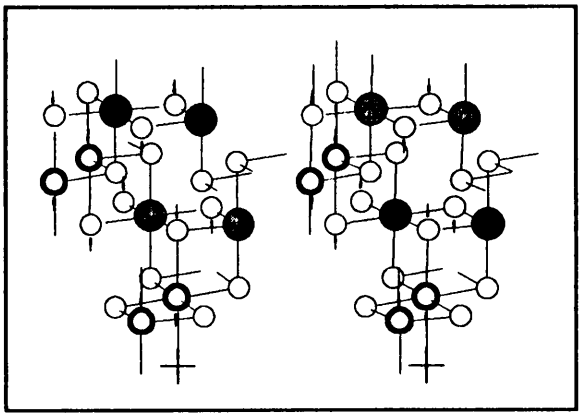

Figure 7.31: B_{2u} applied to set IV.

Chapter 8

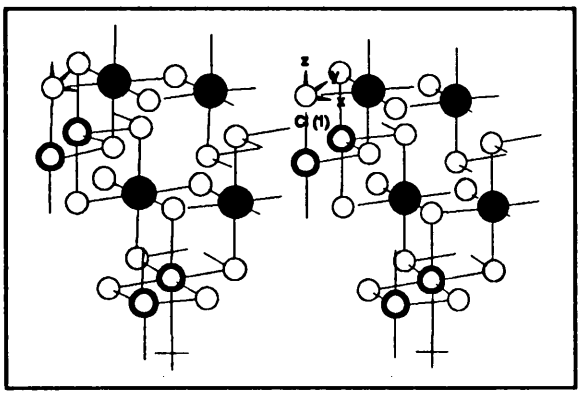

Figure 8.1: A vector aligned with each of the three Cartesian axes on a chlorine atom representing the Cl(1) equivalent set.

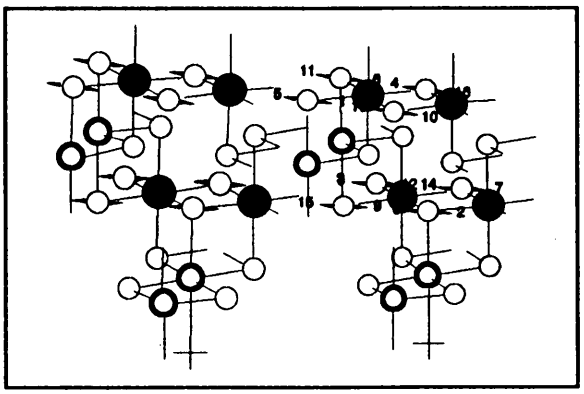

Figure 8.2: The result of applying Spreadsheet 7.1 to a vector aligned with the x-axis on an atom of the Cl(1) equivalent set.

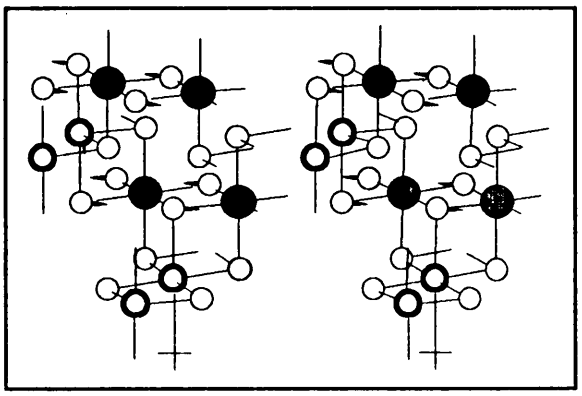

Figure 8.3: Cl (1), x-axis, B_{1g}.

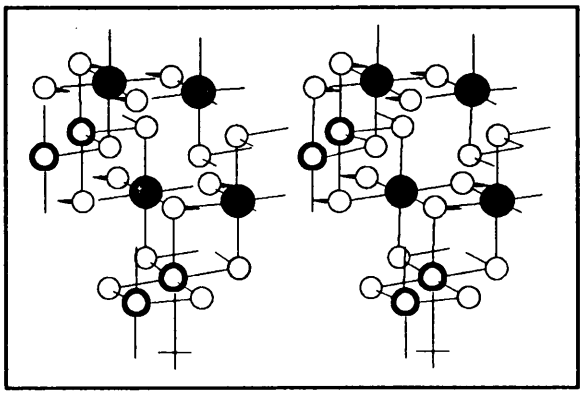

Figure 8.4: Cl (1), x-axis, B_{2g}.

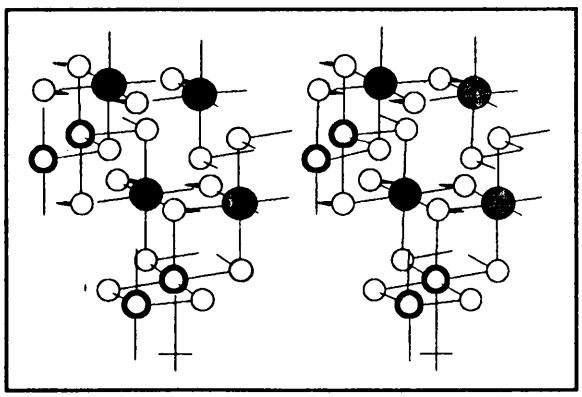

Figure 8.5: Cl (1), x-axis, A_u.

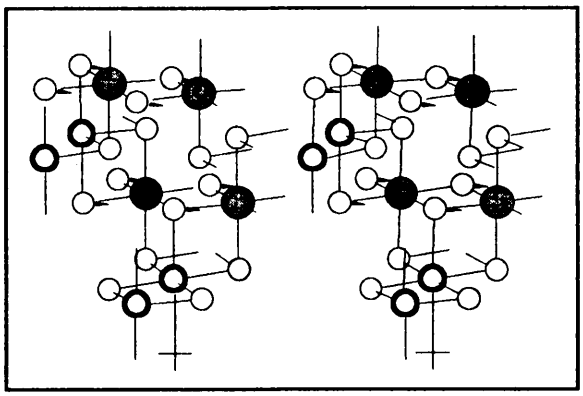

Figure 8.6: Cl (1), x-axis, B_{3u}.

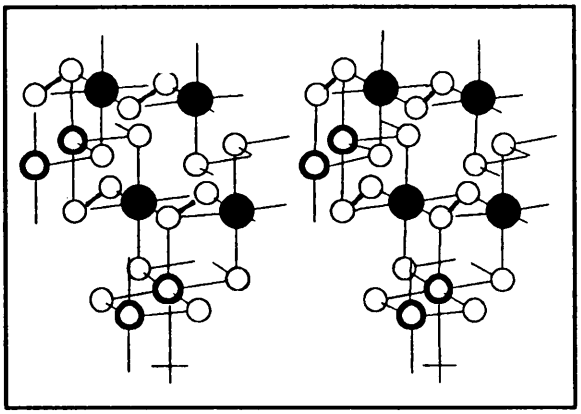

Figure 8.7: Cl (1), y-axis, A_g.

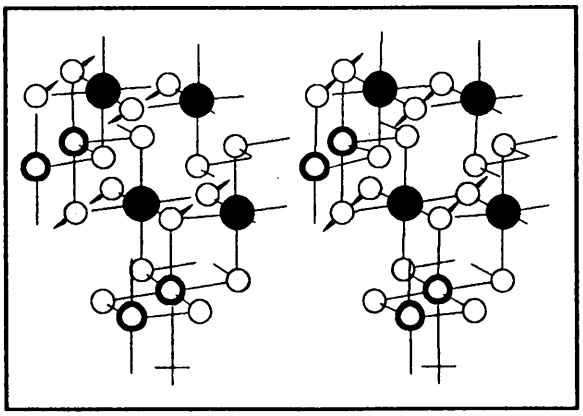

Figure 8.8: Cl (1), y-axis, B_{3g}.

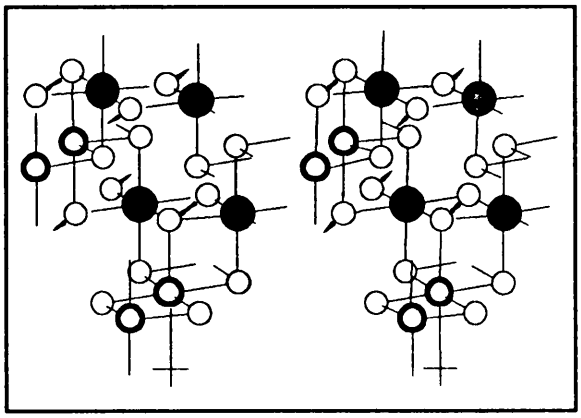

Figure 8.9: Cl (1), y-axis, B_{1u} .

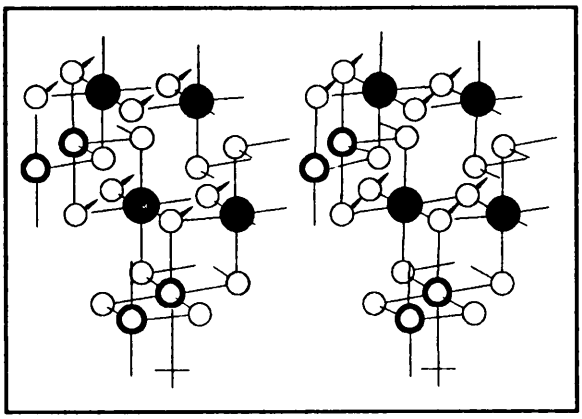

Figure 8.10: Cl (1), y-axis, B_{1u} .

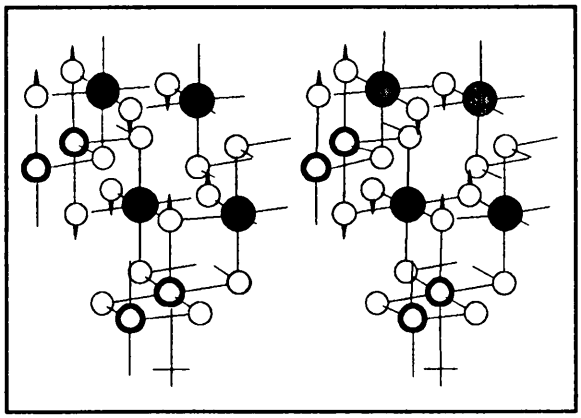

Figure 8.11: Cl (1), z-axis, A_g.

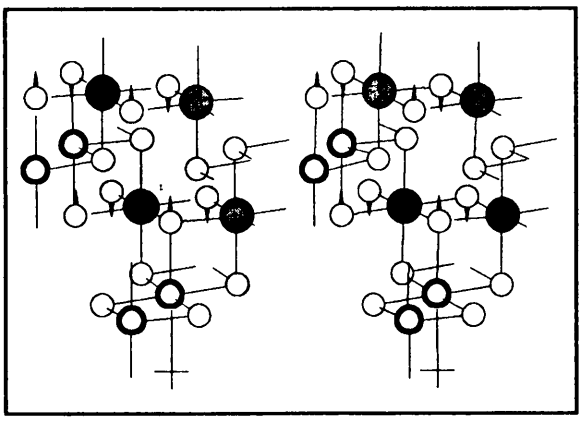

Figure 8.12: Cl (1), z-axis, B_{3g}.

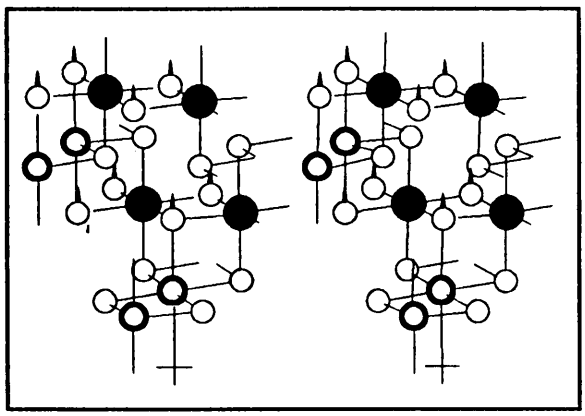

Figure 8.13: Cl (1), z-axis, B_{1u}.

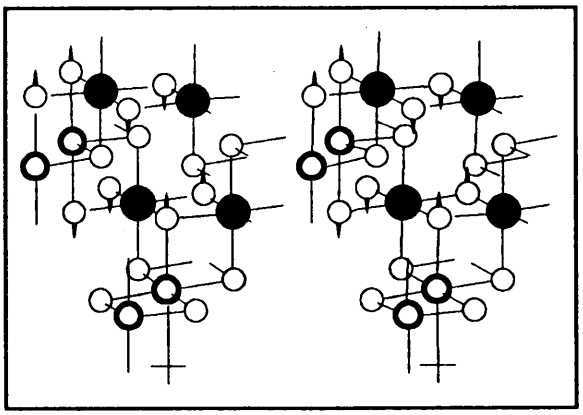

Figure 8.14: Cl (1), z-axis, B_{2u}.

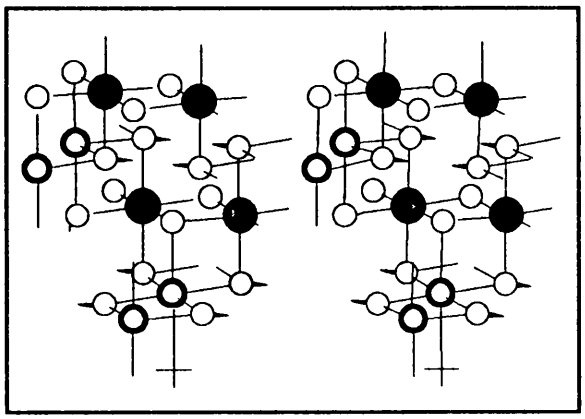

Figure 8.15: Cl (2), x-axis, A_g.

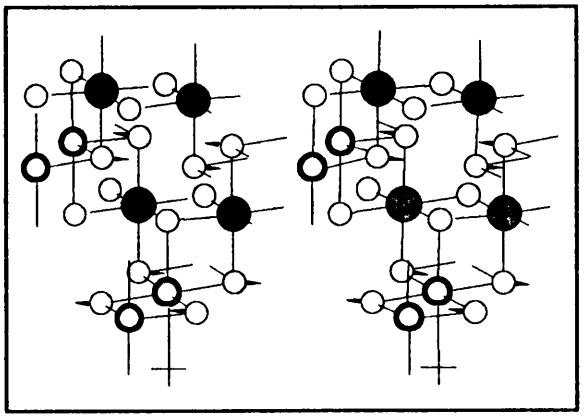

Figure 8.16: Cl (2), x-axis, B_{2g}.

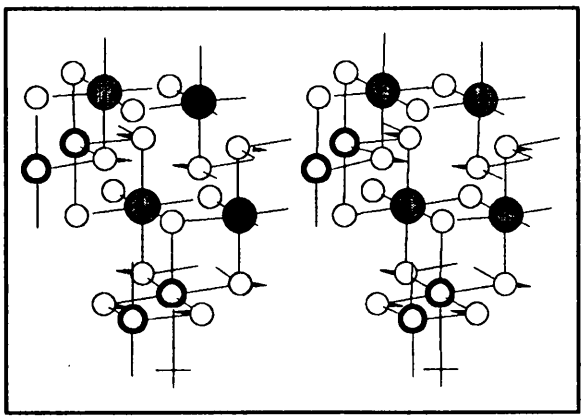

Figure 8.17: Cl (2), x-axis, B_{1u}.

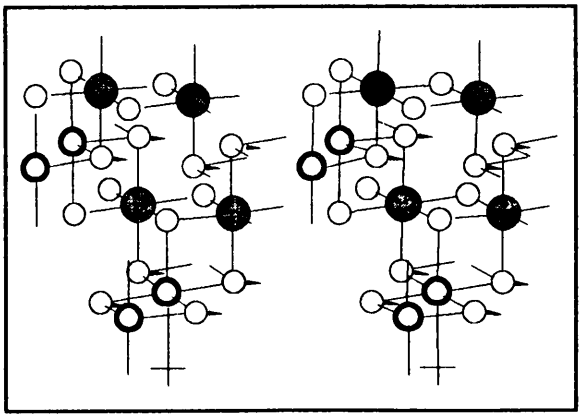

Figure 8.18: Cl (2), x-axis, B_{3u}.

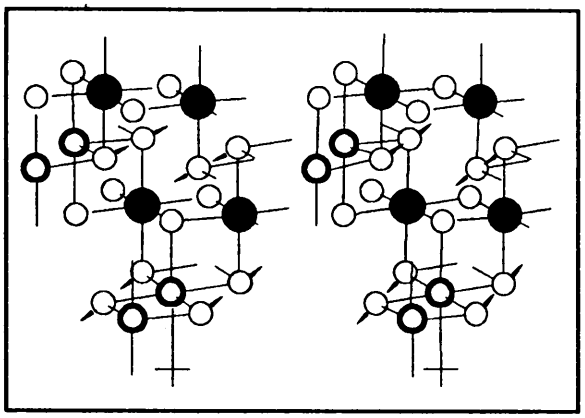

Figure 8.19: Cl (2), y-axis, B_{1g}.

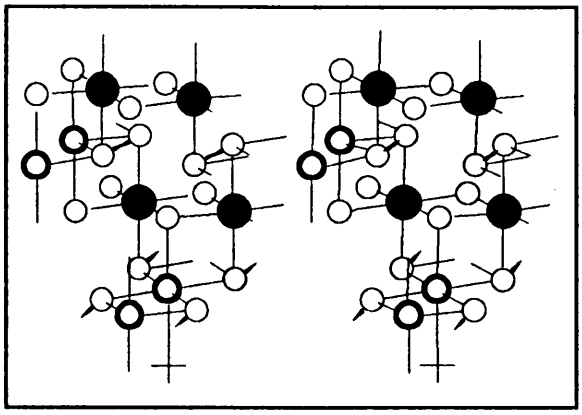

Figure 8.20: Cl (2), y-axis, B_{3g}.

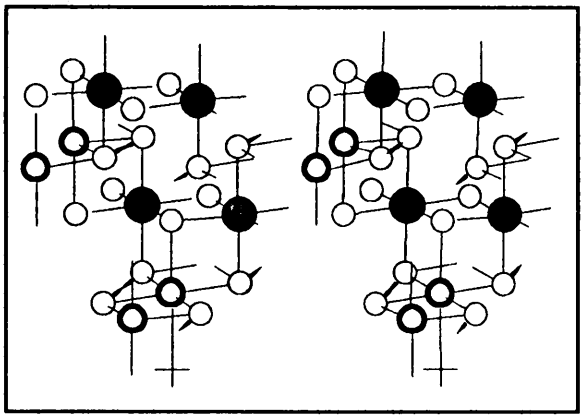

Figure 8.21: Cl (2), y-axis, A_u.

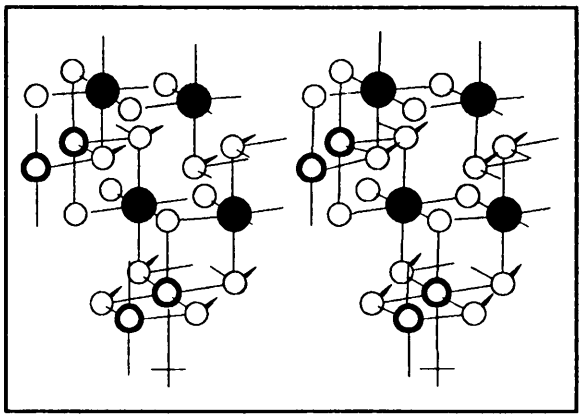

Figure 8.22: Cl (2), y-axis, B_{2u}.

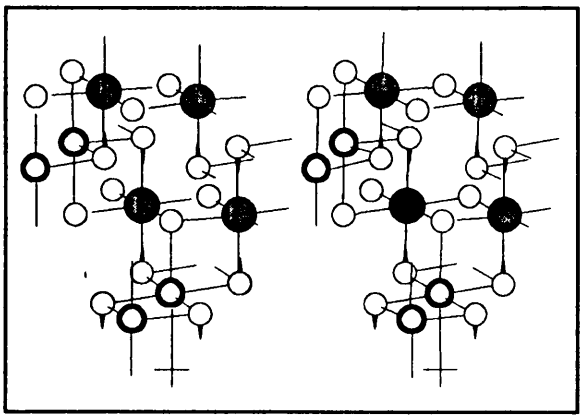

Figure 8.23: Cl (2), z-axis, A_g.

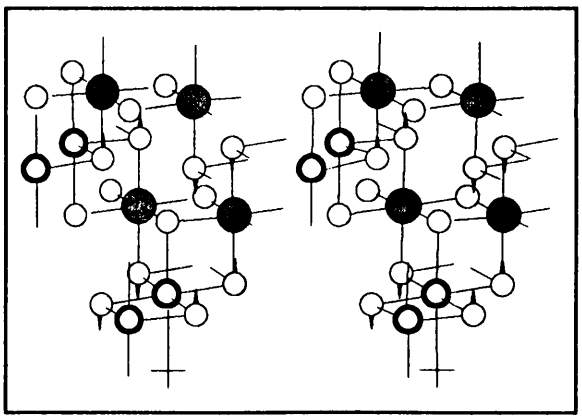

Figure 8.24: Cl (2), z-axis, B_{2g}.

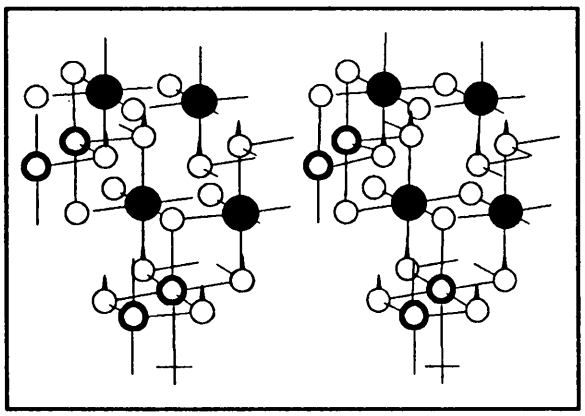

Figure 8.25: Cl (2), z-axis, B_{1u}.

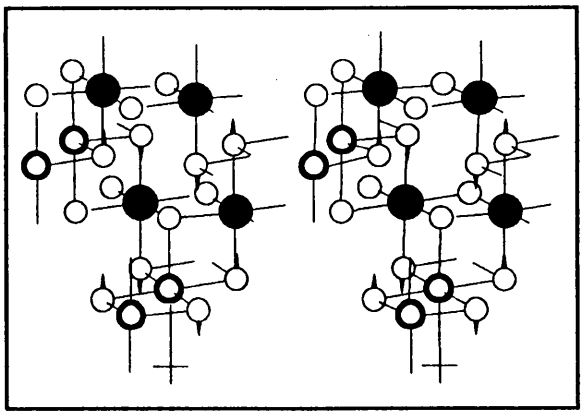

Figure 8.26: Cl (2), z-axis, B_{3u}.

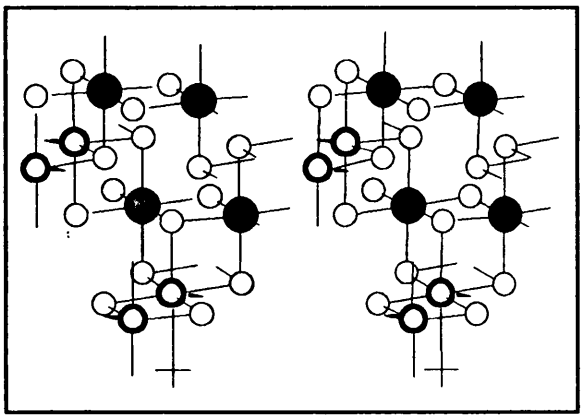

Figure 8.27: Cl (2), z-axis, B_{3u}.

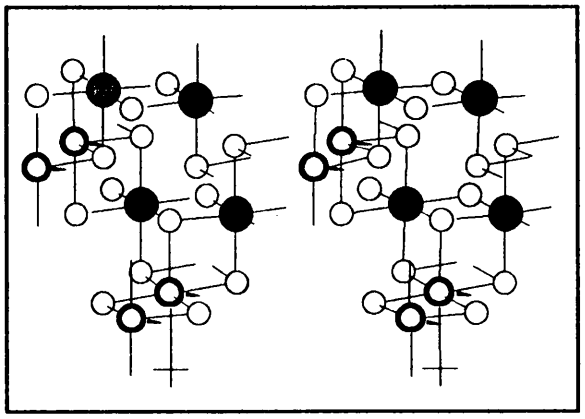

Figure 8.28: Li: O_h, x-axis, B_{3u}.

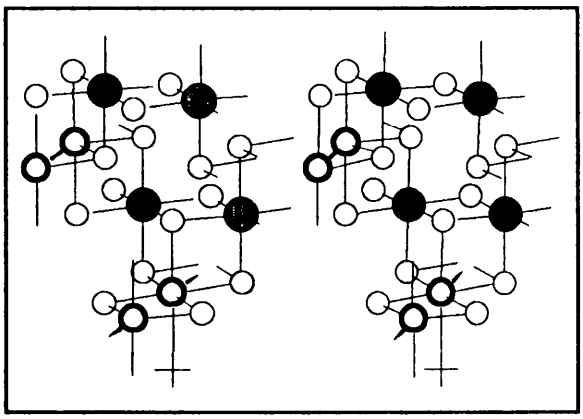

Figure 8.29: Li: O_h, y-axis, B_{1u}.

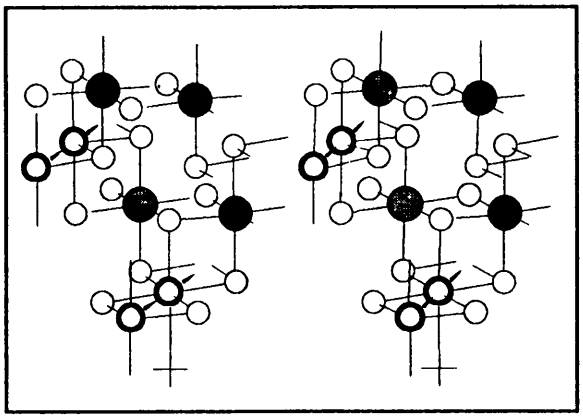

Figure 8.30: Li: O_h, y-axis, B_{1u}.

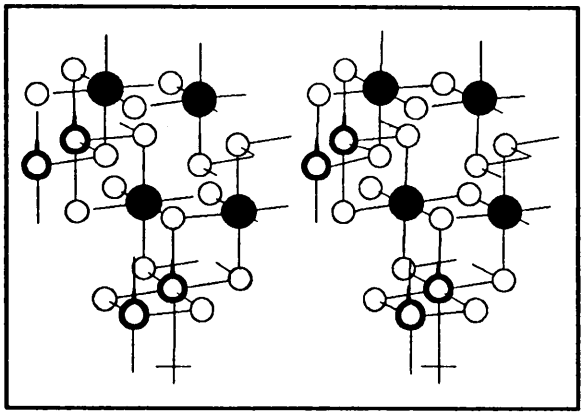

Figure 8.31: Li: O_h, z-axis, B_{1u}.

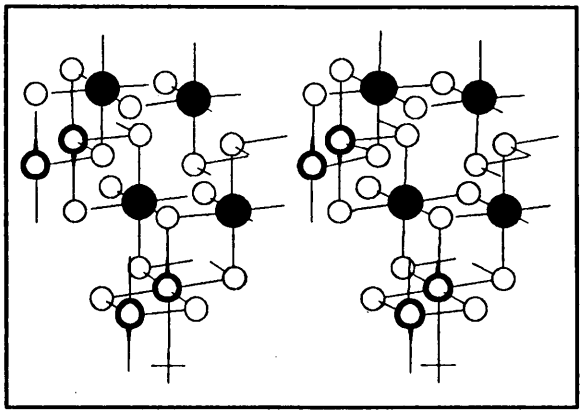

Figure 8.32: Li: O_h, z-axis, B_{2u}.

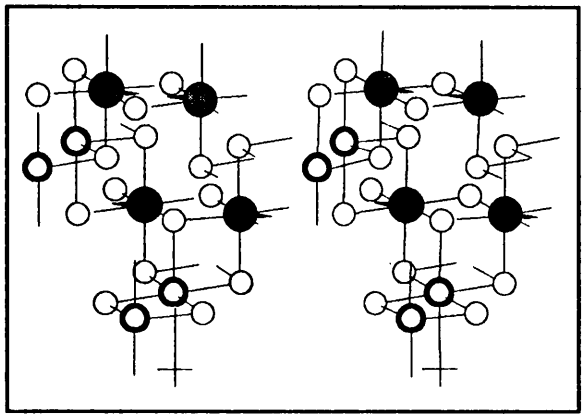

Figure 8.33: M: O_h, x-axis, B_{1u}.

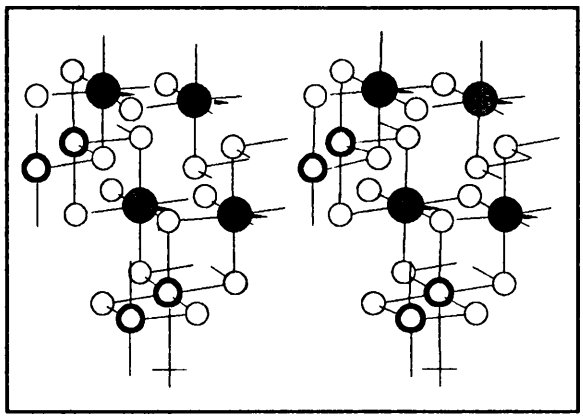

Figure 8.34: M: O_h, x-axis, B_{3u}.

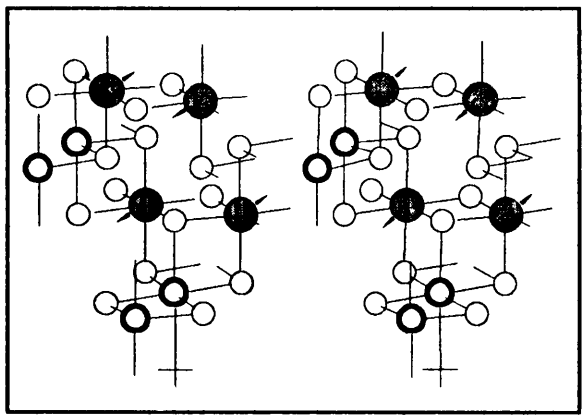

Figure 8.35: M: O_h, y-axis, A_u.

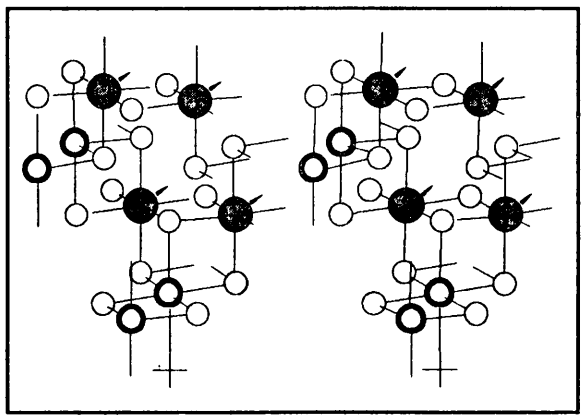

Figure 8.36: M: O_h, y-axis, B_{2u}.

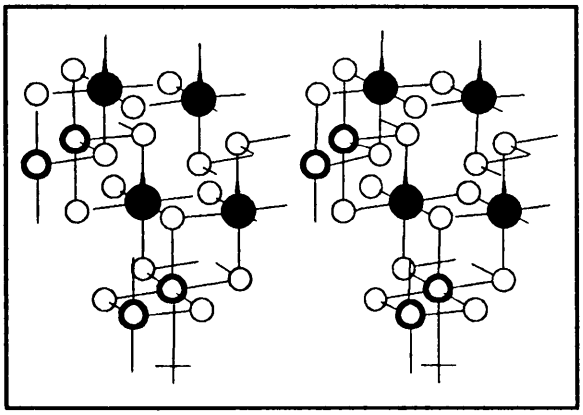

Figure 8.37: M: O_h, z-axis, B_{1u}.

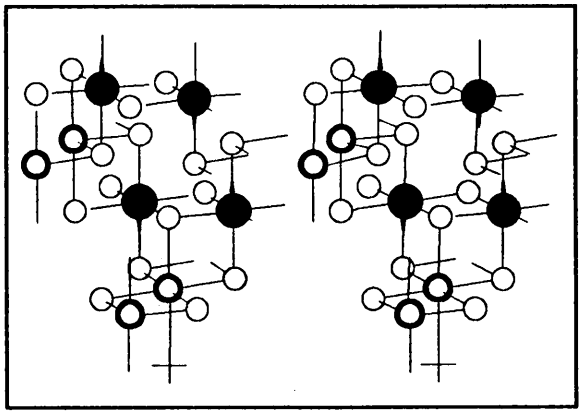

Figure 8.38: M: O_h, z-axis, B_{3u}.

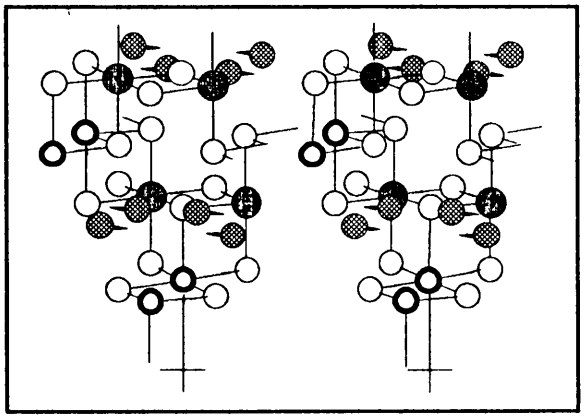

Figure 8.39: Li in the 8i site, x-axis, A_g.

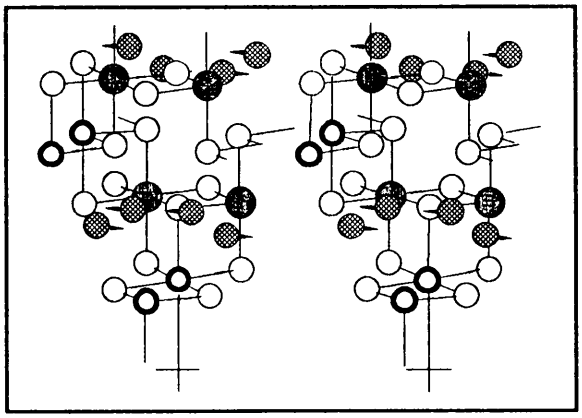

Figure 8.40: Li in the 8i site, x-axis, B_{2g}.

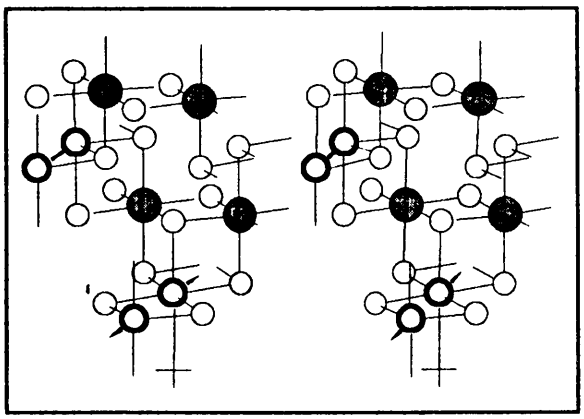

Figure 8.41: Li in the 8i site, x-axis, B_{1u}.

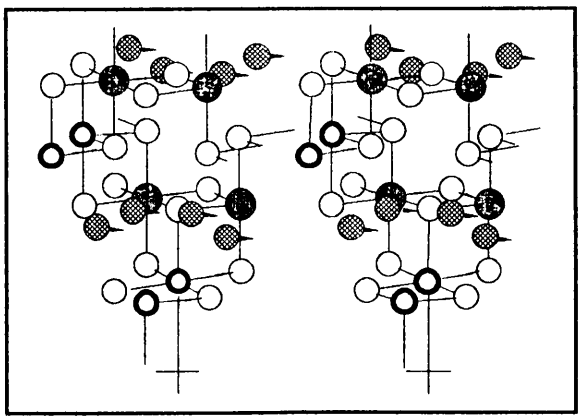

Figure 8.42: Li in the 8i site, x-axis, B_{3u}.

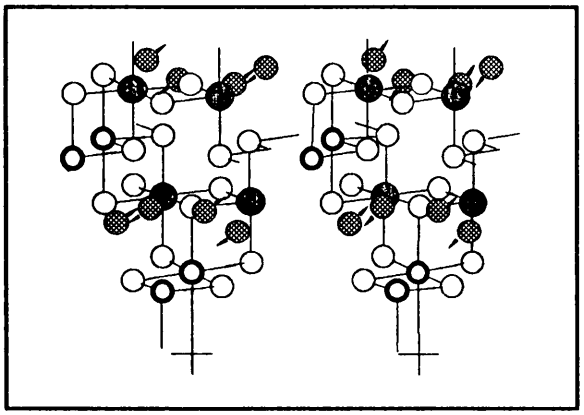

Figure 8.43: Li in the 8i site, y-axis, B_{1g}.

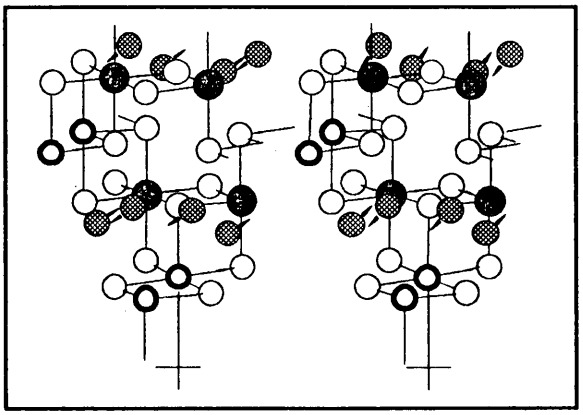

Figure 8.44: Li in the 8i site, y-axis, B_{3g}.

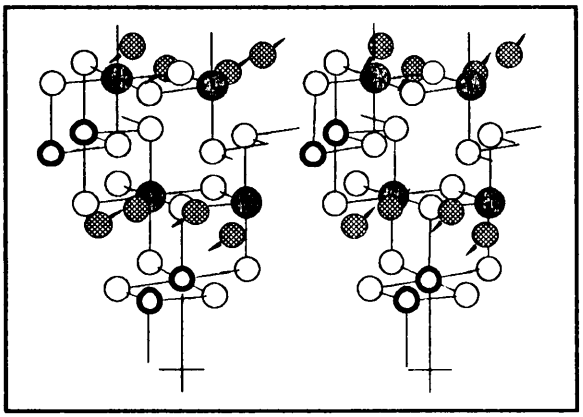

Figure 8.45: Li in the 8i site, y-axis, A_u.

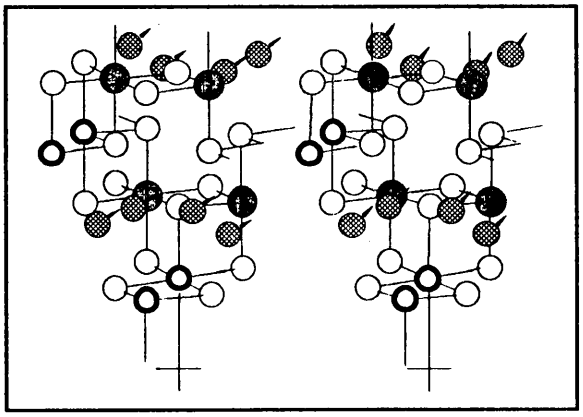

Figure 8.46: Li in the 8i site, y-axis, B_{2u}.

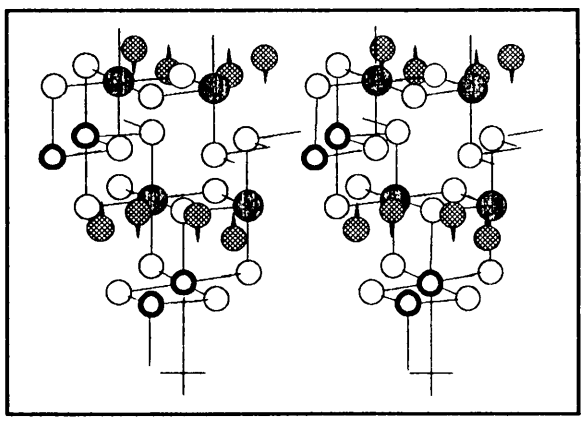

Figure 8.47: Li in the 8i site, z-axis, A_g.

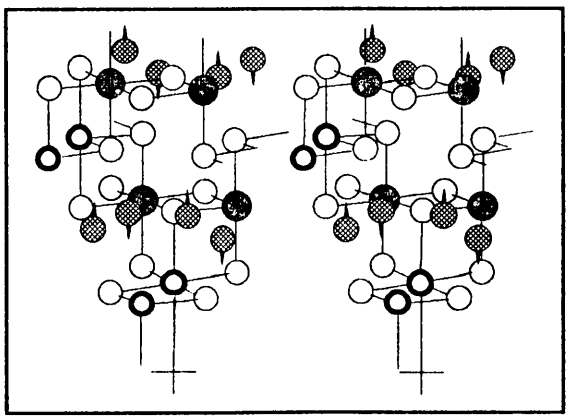

Figure 8.48: Li in the 8i site, z-axis, B_{2g}.

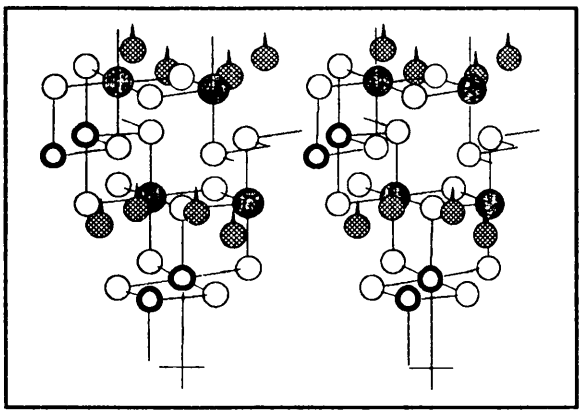

Figure 8.49: Li in the 8i site, z-axis, B_{1u}.

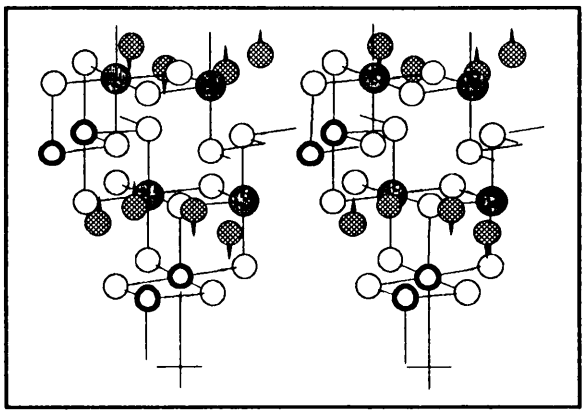

Figure 8.50: Li in the 8i site, z-axis, B_{3u}.

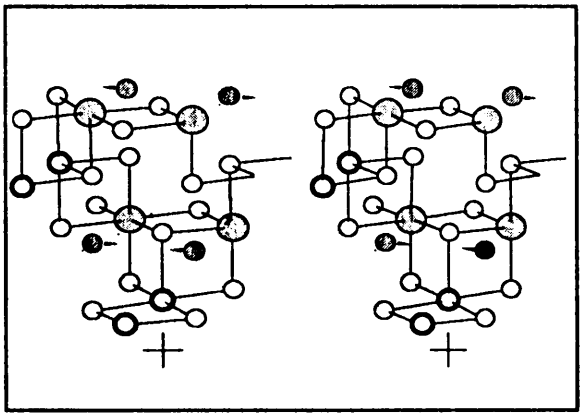

Figure 8.51: Li in the 4c site, x-axis, B_{1u}.

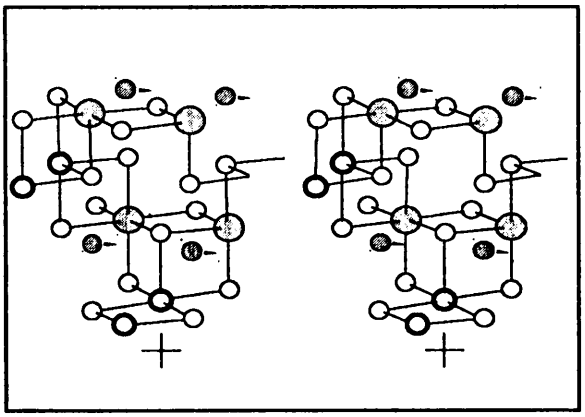

Figure 8.52: Li in the 4c site, x-axis, B_{3u}.

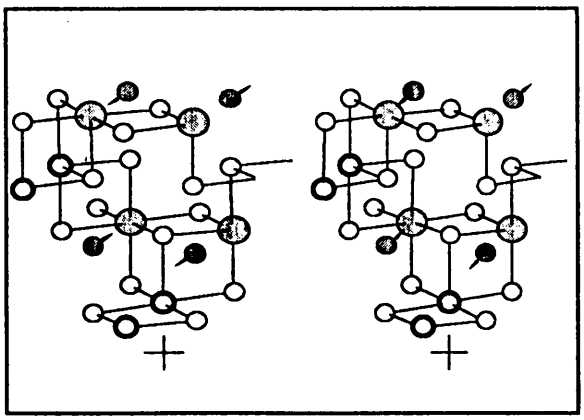

Figure 8.53: Li in the 4c site, y-axis, A_u.

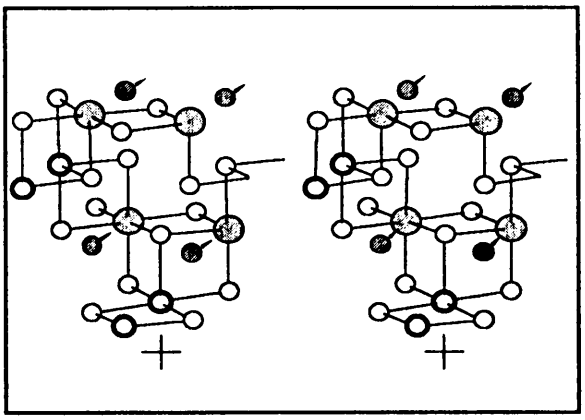

Figure 8.54: Li in the 4c site, y-axis, B_{2u}.

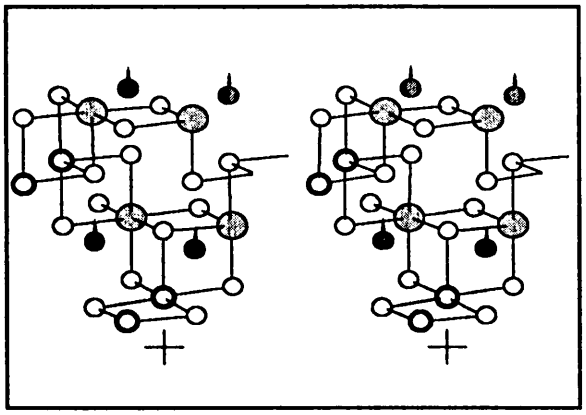

Figure 8.55: Li in the 4c site, z-axis, B_{1u}.

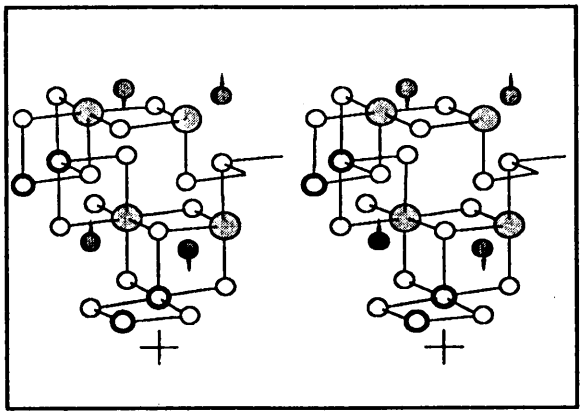

Figure 8.56: Li in the 4c site, z-axis, B_{3u}.

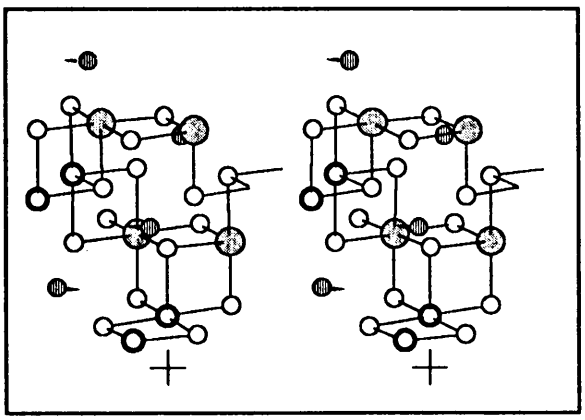

Figure 8.57: Li in the 4e site, x-axis, B_{2g}.

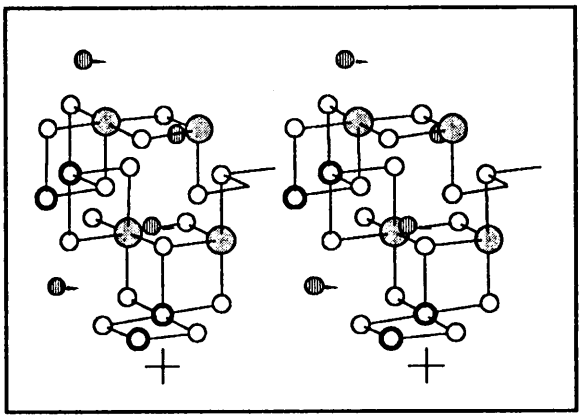

Figure 8.58: Li in the 4e site, x-axis, B_{3u}.

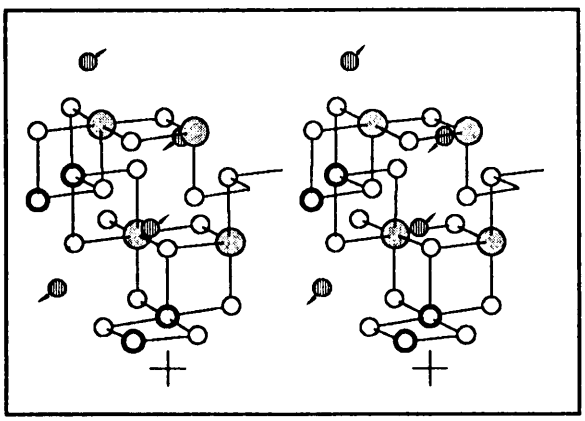

Figure 8.59: Li in the 4e site, y-axis, B_{3g}.

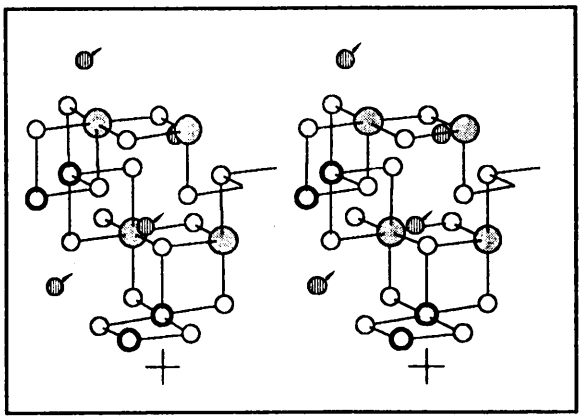

Figure 8.60: Li in the 4e site, y-axis, B_{2u}.

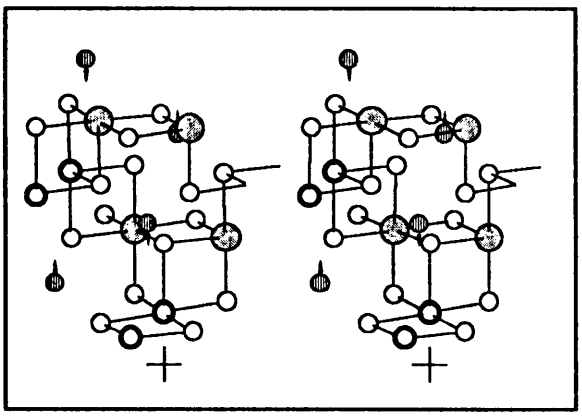

Figure 8.61: Li in the 4e site, z-axis, A_g.

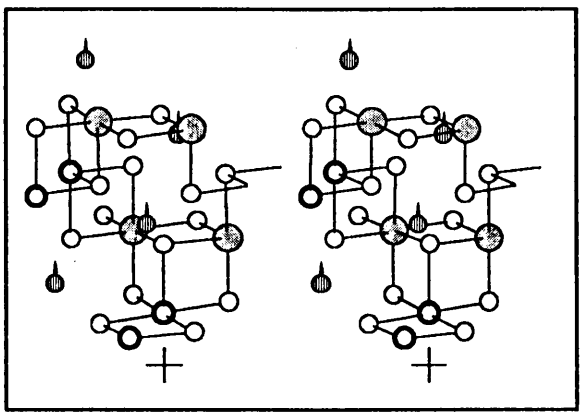

Figure 8.62: Li in the 4e site, z-axis, B_{1u}.

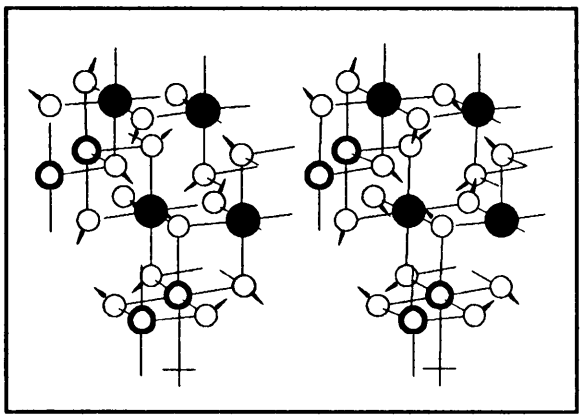

Figure 8.63: Representation of the first combination of A_g modes from Table 8.3.

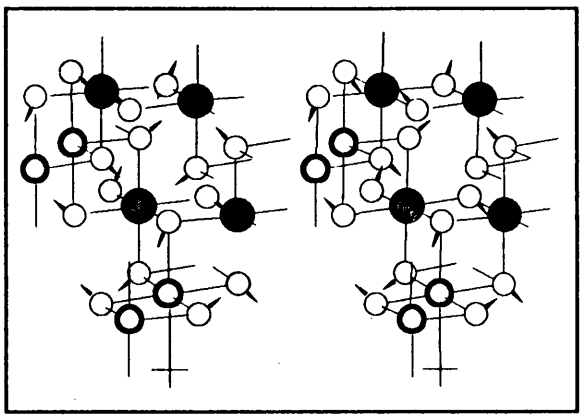

Figure 8.63: Representation of the second combination of A_g modes from Table 8.3.

Appendix A

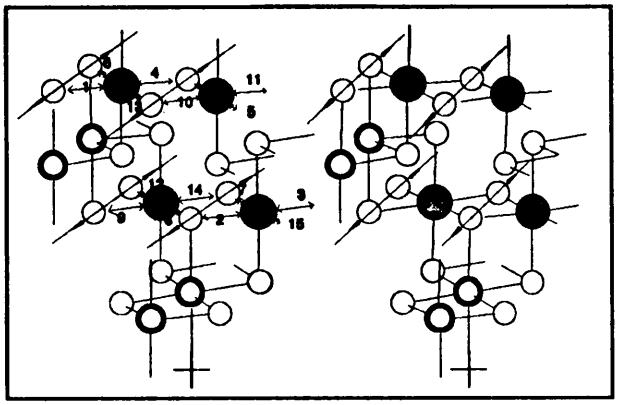

Figure A.4: An example of the guide lines represent a vibration.

Appendix C

Bibliography

Books and monographs

[1] Balkanski, M. (ed.), *Lattice Dynamics*, Flammarion, Paris (1978).

[2] Bhagavantum, S., Venkatarayudu, T., *Theory of Groups and Its Application to Physical Problems*, Audhra University, Waltair, India (1962).

[3] Coblentz, W.W., *Additional Investigations of Infrared Spectra*, Carnegie Institution, Washington D.C. (1908).

[4] Cotton, F.A.,*Chemical Applications of Group Theory*, Wiley-Interscience, New York, (1990 3rd. ed.).

[5] Fateley, W.G., Dollish, N.T., et al, *Infrared and Raman Selection Rules for Molecular and Lattice Vibrations: The Correlation Method*, Wiley-Interscience, New York (1972).

[6] Flurry, R.L. Jr., *Symmetry Groups : Theory and Chemical Applications*, Prentice Hall Inc, Englewood Cliffs, New Yersey (1980).

[7] Greenwood, N.N., Earnshaw, A., *Chemistry of the Elements*, Pergamon Press, Oxford (1984).

[8] Hahn, T. (Ed.), *International Tables for Crystallography Volume A: Space-group symmetry*, D Reidel Publishing Company, Dortrecht/Boston/Lancaster/Tokio (1987 2nd. revised edition).

[9] Hertzberg, G., *Infrared and Raman Spectra of Polyatomic Molecules*, Van Nostrad, New York (1945).

[10] Wilson, E.B. Jr., Decius, J.C., Cross, P.C., *Molecular Vibrations: The Theory of Infrared and Raman Vibrational Spectra*, McGraw-Hill, New York, (1955).

[11] Adams, D.M., Newton, D.C., *Tables for Factor Group and Point Group Analysis*, Beckman-RICC Limited, Sunley House, England

Papers

[12] Akagogi, M., Ross, N.L., et al, *Am. Mineral.*, **69**, 499, (1984).
[13] Badarinath, K.V.S., *Phys. Stat. Sol. (a)*, **91**, K19 (1985).
[14] Baran, E.J., Botto, I.L., *Z. Anorg. Allg. Chem.*, **463**, 185 (1980).
[15] Burdett, J.K., Price, G.D., Price, S.L., *J. Am. Chem. Soc.*, **104**, 92 (1982).
[16] Cros, C., Hanebali, L., et al, *Solid State Ionics*, **9-10**, 139 (1983).
[17] Cynn, H., Sharma, S.K., et al, *Phys. Rev. B: Condens. Matter*, **45**, 500 (1992).
[18] Gasanly, N.M., El-Hamid, S.A., et al, *Phys. Stat. Sol. (b)*, **169**, K115 (1992).
[19] Graves, P.R., Johnston, C., Campaniello, J.J., *Mat. Res. Bull.*, **23**, 1651 (1988).
[20] Gupta, H.C., Geeta, S., et al, *J. Phys. Chem. Solids*, **50**, 925 (1989).
[21] Gupta, H.C., Parashar, A., *Phys. Stat. Sol. (b)*, **160**, K19 (1990).
[22] Gupta, H.C., Sinha, M.M., et al, *Phys. Stat. Sol. (b)*, **169**, K65, (1992).
[23] Guyot, F., Boyer, H., et al, *Phys. Chem. Minerals*, **13**, 91 (1986).
[24] Haas, C., *J. Phys. Chem. Solids*, **26**, 1225, (1965).
[25] Heuer, A.H., Mitchell, T.E., *J. Phys. C: Solid State Phys.*, **8**, L541 (1975).
[26] Himmrich, J., Lutz, H.D., *Solid State Com.*, **79**, 447 (1991).
[27] Ishii, M., Hiraishi, J., Yamanaka, T., *Phys. Chem. Minerals*, **8**, 64 (1982).
[28] Kanno, R., Takeda, Y., et al, *J. Electrochem. Soc.*, **131**, 469 (1984).
[29] Kanno, R., Takeda, Y., et al, *J. Electrochem. Soc.*, **133**, 1053 (1986).
[30] Kanno, R., Takeda, Y., et al, *J. Solid State Chem.*, **71**, 196 (1987).

[31] Kanno, R., Takeda, Y., et al, *J. Solid State Chem.*, **72**, 363 (1988).

[32] Kanno, R., Takeda, Y., et al, *J. Solid State Chem.*, **75**, 41 (1988).

[33] Kanno, R., Takeda, Y., et al, *Solid State Ionics*, **20**, 99 (1986).

[34] Kanno, R., Takeda, Y., Yamamoto, O., *Mater. Res. Bull.*, **16**, 999 (1981).

[35] Kanno, R., Takeda, Y., Yamamoto, O., *Solid State Ionics*, **9-10**, 153 (1983).

[36] Lutz, H.D., Becker, W., et al, *J. Raman Spec.*, **20**, 99 (1989).

[37] Lutz, H.D., Müller, B., Steiner, H.J., *J. Solid State Chem.*, **90**, 54 (1991).

[38] Lutz, H.D., Schmidt, W., Haeuseler, H., *J. Phys. Chem. Solids*, **42**, 287 (1981).

[39] Lutz, H.D., Waeschenbach, G., et al, *J. Solid State Chem.*, **48**, 196 (1983).

[40] Malézieux, J.-M., Piriou, B., *Bull. Minéral.*, **111**, 649 (1988).

[41] McMillan, P., Akaogi, M., *Am. Mineral.*, **72**, 361 (1987).

[42] Porotnikov, N.V., Savenko, V.G., Sidorova, O.V., *Zh. Neorg. Khimii*, **28**, 1653 (1983).

[43] Preudhomme, J., Tartre, P., *Spectrochim. Acta*, **27A**, 845 (1971).

[44] Preudhomme, J., Tartre, P., *Spectrochim. Acta*, **27A**, 961 (1971).

[45] Preudhomme, J., Tartre, P., *Spectrochim. Acta*, **27A**, 1817 (1971).

[46] Preudhomme, J., Tartre, P., *Spectrochim. Acta*, **28A**, 69 (1972).

[47] Shaplygin, I.S., Lazarev, V.B., *Zh. Neorg. Khimii*, **25**, 906 (1980).

[48] Shirai, H., Yoshiyuki, M., Nakagawa, I., *J Phys. Soc. Japan*, **51**, 592 (1982).

[49] Soubeyroux, J.L., Cros, C., et al, *Solid State Ionics*, **15**, 293 (1985).

[50] Striefler, M.E., Barsch, G. R., Syun-Iti, A., *Spectrochim. Acta*, **36A**, 275 (1980).

[51] Tartre, P., *Acta Cryst.*, **16**, 228 (1963).

[52] Tobin, M.C., *J. Chem. Phys.*, **23**, 891 (1955).

[53] Tobin, M.C., *J. Mol. Spectr.*, **4**, 349 (1960).

[54] Van Loon, C.J.J., De Jong, J., *Acta Crystallogr. Sect. B*, **B31**, 2549 (1975).

[55] Wakaki, M., *Jap. J. Appl. Phys. Part 1*, **24**, 1471 (1985).

[56] Wakamura, K., Iwatani, H., Takarabe, K., *J. Phys. Chem. Solids.*, **48**, 857 (1987).

[57] Wakamura, K., *J. Solid State Chem.*, **78**, 197 (1989).

[58] Waldron, R.D., *Phys. Rev.*, **99**, 1727 (1955).

[59] White, W.B., De Angelis, B.A., *Spectrochim. Acta*, **23A**, 985 (1967).

[60] Winston, H., Halford, R.S., *J. Chem. Phys.*, **17**, 607 (1949).

[61] Wussow, K., Haeuseler, H., et al, *J. Solid State Chem.*, **78**, 117, (1989).

[62] Yamanaka, T., Ishii, M., *Phys. Chem. Minerals*, **13**, 156 (1986).

[63] Zarembowitch, J., Gouteron, J., Lejus, A.M., *Phys. Stat. Sol. (b)*, **94**, 249 (1979).

Computer programs

[64] Alchemy II Rel.2.10 © Tripos Associates Inc. 1986 1989.

[65] Alchemy III Rel.1.00 © Tripos Associates Inc. 1986 1992.

[66] CorelDRAW! Ver3.00 Rel.B © Corel Corporation 1992

[67] CorelTRACE! Ver.3.00 Rel.B © Corel Corporation 1992

[68] DrawPerfect Rel.1.1 © WordPerfect Corporation, 1990.

[69] Image Alchemy Ver.1.5 © Handmade Sofware, Inc. 1990 1991. ***

[70] Lotus123 Rel.2.3 © Lotus Development Corporation, 1990 1991.

[71] Turbo Pascal Ver.6.0 © Borland International Inc. 1983 1990.

[72] WordPerfect for Windows Ver.5.1 © WordPerfect Corporation 1991.

*** This program is shareware and available in the SIMTEL20 directory as ALCH16.ZIP